Cenozoic Denudation of the Raton Basin and Vicinity, Northeastern New Mexico and Southeastern Colorado, Determined Using Apatite Fission-track Thermochronology and Sonic Log Analysis

By

Marta Hemmerich

Submitted in Partial Fulfillment of the Requirements
For the Degree of Master of Science in Geology
August, 2001

Department of Earth and Environmental Science
New Mexico Institute of Mining and Technology
Socorro, New Mexico

Abstract

Little is known about the thermal and exhumation histories of the Raton Basin and vicinity in northeastern New Mexico and southeastern Colorado. As a result, it is one of the last "frontier" and "underdeveloped" basins in the western United States. In this study, the sonic logs from 42 wells within the Raton Basin and surrounding areas in northeastern New Mexico and southeastern Colorado were digitized at five-foot intervals and the amount of sediment that has been eroded was estimated using two different methods: 1) the multiple unit method, which treats all lithologies as a package and bases erosion estimates on sonic log data from the entire section of interest and 2) the single unit method which examines the sonic velocity of individual rock units to determine the amount of erosion. The results of these different sonic log methods were compared to each other and to two different thermal techniques used to estimate denudation values: apatite fission-track thermochronology and vitrinite reflectance of coal ranks. The timing and amount of exhumation experienced by four wells within the study area were determined by apatite fission-track thermochronology. These data collectively indicate that the rocks within the southern portions of the study area experienced more denudation as a result of uplift and erosion than the rocks in the northern portions, which were heated and then subsequently cooled. Apatite fission-track thermochronology constrains the onset of cooling to be approximately 30 Ma, with ages decreasing westward. Both sonic-log methods and the apatite fission-track thermochronology indicate that the

rocks within the Raton Basin and surrounding area have undergone as much as two and a half kilometers of exhumation in the west and south, and as little as a half a kilometer of exhumation in the east and north.

Introduction

A number of lines of geologic and thermochronologic evidence indicate that rocks now at the surface along the High Plains – Southern Rocky Mountain boundary in northeastern New Mexico were at temperatures above ~ 110^0 C prior to about 30 Ma and that these rocks where exhumed during late Oligocene to Miocene time (Kelley and Chapin, 1995). These lines of evidence include previous apatite fission track (AFT) work, an unconformity between the late Miocene Ogallala Formation and Permian rocks in eastern New Mexico, and exposed Miocene to Oligocene plutons (e.g. the Spanish Peaks intrusions) that cooled beneath the surface, but now stand about 1 km above the surrounding plains (Close and Dutcher, 1990; Kelley and Chapin, 1995). Other work suggests that rocks now at approximately 80^0 C at depths of ~ 2.5 km in the Anadarko Basin, Oklahoma, were above approximately 110^0 C prior to around 40 Ma (Carter et al., 1998). The cause of mid-Tertiary cooling, starting at ~ 30 Ma in northeastern New Mexico and at ~ 40 Ma in Oklahoma, could be: 1) relaxation of isotherms following a heating event, with affects extending hundreds of kilometers east of the Rio Grande rift; 2) regional epeirogenic surface uplift, which triggered denudation of the High Plains; or 3) some combination of the latter two mechanisms. An understanding of the affects of heating versus denudation on the southern High Plains is important to evaluating the regional tectonic history of the western United States. Furthermore, constraining the timing, magnitude, and aerial extent of heating and denudation is useful in evaluating the petroleum potential of the southern High Plains.

In this study, I examined portions of southeastern Colorado and northeastern New Mexico between the Sangre de Cristo Mountains along the Southern Rocky Mountain front on the west and the eastern state lines of Colorado and New Mexico on the southern High Plains on the east. The area was chosen because 1) AFT data were already available on either end of this broad transect (Kelley and Chapin, 1995; Carter et al., 1998) and 2) it straddles the boundary between these two fundamentally different physiographic provinces.

The purpose of this investigation was to use sonic well log velocities as well as AFT thermochronology to evaluate the denudational and thermal history of the transition between the Southern Rocky Mountains and the High Plains. The sonic velocities have been used as a measure of porosity reduction due to burial (cf. Magara, 1976). Subsequently, data on maximum burial depths were applied to gauge the amount of material eroded from the area. The thermal history was evaluated with AFT thermochronology. The results of these different techniques are integrated to estimate how much of the post mid-Tertiary cooling observed in the area might be due to denudation (constrained by sonic logs) versus relaxation of isotherms following a regional thermal event (constrained by AFT data). My results are compared to vitrinite reflectance data from a previous study (Scott and Kaiser, 1991), which serves as an independent thermal indicator to constrain maximum paleotemperatures.

Geologic Setting

Southeastern Colorado and northeastern New Mexico have been affected by at least three significant tectonic events during Phanerozoic time: Pennsylvanian to early Permian Ancestral Rocky Mountain tectonism, late Cretaceous to middle Eocene Laramide Orogeny, and the latest Eocene to Recent Rio Grande rift extension and associated volcanism. The most prominent structural feature of the study area is the Raton Basin, which was a large depocenter during both Ancestral Rocky Mountain and Laramide deformation. The Raton Basin, encompassing the Las Vegas sub-basin to the south and Huerfano Park to the north, is a Laramide foreland basin straddling the southern Rocky Mountains – High Plains boundary. The basin is asymmetric, with steeply dipping beds on the western limb near the Sangre de Cristo Mountains (Figure 1) and gently dipping beds on the eastern flank (Cline, 1953; Baltz, 1965; Woodward, 1984; Woodward, 1987a). The basin trends north-south in New Mexico, but curves northwestward in Colorado. At its widest points, the basin is about 280 km long and about 105 km wide (Woodward, 1987a). The surrounding area contains a number of structural features that were active during Pennsylvanian-Permian Ancestral Rocky Mountain and Late Cretaceous-early Tertiary Laramide deformation, including the Sierra Grande arch, the Apishapa arch, and the Las Animas arch (Figure 2). In addition, Laramide age thrust faults are found on the east side of the Sangre de Cristo Mountains (SDCM). Superimposed on these older features are 25 Ma intrusive centers at Spanish Peaks and Mt. Maestas in Colorado (Penn et al., 1992), 37-20 Ma sill complexes

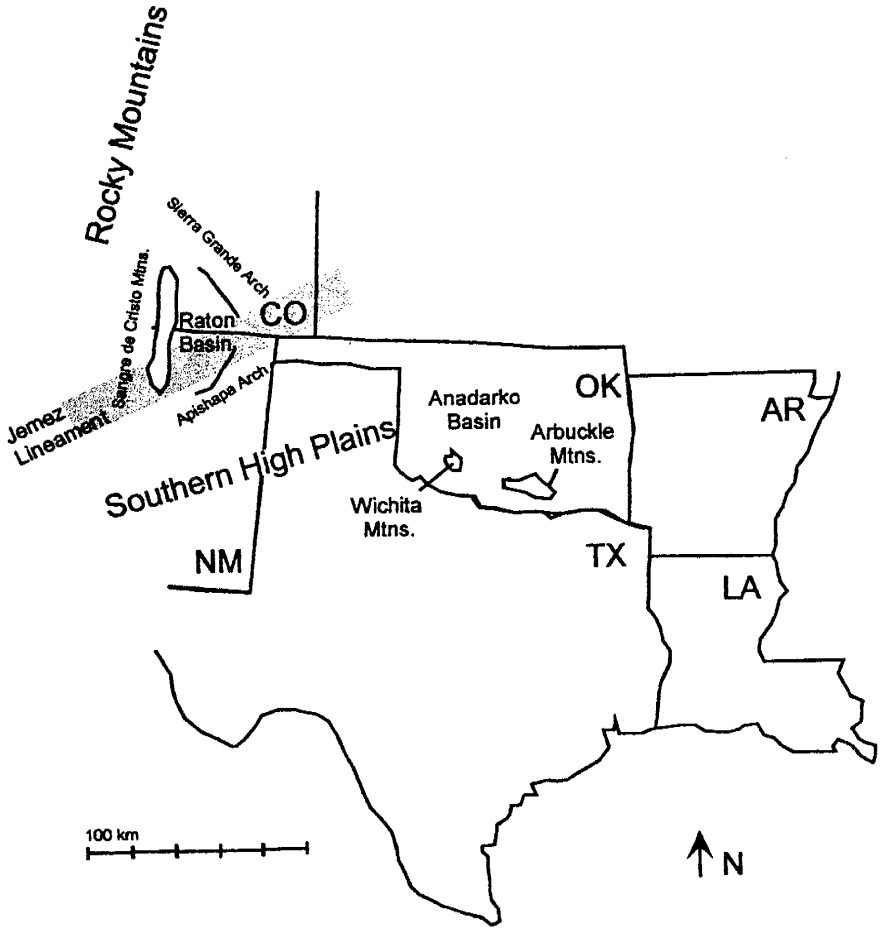

Figure 1. Regional map showing the relationship of the Raton Basin to the southern High Plains and the southern Rocky Mountains. Modified from Viele and Thomas (1989).

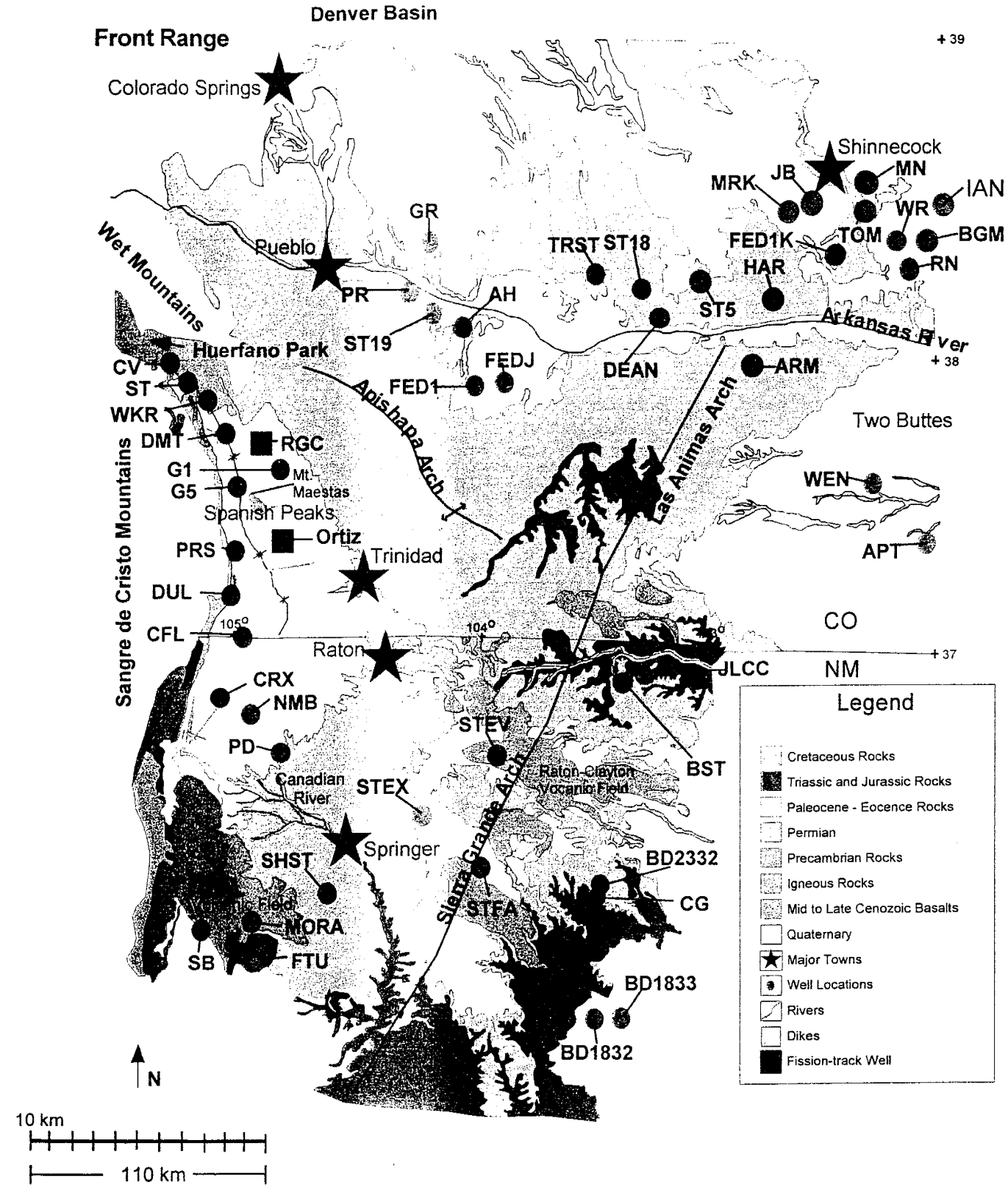

Figure 2. Simplified geologic map of the Raton Basin and surrounding areas. Well locations, major towns, as well as structural features are displayed. Modified from Dane and Bachman (1965) and Tweto (1979). An explanation of abbreviations is given on the following page.

Figure 2. Key to well abbreviations.

AH = Arnold Harriman 1
APT = A.P. Tanner Unit 1
ARM = Armstrong
BD1832 = BDCDGU 1832 #251G
BD1833 = BDCDGU 1833 #051F
BD2332 = BDCDGU 2332 #241
BGM = Baughman
BST = Union "B" State
CFL = CF & L 1
CG = Caroline Gonzales 1
CRX = Castle Rock 1G-90-2
CV = Cuerno Verde
DEAN = Dean 1-22
DMT = Dike Mountain 1-10
DUL = Duling 1A
DOG = Dog Spring
FED1 = Federal #1 (Otero Co.)
FED1K = Federal #1 (Kiowa Co.)
FEDJ = Federal Jordan
FTU = Ft. Union 1
G1 = Goemmer Land Co. 1
G5 = Goëmmer 5
GR =11-31 Green
HAR = Hardy
IAN = Iannitti
JB = John Brown
JLCC = Jolla Land and Cattle Co.
MED = Medina 21
MORA = Mora
MRK = Merrick
MN = Meek-Newsom
NMB = New Mexico B 3
PD = Phelps Dodge 1
PR = Porter 1-28
PRS = Parsons
RN = Reinert
SB = Salman Ranch 1-B
SHST = Shell State 1
ST = Sam Taylor 2
ST5 = State 1-5
ST18 = State 1-18
ST19 = State 1-19
STEV = State EV 1
STEX = State EX 1
STFA = State FA 1
TOM = Thomas
TRST = True State
WEN = W.E. Niles
WKR = Walker Ranch 1
WR = William Rose

in the Raton-Springer area in New Mexico (Scott et al., 1990), and the ~ 37 Ma igneous rocks at Two Buttes (Davis et al., 1996). The youngest igneous features are Miocene to Pleistocene volcanic rocks located along the Jemez Lineament (~ 56 Ka – 9.0 Ma Ocate and Raton-Clayton volcanic fields) (Figure 2). The tectonic elements that structurally characterize the study area and define the Raton Basin proper are discussed further in the following paragraphs.

Sangre de Cristo Mountains (SDCM)

The SDCM are one of the largest positive features of the Rocky Mountain foreland. They trend northward for a length of about 320 km, exposing Proterozoic crystalline and Pennsylvanian and Permian sedimentary rocks. The SDCM are a fault-controlled mountain range, bound by Cenozoic normal faults on the west and Laramide-aged reverse faults toward the east (Baltz, 1965; Woodward and Snyder, 1976). A seismic line from the crest of the SDCM on the west to Walsenburg in the northern tip of the Raton Basin shows that the western flank of the Raton Basin near the SDCM is structurally complex with 16 to 24 km of horizontal overstep, three major thrust sheets, and at least part of a major fold (Applegate and Rose, 1985).

Arches

Less dramatic than the SDCM, the Sierra Grande arch is a low, broad feature of Late Pennsylvanian or Permian age (Miller et al., 1963) that creates

the eastern boundary of the Raton Basin. Mesozoic sedimentary and Cenozoic volcanic strata cap this gently dipping structural high (Woodward, 1987a).

The Apishapa arch is an extension of the Wet Mountains that stretches for about 150 km in Colorado (Woodward, 1987b). It is a slightly faulted, saddle-like feature that merges gently into the Denver Basin to the north and into the northern part of the Sierra Grande arch (Baltz, 1965; Woodward, 1987a). The arch was first elevated during the late Paleozoic, but the present configuration is largely due to Laramide reactivation (Mallory, 1977; Woodward, 1987b). The Las Animas arch is another structural feature in the study area that has an Ancestral Rocky Mountain and Laramide history (Rascoe, 1978; Clair and Volk, 1968).

Rio Grande Rift, Jemez Lineament, and Related Features

Other structural influences on the study area include the Rio Grande rift and Jemez Lineament. The Rio Grande rift is a north-trending break in the lithosphere separating the Colorado Plateau on the west from the High Plains on the east. The rift stretches north-south approximately 550 km from central Colorado through New Mexico and into Mexico. Clarkson and Reiter (1984) surmise that the magmatic source of volcanic rocks of the rift is deep and that modern heat flow has been affected by the rift as far east as the Raton Basin and Great Plains along the Jemez lineament.

The Jemez lineament (Figure 1) defines one of two significant volcanic trends that cross the area. It is a northeast-trending zone of <10 Ma volcanism extending from east-central Arizona to southeastern Colorado. The mafic to

intermediate composition flows associated with volcanic centers along the Jemez lineament are aerially extensive. The late Cenozoic Ocate and Raton-Clayton volcanic fields (Figure 2) form the northeastern segment of the lineament. The Ocate field straddles the margin of the Sangre de Cristo Mountains and the High Plains just south of the Cimarron Mountains. The sequence of rock types erupted in the Ocate field are, from oldest to youngest, alkaline basalt, trachyandesite, basalt, and trachybasalt. The Ocate field has been described in terms of three broad stages of volcanism. The ages of the volcanic flows that cap the highest mesas range from 8.3 to 5.3 Ma in age. Volcanic rocks on the intermediate level surface are 4.7 to 3.8 Ma in age. The lowest surfaces are covered by 3.8 to 0.8 Ma lavas (O'Neill and Mehnert, 1988). The latter authors suggest that, prior to ~ 5.5 Ma, a period of tectonic stability allowed a late Miocene surface to develop on the Sangre de Cristo Mountains and the High Plains. That surface was dissected starting after 5.5 Ma, with erosion continuing today.

The Raton-Clayton field, on the High Plains along the New Mexico-Colorado state line, is the second volcanic field associated with the Jemez lineament. Here, the sequence of volcanic rocks erupted is generally similar to that found at the Ocate Field: dacite, alkaline basalt, trachyandesite, basalt, and nephelinite basanite, from oldest to youngest. Volcanic flows on the highest mesas in the Raton-Clayton field are 9.0 to 3.6 Ma in age, the intermediate elevation mesas are topped by 3.0 to 2.2 Ma flows, and the lowest areas are covered by 1.7 Ma to 56 Ka volcanics (Stroud and McIntosh, 1996). Stroud

(1997) notes that accelerated dissection of the Raton-Clayton area did not begin until after 3.6 Ma, later than the timing suggested for the Ocate field.

The second volcanic trend that crosses the study area is the Rocky Mountain alkalic province, which includes late Eocene – Oligocene Cenozoic volcanic centers trending roughly north-south along the Great Plains margin from Canada to Mexico (Allen and McLemore, 1991). The magmatic volume associated with these centers is generally quite small (Davis et al., 1996).

Middle Tertiary sill complexes that are part of the Rocky Mountain alkalic province occur at several localities in northeastern New Mexico. The Chico sill complex in the Raton-Springer area consists of ~ 300 m in total thickness of phonolitic to trachytic intrusives that range in age from 37 to 20 Ma (Scott et al., 1990). Major element geochemistry indicates that these alkalic rocks were likely derived from melting of the lower crust (Scott et al., 1990). Syenite to rhyodacite sills that may be related to the Latir volcanic field are found in the Cimarron area. Finally, the Turkey Mountain dome near Wagon Mound is likely underlain by an intrusion (Hayes, 1957).

Alkalic mafic intrusions at Two Buttes in southeastern Colorado yield K-Ar ages on phlogopite that average ~37 Ma (Davis et al., 1996). Gibson et al. (1993) determined phlogopite K-Ar dates of 27 to 35 Ma on the same intrusions. An apatite fission-track age of 25.7 ± 5 Ma was determined by Pilione et al. (1977). Davis et al. (1996) used isotopic and trace element data to suggest that these alkalic rocks were derived from the lithospheric mantle. These authors

attribute this volcanism to the interaction between a Cenozoic subducted slab and the western edge of the cold cratonic mantle that underlies the High Plains.

Two other features associated with the Rocky Mountain alkalic province are the Spanish Peaks (Figure 2) and adjacent Mt. Maestas. Recently high-precision $^{40}Ar/^{39}Ar$ radiometric dating has provided a detailed chronology for the igneous rocks, indicating that most of the plutons in this area were emplaced between 27 and 21 million years ago (Penn and Lindsey, 1996; Miggins et al., 1999). Both mountains are comprised of monzonite, granodiorite porphyry, granite porphyry, and syenite porphyry (Close and Dutcher, 1990; Penn and Lindsey, 1996). The current landscape was formed by erosion of the softer sediments that the magma was intruded into; the erosion has left the igneous rocks prominently exposed. Eocene strata found on the upper portions of the Spanish Peaks have been used to confirm that erosion removed at least 1 km of sediment from this area since ~25 Ma (Close and Dutcher, 1990; Kelley and Chapin, 1995).

Stratigraphy

Five stratigraphic units found within the study area were used for the sonic log portion of this project. These units, which range from early to late Cretaceous in age, were selected for three reasons: 1) they postdate Ancestral Rocky Mountain tectonism and were thus only affected by the Laramide Orogeny and younger events; 2) the sonic transit time signatures of these units are distinct; and 3) the units are present over large portions of the study area. Only these five

units are described in this report. Readers are referred to Baltz (1965) for an excellent detailed description of the complete stratigraphy of the basin (Figure 3).

The Lower Cretaceous Dakota Sandstone is a gray to buff-colored beach deposit composed of fine-grained sandstones and interbedded gray shales that formed during a transgression. This unit is commonly only 10 to 20 m thick, but thickens both north and west and can reach as much as 45 m thick in the subsurface of Colorado (Baltz, 1965; Speer, 1976). On average, the thickness of the Dakota Sandstone within wells of the study area is 20 m.

The dark gray shales of the Upper Cretaceous Graneros Shale sit on top of the Dakota Sandstone and are locally interspersed with minor beds of limestone and sandstone. The Graneros Shale varies from 35 to 116 m thick in the Raton Basin, but is commonly 66 to 76 m thick in the Las Vegas sub-basin (Baltz, 1965; Woodward, 1987a). Within the wells of the study area, the average thickness of the Graneros Shale is 51 m.

The Upper Cretaceous Greenhorn Formation sits conformably on the Graneros Shale. It ranges from 6 to 27 m thick (Woodward, 1987a). It includes thin limestone beds and calcareous, chalky shales, with minor sandstone beds. In the area of interest, the Greenhorn Formation is characterized by limestone at the top of the unit and shale at the bottom.

The marine Niobrara Formation, also Upper Cretaceous in age, averages 170 m thick but can reach thicknesses in excess of 192 m. The Niobrara Formation is absent in the Las Vegas sub-basin due to Neogene erosion (Baltz, 1965; Jacob, 1983); where present, it is an assemblage of limestone

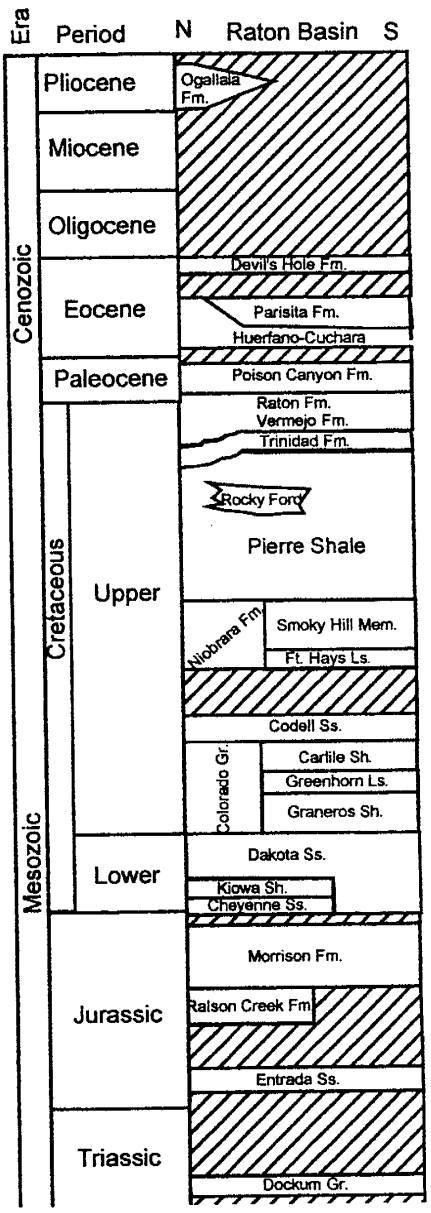

Figure 3. Stratigraphic column for the Raton Basin and surrounding regions in New Mexico and Colorado. Diagonal lines represent unconformities.

interbedded with shale and sandy shale. The Niobrara Formation is composed of two members, the basal Ft. Hays Limestone and the overlying Smoky Hill member.

The Pierre Shale, which is the youngest unit examined, lies atop the Niobrara Formation. This thick unit, 480 m to 1760 m, consists of dark gray, sandy, non-calcareous marine shale. It contains local thin beds of limestone and sandstone, especially near the top of the unit (Jacobs, 1983; Woodward, 1987a). Weimer (1980) comments that the presence of sand and thickness variations in the Pierre Shale record the onset of Laramide deformation.

Sonic Log Velocities: Principles and Methods

Introduction

Since 1930, graphs of porosity versus depth have been used to decipher depth-controlled changes in porosity (Heasler and Kharitonova, 1996). Holding special use for petroleum companies, these graphs can provide a clearer understanding of porosity loss due to burial and allow for the prediction of porosity at depths of interest. For the purpose of this study, depth versus porosity curves are used as a measure of compaction. As a rock unit undergoes burial it also undergoes porosity reduction. Once a unit is compacted, it cannot return to its original state, even after the removal of overburden by erosion. A unit that resides at a shallower depth than required to explain a high amount of compaction is considered "overcompacted" with respect to its current position in the lithologic column. An "undercompacted" unit is one that shows less

compaction than expected for its stratigraphic position (for example, due to elevated fluid pressure; Figure 4). Over- and undercompaction is determined by comparison to a "control" well, or a well that displays the normal compaction trend and has the least amount of alteration for a specific package of rock. The porosity-depth relationship in each well in a region is compared to the control well to determine the current status of compaction. Comparison of all wells and rock units to this "normal" well enables one to quantify geologic processes, such as amount of exhumation and porosity loss as a function of depth. The determination of relative amounts of exhumation is the focus of this study.

Sonic Transit Times

Sonic logs are measured in interval transit time (Δt, tt) as microseconds per foot ($\mu s/ft$). For the purposes of this study, where the sonic log data are discussed, they are referred to in the standard English units of feet; however, the metric conversion is also supplied. The transit time is the length of time it takes an emitted sound wave to travel through the rock unit to a receiver. The transit time is the reciprocal of velocity; thus rocks with a faster transit time have slow sonic velocity (Heasler and Kharitonova, 1996; Hillis, 1995). Many factors affect the sonic transit time, including porosity, lithology, temperature, borehole geometry, and fluid pressure and content (Heasler and Kharitonova, 1996.) A variety of factors influence transit time, but it is most strongly correlated with porosity. This enables one to link compaction to transit times since porosity decreases with increasing compaction.

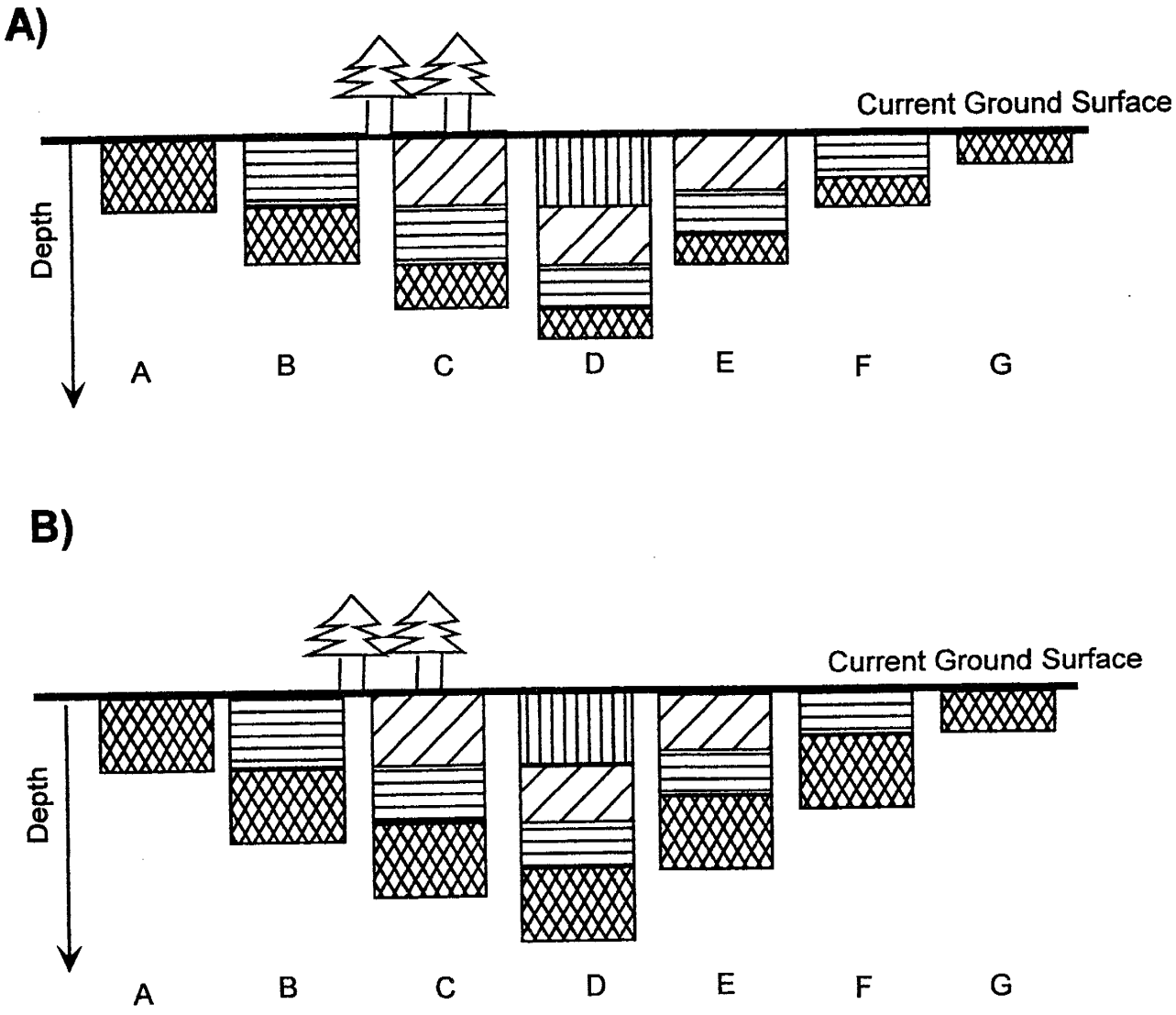

Figure 4. Cartoon showing example of A) overcompaction and B) undercompaction.

A) Column A represents a specific unit that undergoes burial in columns B and C. Maximum burial occurs by column D. Columns E and F represent subsequent erosion. Compare the thickness of the crosshatched unit from column A to column G. The crosshatched unit in column G is overcompacted with respect to its current depth.

B) Column A represents a specific unit that undergoes burial in columns B and C. Maximum burial occurs by column D. Columns E and F represent subsequent erosion. Compare the thickness of the crosshatched unit from column A to column G. The thickness remains constant through burial and erosion. The crosshatched unit remains undercompacted with respect to its current depth.

The assumptions associated with use of sonic transit times to determine compaction amounts are based primarily on the idea that the mechanical process of rock compaction is the governing force controlling the magnitude of porosity. Diagenesis, other chemical reactions, and rock heterogeneities are assumed to be less critical in comparison.

Single Unit Sonic Transit Time Analysis

Maximum burial depths can be estimated from stratigraphic units that exhibit vertically and laterally consistent relationships between depth and compaction (Hillis, 1995). The best units to use are those that show little bulk facies change and that are widely distributed through the area.

Sonic log studies can be used to estimate the magnitude of exhumation when the unit of interest within a given well is compared to the same unit within a control well. The average transit time for each unit in a given well was calculated from the sonic log picks and plotted against depth to the midpoint of the unit. In an area of suspected denudation, the wells that exhibit the highest Δt (lowest velocity) for a given depth were used to define a normal compaction curve. The velocity (inverse Δt) is correlated with depth as follows:

$$1/v = a + b \exp(-d/c)$$

where a, b, and c are constants, v is velocity and d represents depth (Hillis, 1995). For the intervals of depth considered in this study (surface to about 1524 m), this equation produces a linear relationship. Thus, any two wells that define a straight line with no points falling to the right of that line establish the normal

compaction trend for that unit (Figure 5). In cases where several different linear trends were identified, the line that provided the most geologically realistic trend – usually the most abrupt decrease in Δt with depth – was used. Apparent exhumation, the vertical displacement of each well, was determined with respect to the defined normal compaction trend. This value can be estimated directly from a transit time versus depth plot (Figure 5), but for accuracy it was determined numerically using the following equation:

$$E_a = 1/m(\Delta t_u - \Delta t_0) - d_u$$

where E_a is the apparent exhumation, m is the gradient of the compaction trend line, Δt_0 is the interval transit time at the surface determined from the normal compaction trend, Δt_u is the average transit time of the unit of interest, and d_u is the depth to the midpoint of the unit for an individual well (Hillis, 1995).

Multiple Unit Sonic Transit Times Analysis

As mentioned previously, several models exist that relate porosity changes to burial depth. Equations that describe porosity trends have been proposed to be linear (Selley, 1978; Magara, 1980; Hillis, 1995), parabolic (Liu and Roaldset, 1994), and exponential (Athy, 1930; Heasler and Kharitonova, 1996). The exponential equation best describes the data; plots of transit time versus depth graphically illustrate an exponential decay in travel time with depth (Figure 6). The exponential form for the sonic logs is given by:

$$(1) \quad tt = tt_0 \exp(-bx)$$

Greenhorn Limestone Normal Compaction Trend

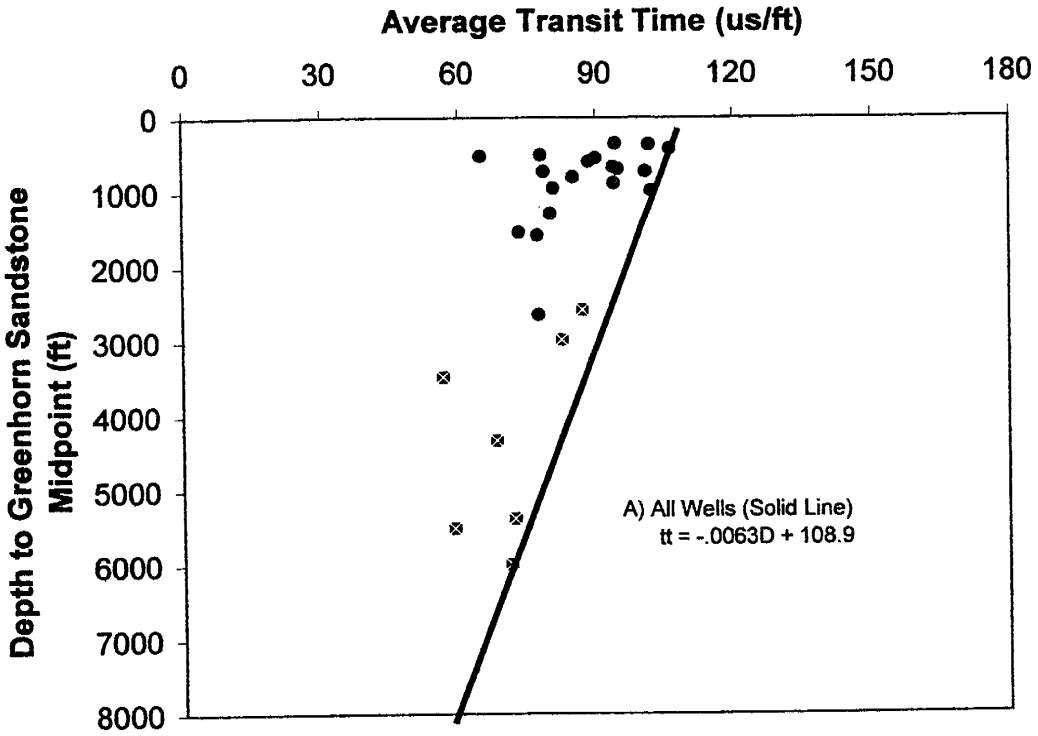

Figure 5. Plot showing the compaction trend for the Greenhorn Limestone. The average transit time was plotted against the depth to midpoint for each well within the study area. Solid circles are High Plains wells. Crossed circles are Raton Basin wells. The points farthest to the right, that form a line define the least compaction trend. In this case, there was only one possible normal compaction trend, solid line.

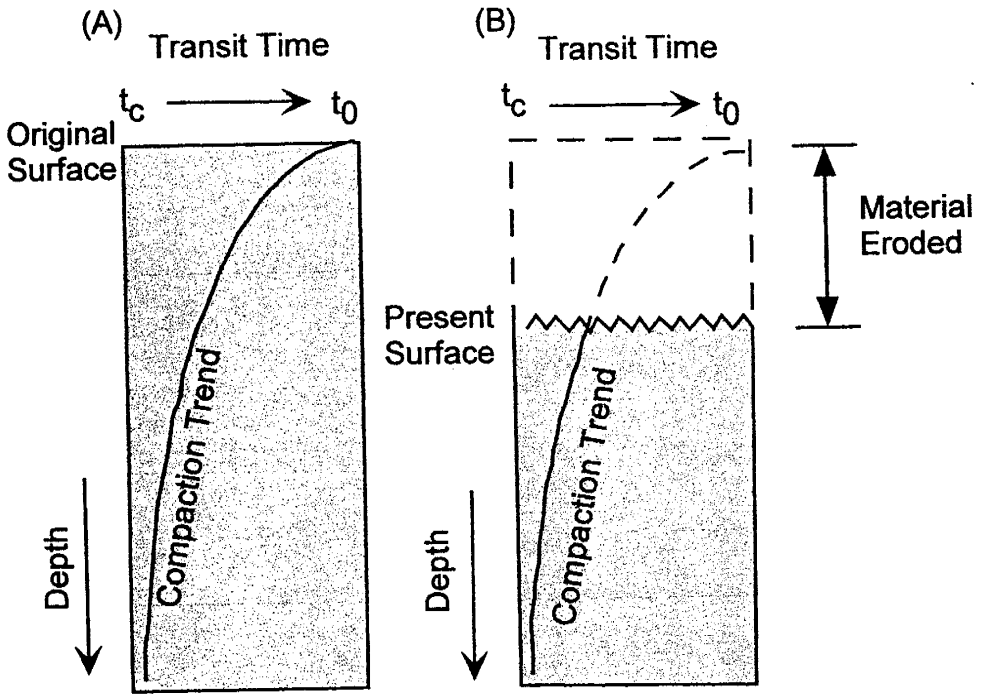

Figure 6. Cartoon illustrating the multiple unit sonic log method. The symbol t_c is the shift constant, usually 40 to 65 μs/ft. Modified from Magara (1976) and Heasler and Kharitonova (1996).

A) An example of a well in an area that has not undergone erosion. The vertical axis is depth and the horizontal axis is sonic transit time. The compaction curve is determined by fitting an exponential curve to the digitized sonic log. In the case of no erosion, the compaction trend approaches higher transit time values (t_0) where t_0 represents the original surface transit time (taken as the transit time of free-flowing water, 180 μs/ft).

B) An example of a well in an area that has experienced erosion. The compaction curve does not reach the higher values of transit time (t_0). This implies that erosion removed sediment subsequent to deposition. The vertical distance from the extrapolation of the curve back to t_0 to the present-day surface is the estimate of the amount of sediment eroded.

where tt is the sonic transit time , tt_0 is the transit time at the surface (x = 0), b represents the exponential decay constant, and x is depth. A plot of this curve, however, tends to deviate from the actual data at depths greater than 5000 to 8000 ft (1500 m to 2450 m). One of the most significant reasons for this divergence is that equation 1 inaccurately predicts that a totally compacted rock has a sonic velocity of zero. Intuitively, a solid rock has measurable sonic velocity. Indeed, observations of depth versus transit time demonstrate that the transit time stabilizes at 30 to 40 μs/ft, not zero, at depths of 5000 to 8000 ft (1500 to 2450 m). Consequently, a more realistic relationship between transit time and depth is given by:

$$(2)\quad tt = tt_0 \exp(-bx) + c$$

where tt is the predicted transit time, tt_0 is the surface transit time (x = 0), x is depth, b is the decay constant, and c is a logarithmic correction, or shift constant, that is determined independently for each well and approximates the rock matrix transit time (Heasler and Kharitonova, 1996).

The correction term (shift constant) was determined by 1) fitting a standard least-squares regression to a modified form of Equation 2, and 2) adjusting the equation to a linear form as follows:

$$tt - c = tt_0 \exp(-bx).$$

Taking the natural logarithm of both sides yields:

$$(3)\quad \ln(tt - c) = \ln(tt_0) - bx.$$

This is a linear form (y = mx + b) of equation (2) which allows for easy statistical analysis. The least-squares regression minimizes the sum of the squares of

deviation of the data points from the regression line (Moore and McCabe, 1993). Equation 3 was used with shift constant values (c) ranging from 40 to 100 and errors were evaluated using the Root Mean Square (RMS) and Average Absolute Value (AAV). The equations and explanations for both RMS and AAV are detailed in Appendix A. The lowest values of RMS and AAV determined with a particular shift constant correspond to the best fit. In general, the RMS analysis tends to be less accurate than AAV, since the RMS uses the square of the error. Thus, in cases where the RMS values calculated using different shift constants are very similar, the one with the smallest AAV is taken to be more reliable.

Once the appropriate shift constant was established for each of the wells, the amount of exhumation was estimated. The basis for this technique is shown in Figure 6. The principal assumption is that t_0, the surface transit time, is approximated by 180 μs/ft, the transit time of unconfined water, appropriate for marine sediments. The extrapolation of the corrected compaction curve back to the initial transit time (180 μs/ft) allows the vertical difference between the current surface and the original depositional surface to be measured and the amount of erosion to be estimated (Figure 7). The multiple unit method also enabled me to include more wells, such as wells that had Mesozoic (e.g., Jurassic Morrison Formation, Jurassic Entrada Sandstone, Triassic Santa Rosa Formation) but not Cretaceous sediments.

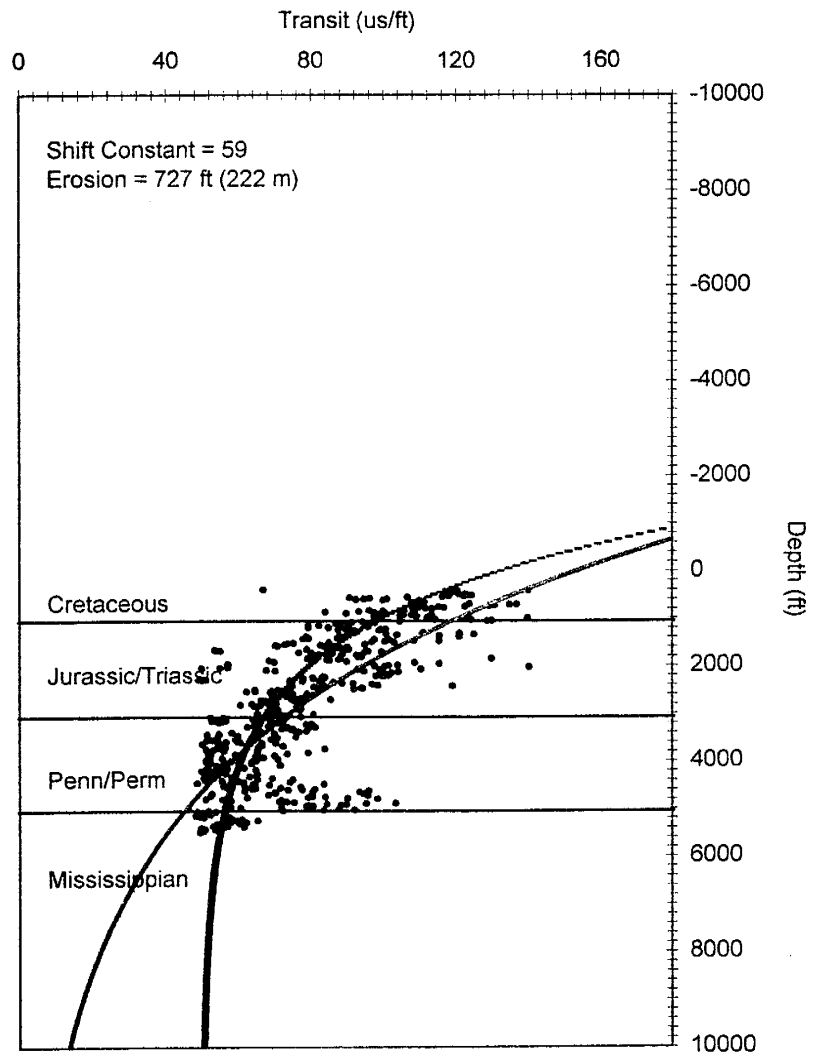

Figure 7. Example of multiple unit method as used in this study. The scatter plot of data is from the Reinert well in southeastern Colorado, which was digitized in five-foot intervals. The compaction trend is the best fit exponential curve (black; shift constant of 59) as determined from Equation 3. Based on an extrapolation of the curve back to 180 μs/ft (representing the original surface), 727 ft or 222 m of sediment has been eroded. The uncorrected curve (red; shift constant of 0) estimates only 220 ft or 67 m of erosion.

Fission-track Analysis: Principles and Methods

Introduction

The natural, spontaneous fissioning of U^{238} causes physical, submicroscopic damage to the crystal lattice. The zone of damage, referred to as a fission track (FT), remains until the atomic structure of the crystal lattice returns to its former state, which requires diffusive mass transfer at elevated temperatures. The healing process causes the fission tracks to shorten and thin and eventually disappear. This property of shortening and erasure of tracks is known as *annealing.*

Because the process of annealing is temperature dependent, apatite fission-track ages and length decrease as a function of depth (Naeser, 1979; Carlson, 1990). For temperatures cooler than approximately 60^0 C, any tracks generated will be almost completely preserved; annealing is negligible. The ages obtained from detrital grains in sandstone from these shallow depths correspond to or are older than the stratigraphic age of the rock unit provided there has not been heating subsequent to deposition. Generally, the track lengths are between 13 to 15 μm. The temperature zone between 60 to 70^0 C and 110 to 140^0 C, depending on the chemical composition of the apatite (tracks in fluorapatites anneal faster than those in chlorapatites), is known as the partial annealing zone (PAZ; Naeser, 1979). In this zone, the tracks are partially annealed, so that the mean track lengths are 8 to 13 μm. Temperatures greater than approximately 110^0 C will cause any fission tracks that form in a fluorapatite to be completely healed and the age of the sample will be zero. The X^2-test is applied to samples

to statistically determine whether multiple age populations are present within a sample (Galbraith, 1981).

If a terrane experiences a tectonic event resulting in rapid denudation and cooling, the PAZ can be preserved in the fission-track record. Ages below the base of a fossil PAZ record the approximate timing of onset of the cooling event. The break-in-slope on an age-depth curve can be used to estimate the paleodepth to the bottom of the PAZ, assuming a reasonable range of paleo-geothermal gradients. AFT analysis can therefore be an effective approach for estimating exhumation values.

Apatite fission-track ages and track-length distributions can be modeled to further quantify the time-temperature history of a given sample. Samples with significant numbers of confined tracks (approximately 50) were modeled using AFTSolve© (Ketchum et al., 1999, 2000) to fit thermal history curves to the observed ages and track lengths. The AFTSolve© program combines track-length data, sample ages, and time constraints from independent geological information to generate a series of possible paths that describe the time/temperature history for that sample. The program will generate any number of requested paths, and outputs include a best-fit line, a 'good' fit area and an 'acceptable' fit area, when applicable. These thermal history results provide an independent set of denudation estimates for the Raton Basin and vicinity and provide information on the timing of cooling.

Procedures

Sonic Log Velocity Analysis

A total of 42 wells were selected for use in the sonic log portion of this study. Wells were chosen based on 1) availability of sonic log velocity data that spanned at least 3000 ft (915 m) of drill core and contained data in the upper 900 ft (275 m) of the core; and 2) the location and spacing of the wells within the study area. Some of these wells are located in the Raton basin, but many of the wells are from a transect along the Arkansas River in southeastern Colorado, along the southern margin of the Denver basin, and some of the wells in northeastern New Mexico lie on and to the east of the Sierra Grande arch. Each sonic log was digitized at 5 ft intervals using Neuralog software. This interval was chosen because the vertical resolution of the sonic log tool is 2 ft. Therefore 5 ft intervals characterized the log fairly well. Certain gamma logs were selected for correlation purposes and were digitized by hand using Sigma Scan software.

Several sonic logs in the study area met the criteria outlined above but could not be used in this analysis for various reasons. Table 1 provides a list of logs that were considered, but ultimately eliminated from the study.

Single Unit Method

The evaluation of lateral compaction trends in a single lithologic unit that is present throughout an area forms the basis of the single unit method. As mentioned previously, five units were chosen for this portion of the study: all five have characteristic sonic log signatures throughout the studied area (Figure 8).

Well Name	Location	Reason for Elimination
Parsons 1	T. 32S, R. 68 W., sec 18	Well in frontal fault zone of SDCM
Dike Mtn.1-10	T. 28S, R. 69W, sec.10	Well penetrates multiple dikes
Dean #1-22	T. 22S., R. 52 W., Sec 22	Well did not contain Cretaceous
Armstrong	T. 24S, R. 48 W., Sec 5	Well did not contain Cretaceous
Duling 1-A	T. 33S, R 69W, Sec 26	Well contained faults and overthickened units
A.P. Tanner	T. 31S, R. 42W., Sec 14	Well did not contain Cretaceous
Salman B	T. 21N, R. 17E, Sec 21	Well contained a fault; sonic log incomplete
W.E. Niles	T. 29S, R. 44W, Sec 2	Well did not contain Cretaceous
State 1-5	T. 21S, R. 50W, Sec 5	Well did not contain Cretaceous

Table 1. The name, location, and explanation for several wells that contained sonic log data, but for the reasons listed were not practical for use in this study.

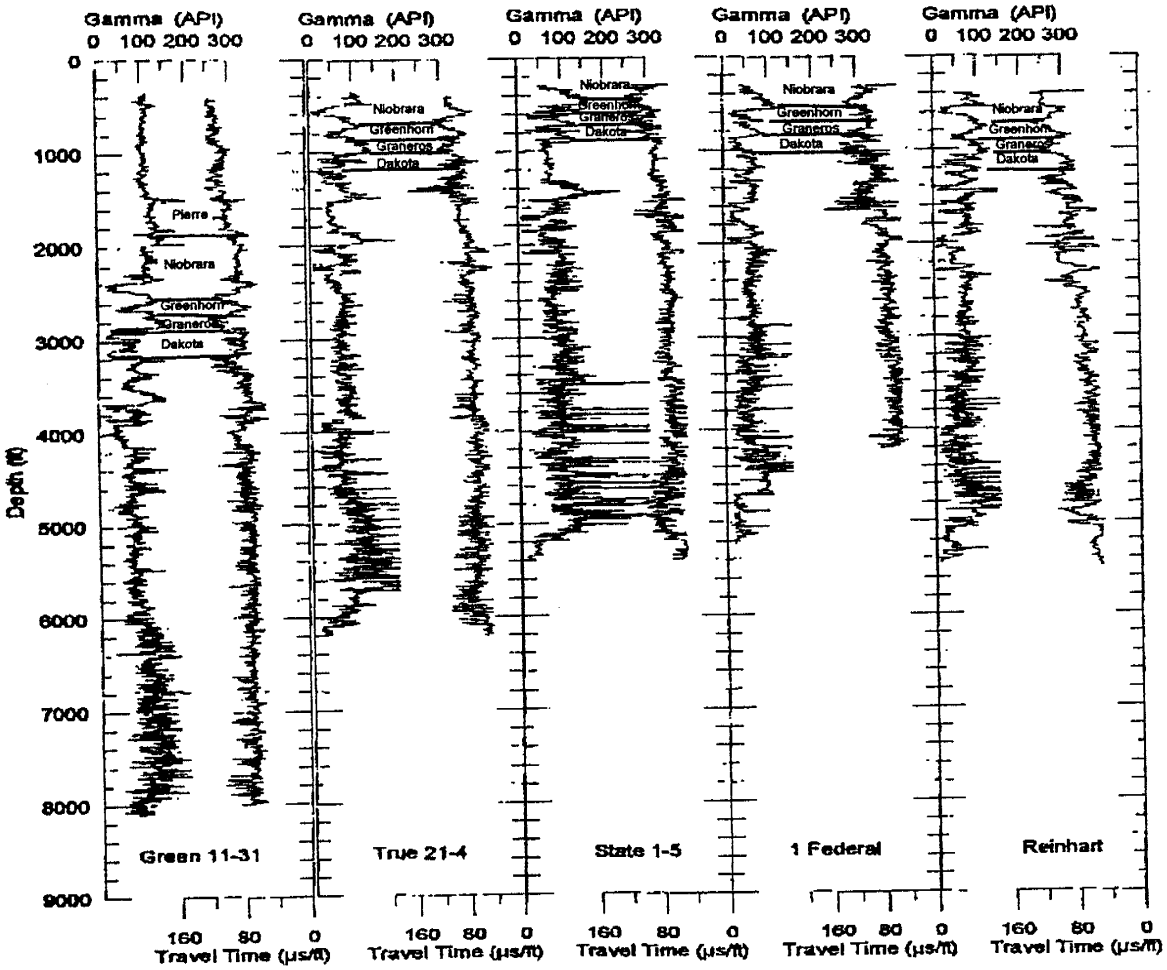

Figure 8. Gamma log (to the left) and sonic log (to the right) for five representative wells within the study area. The stratigraphic units used in the single unit method are also indicated. These wells follow the Arkansas River in Colorado (Figure 2).

All five are Cretaceous in age and were therefore affected only by Laramide age burial and post-Laramide exhumation events. Of the units studied, two distinct sonic log "types" can be identified. The first group comprises limestone, shale, and chalk, while the second type is primarily sandstone. The transit time signatures of the different lithologic components of the Greenhorn Formation allowed it to be easily subdivided into two sections: the Greenhorn limestone and the Greenhorn shale. The single unit analysis was performed independently on the shale and limestone in this unit in order to compare the results from these two lithologies. Because denudation values are estimated by comparison to normal compaction trends, one primary assumption is that porosity loss is due to compaction and not to diagenesis or hydrothermal alteration. Despite the possible errors, a sandstone unit was also studied to evaluate the sensitivity of the technique to lithology.

The tops and bases of each of the selected units were picked directly off the sonic and gamma logs, cross referenced with any other available log suites and scout tickets, and verified with published structure contour maps (Haun, 1968; Weimer, 1980; Woodward, 1984).

Sonic Log Velocity Multiple Unit Method

Each digitized sonic log was run through a Minitab statistical program that computed regression values for the variables in equation 3 to determine a shift constant (c) as described in the Principles section. Ideally, the corrected curve should be fit to the synorogenic Paleocene to Eocene units only (Heasler and Kharitonova, 1996). However, the limited spatial and vertical distribution of these

units in the area precluded this analysis. Instead, the curves were fit to units younger than the middle Permian, since these units should have been affected by only one significant burial event, that associated with Cretaceous deposition and potentially tectonic burial or deposition related to Laramide deformation. This strategy ignores the unconformities that developed in the Cretaceous section during sea level changes and minor Mesozoic tectonic disturbances that preceded the main episodes of Laramide deformation (Weimer, 1980). This analysis also ignores the influence of Ogallala deposition (<100 m thick across the study area; Hawley, 1984, during the Pliocene (5 –12 Ma).

Another factor to consider in multiple unit analysis is the fact that the analyzed section is a mixture of shale, limestone, and sandstone. Usually compaction trends are determined for a single lithology (e.g. Magara, 1976). In most cases in the study area, the units are too thin or too geographically restricted for effective individual analysis. Heasler and Kharitonova (1996) evaluated erosion estimates determined from sandstone and from mixed lithologies in the Big Horn basin of Wyoming and found that these two data sets gave similar results. Consequently, all lithologies were used in this analysis.

If the shallow (<3000 ft or 915 m) portions of the well are not recorded on the sonic log, the result will be erroneous erosion estimates. It is the upper portion of log that defines the extrapolation of the curve to 180 μs/ft. If a fair amount of data is missing, the upper portion of the curve cannot be accurately extrapolated. Sonic logs that began at depths greater than 3000 ft (915 m) were therefore not used in this study.

Apatite Fission-track Thermochronology

Sixteen sandstone core samples were collected from four wells in the vicinity of the Raton Basin for AFT analysis. The sampling strategy for this portion of the study was based on obtaining the maximum depth spread among apatite-bearing strata. More samples were not available because of either a lack of apatite-bearing lithologies or a lack of drill core. Two samples were collected from the Mora Ranch 1 well, in Mora County, New Mexico, at depths of 2663 m and 2777 m (Table 2). Three samples were taken from the Lake Meredith Salinity Control Project Pilot Hole (hereafter referred to as the Logan well) near the town of Logan in Quay County, New Mexico. Sample depths were 22 m, 767 m and 905 m. The third well examined was the 1 RGC–CO well from Huerfano County, CO. Ten samples were collected between 225 m and 1158 m. The fourth well, the 14-12 1 Ortiz well in Las Animas County, CO, only had one core sample at 194 m. All of the wells, except for the Mora Ranch 1 well, contained enough apatite to be dated using the external detector method (Naeser, 1979). The methods used to obtain AFT dates and lengths follow Kelley et al. (1992). Confined tracks lengths were measured using a petrographic microscope fitted with a 100x dry objective and digitizing pad. Only horizontal, completely confined tracks were measured. Electron microprobe analysis was used on four samples to determine apatite composition (chlor- versus fluorapatite, Table 3).

Table 2. Apatite fission-track data from the Raton Basin and vicinity.

Sample Number	Rock Type	Latitude Longitude	Depth m (ft)	Number of Grains Dated	ρ_s $_5$ x 10_5 t/cm^2	ρ_I $_5$ x 10_5 t/cm^2	ρ_d x 10^5 t/cm^2	Central Age (Ma) (± 1 S.E.)	P(x)^2 %	Mean Track Length ± 1 S.E. (μm)	Standard Deviation Track Length
Log73	Triassic Santa Rosa SS	35°25' -103°45	22 (73)	20	2.1 (1550)	.56 (3904).	1.160	134.8 ± 4.6	94	12.00 ± 0.43	1.84
Log2515	Permian Yeso Form	35°25' -103°45	767 (2515)	20	.34 (176)	.11 (646)	1.188	123.7 ± 9.	91	14.08 ± 3.2	3.30
Log2970	Permian Abo Form	35°25' -103°45	905 (2970)	14	1.91 (81)	.37 (1459)	1.216	21.6 ± 2.	67	n.d.	
RGC738	Tertiary Raton Form	37°57 -104°83	225 (738)	14	1.9 (89)	.36 (1617)	1.198	26.6 ±3.	95	12.50 ± 3.7	2.69
RGC1089	Tertiary Raton Form	37°57 -104°83	332 (1089)	19	1.42 (71)	.32 (1741)	1.176	17.4 ± 2.	88	n.d.	
RGC1424	Tertiary Raton Form	37°57 -104°83	434 (1424)	18	1.26 (54)	.28 (1021)	1.153	26.4 ± 3.	96	n.d.	
RGC1816	Tertiary Raton Form	37°57 -104°83	554 (1816)	12	1.14 (35)	.17 (490)	1.130	36.5 ± 6.	94	n.d.	
RCG2187	Tertiary Raton Form	37°57 -104°83	667 (2187)	20	2.8 (136)	2.78 (1627)	1.108	41.5 ± 3.	94	n.d.	
RGC2729	Tertiary Raton Form	37°57 -104°83	832 (2729)	10	1.1 (50)	1.08 (940)	1.085	19.1 ± 2.	95	n.d.	
RGC3335	Cretaceous Vermejo Form	37°57 -104°83	1017 (3335)	19	1.7 (90)	.17 (1509)	1.062	19.9 ± 2.	96	11.65 ± .58	2.10
RGC3629	Igneous	37°57 -104°83	1106 (3629)	20	1.8 (60)	.18 (235)	1.040	77.6 ± 1.	68	12.19 ± 1.2	1.62
RGC3799	Igneous	37°57 -104°83	1158 (3799)	6	1.44 (48)	.14 (177)	1.017	14.1 ± 2.	46	12.00 ± 2.0	1.41
Mora8737	Igneous	36°10'N 104°57'W	2663 (8738)	1	–	–	–	–	–	–	–
Mora9112	Igneous	36°10'N 104°57'W	2777 (9112)	0	–	–	–	–	–	–	–
*Ortiz	Tertiary Raton Form		194 (636)	20	–	–	–	20.8	–	–	–

ρ_s – spontaneous track density ρ_I = induced track density ρ_d = track density in muscovite detector covering

The number in parenthesis is the number of tracks counted for ages and fluence calibration or the number of tracks measured for lengths.

S.E. – standard error $P(\chi)^2$ – Chi-squared probability n.d. – no data – = unable to determine

Table 3. Results of chemical analysis on certain AFT samples. The geoanalysis is based on 2 oxygens.

Sample Identification		P2O5	SiO2	SO2	Y2O3	La2O3	Ce2O3	Nd2O3	MgO	CaO	MnO	FeO	SrO	H2O	F	Cl	Total
Dur-Ap-1	#1	40.141	0.369	0.297	0.088	0.529	0.507	0.182	0	53.555	0	0.037	0.048	0.03	3.399	0.358	**99.54**
Dur-Ap-2	#2	41.229	0.368	0.26	0.098	0.443	0.579	0.134	0	53.497	0	0.043	0.042	0.034	3.435	0.376	**100.538**
Bee-Ap-1	#3	40.79	0.173	0.313	0	0.15	0.206	0.14	0.023	54.049	0.024	0.01	0.411	0	3.732	0.019	**100.04**
Bee-Ap-2	#4	41.064	0.184	0.363	0	0.147	0.393	0.092	0.003	54.155	0	0.016	0.488	0	3.789	0.002	**100.705**
RGC738 Grain 20	#15	40.071	0.411	0.169	0.156	0.048	0	0.002	0.043	52.746	0.082	0.093	0.004	0.132	3.295	0.074	**97.326**
RGC738 Grain 20-2	#16	40.723	0.284	0.059	0.29	0	0.005	0	0.023	54.044	0.106	0.048	0.018	0.171	3.291	0.038	**99.1**
RGC738 Grain 19	#17	41.68	0.041	0.02	0.035	0.003	0.014	0	0.003	54.628	0.088	0.044	0.056	0.389	2.839	0.113	**99.953**
RGC738 Grain 18	#18	41.475	0.06	0.013	0.043	0	0.076	0.025	0.011	54.174	0.104	0.038	0.045	0.406	2.793	0.092	**99.355**
RGC738 Grain 16	#19	41.588	0.026	0.081	0.021	0	0.015	0.02	0.013	54.215	0.101	0.019	0.085	0.537	2.365	0.392	**99.478**
RGC 738 Grain 13	#20	41.117	0.38	0.053	0.076	0.014	0.005	0.013	0.143	53.672	0.076	0.05	0.03	0.375	2.822	0.14	**98.966**
RGC738 Grain 14	#21	40.918	0.211	0.028	0.161	0.022	0.023	0.038	0.104	54.738	0.058	0.009	0.029	0.118	3.429	0.033	**99.916**
RGC738 Grain 15	#22	41.547	0.207	0.118	0	0.053	0.012	0.056	0.044	53.712	0.044	0.044	0.387	0.07	3.539	0.039	**99.872**
RGC738 Grain 4	#23	41.69	0.142	0.164	0	0.038	0.008	0.031	0.049	54.299	0.05	0.012	0.054	0.187	3.286	0.079	**100.089**
RGC738 Grain 5	#24	42.289	0.115	0.135	0.071	0	0.07	0.034	0.046	54.543	0.075	0.012	0.039	0.166	3.378	0.061	**101.034**
RGC738 Grain 8	#25	40.624	0.273	0.151	0.044	0.076	0.02	0.02	0.063	54.037	0.036	0.031	0.071	0.203	3.224	0.03	**98.903**
RGC738 Grain 6	#26	41.726	0.098	0.044	0.047	0.026	0.062	0.023	0	54.989	0.115	0.099	0.057	0	3.88	0.012	**101.178**
RGC738 Grain 12	#27	40.935	0.322	0.024	0.225	0.067	0.125	0.185	0.015	54.016	0.057	0.065	0.067	0.04	3.582	0.039	**99.764**
RGC738 Grain 11	#28	41.192	0.13	0.024	0.012	0	0.008	0	0.045	54.391	0.039	0.043	0	0.615	2.374	0.035	**98.908**
RGC738 Grain 10	#29	40.594	0.205	0.018	0	0.012	0.064	0.043	0.051	54.096	0.063	0.026	0.026	0.23	3.15	0.038	**98.616**
RGC738 Grain 17	#30	38.761	0.403	0.122	0.162	0.019	0	0.061	0.086	51.873	0.086	0.059	0.005	0.241	2.997	0.022	**94.897**
Dur-Ap-3	#35	41.303	0.347	0.292	0.046	0.468	0.539	0.167	0.001	53.58	0.019	0.062	0.089	0.116	3.28	0.354	**100.663**
Dur-Ap-4	#36	40.465	0.382	0.285	0.103	0.49	0.505	0.164	0.012	53.37	0.034	0.079	0.076	0	3.477	0.36	**99.802**
Bee-Ap-3	#37	40.84	0.23	0.326	0	0.125	0.313	0.186	0	53.939	0	0.034	0.437	0.001	3.681	0.013	**100.125**
Bee-Ap-4	#38	40.894	0.314	0.369	0	0.118	0.292	0.172	0.012	54.289	0.046	0.057	0.416	0	4.012	0.009	**101**

Results

Single Unit Method

The normal compaction trend for each unit was determined from a plot of average interval transit time versus depth to midpoint of that unit (Figure 9). All the wells containing the desired units were included in these plots. Wells in the Raton basin, which lie near the mountain front, are plotted with a different symbol than those that lie on the High Plains to the east of the Raton basin. These plots show that several wells along the SDCM front in Huerfano Park and in the northern Raton Basin in Colorado have the smallest amount of over-compaction, hence the lease amount of erosion.

The latter wells lie in a part of the study area where the Paleocene to Eocene synorogenic sedimentary units are still preserved and the stratigraphic column is nearly complete (Figure 2). As can be seen in Figure 9, the High Plains wells form a separate group of points distinct from the Raton basin wells. The calculated equations and control wells for the compaction trend for each unit are listed in Table 4. In all cases, the Walker Ranch well, which lies on the axis of the Raton basin, was a control well. Consequently, this well always provided an erosion estimate of zero based on this analysis. In terms of this study, the Walker Ranch well has experienced the least amount of erosion; however, it is known from the preservation of Eocene sediments at high elevation on Spanish Peaks that there has been ~ 1 km of erosion in this region (Close and Dutcher, 1990; Kelley and Chapin, 1995). The location of the second control well for each unit used to define the normal compaction trend is more geographically diverse.

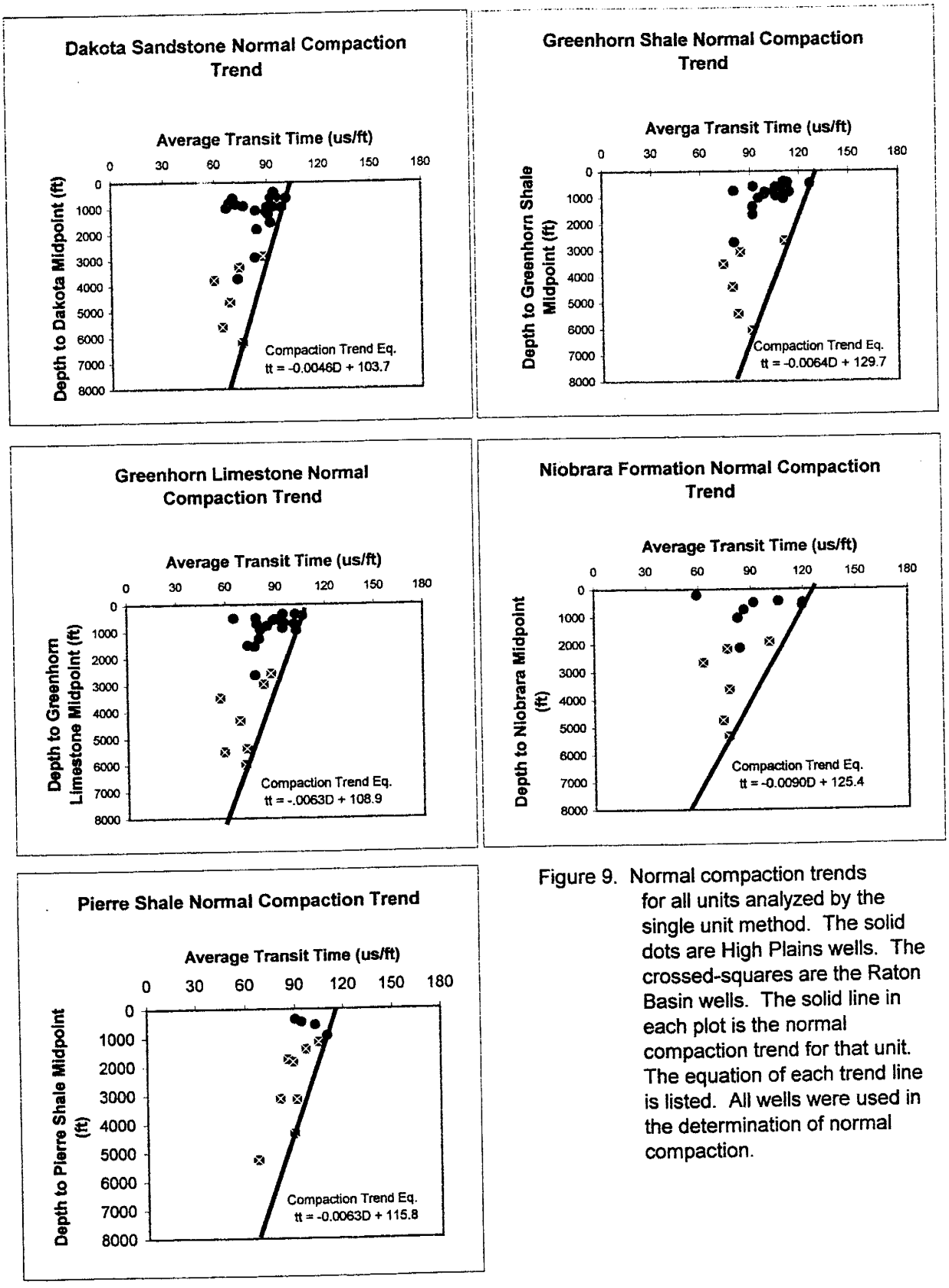

Figure 9. Normal compaction trends for all units analyzed by the single unit method. The solid dots are High Plains wells. The crossed-squares are the Raton Basin wells. The solid line in each plot is the normal compaction trend for that unit. The equation of each trend line is listed. All wells were used in the determination of normal compaction.

Unit	Control Wells	Equation of Normal Compaction
Dakota Sandstone	Federal #1 (Kiowa) Walker Ranch (Huerfano)	-0.0046D + 103.7 = Δt
Graneros Shale	Federal Jordan (Otero) Walker Ranch (Huerfano)	-0.0099D + 152.3 = Δt
Greenhorn Limestone	Hardy (Kiowa) Walker Ranch (Huerfano)	-0.0063D + 108.9 = Δt
Greenhorn Shale	Hardy (Kiowa) Walker Ranch (Huerfano)	-0.0064D + 129.7 = Δt
Niobrara Shale	Iannitti (Kiowa) Walker Ranch (Huerfano)	-0.0090D + 125.4 = Δt
Pierre Shale	11-31 Green (Pueblo) Walker Ranch (Huerfano)	-0.0063D + 115.8 = Δt

Table 4. Control wells and the resulting equations for the compaction trend lines for each rock unit, derived from plots shown in Figure 9.

The location of the second control wells, which are all located along the Arkansas River transect, varies from unit to unit and has no obvious geographic pattern (Figure 10 and Appendix B).

The values of erosion estimated from this method are listed in Appendix B and are displayed spatially in Figure 10. Contour lines constructed from the erosion estimates of the single unit method portray possible denudation trends.

Figure 10 consists of a series of contour maps derived from the erosion estimates from each of the five units, as well as a map based on the *average* of the single unit erosion estimates (Figure 10g). The single unit method provides the opportunity to evaluate the difference in erosion estimated from individual units and to average the values for a given well.

The most obvious trend occurs along the western portion of the Raton Basin proper. In every unit, the trend is the same: erosion values decrease northward. Consistently, the southern part of the basin shows on the order of 2 km of erosion and the amount of erosion systematically decreases to the north. A systematic east-west trend in erosion along the Arkansas River transect is not as obvious. The eastern portion appears to have undergone less erosion (from 0 to 500 m) and the values increase to about 1500 m on the west end of the transect (Figure 10.)

Assuming that the compaction experienced by the units sampled in a given well records only maximum burial and subsequent exhumation (that postdates the youngest unit analyzed), each unit should provide erosion estimates that are consistent with those derived from the other units. If this

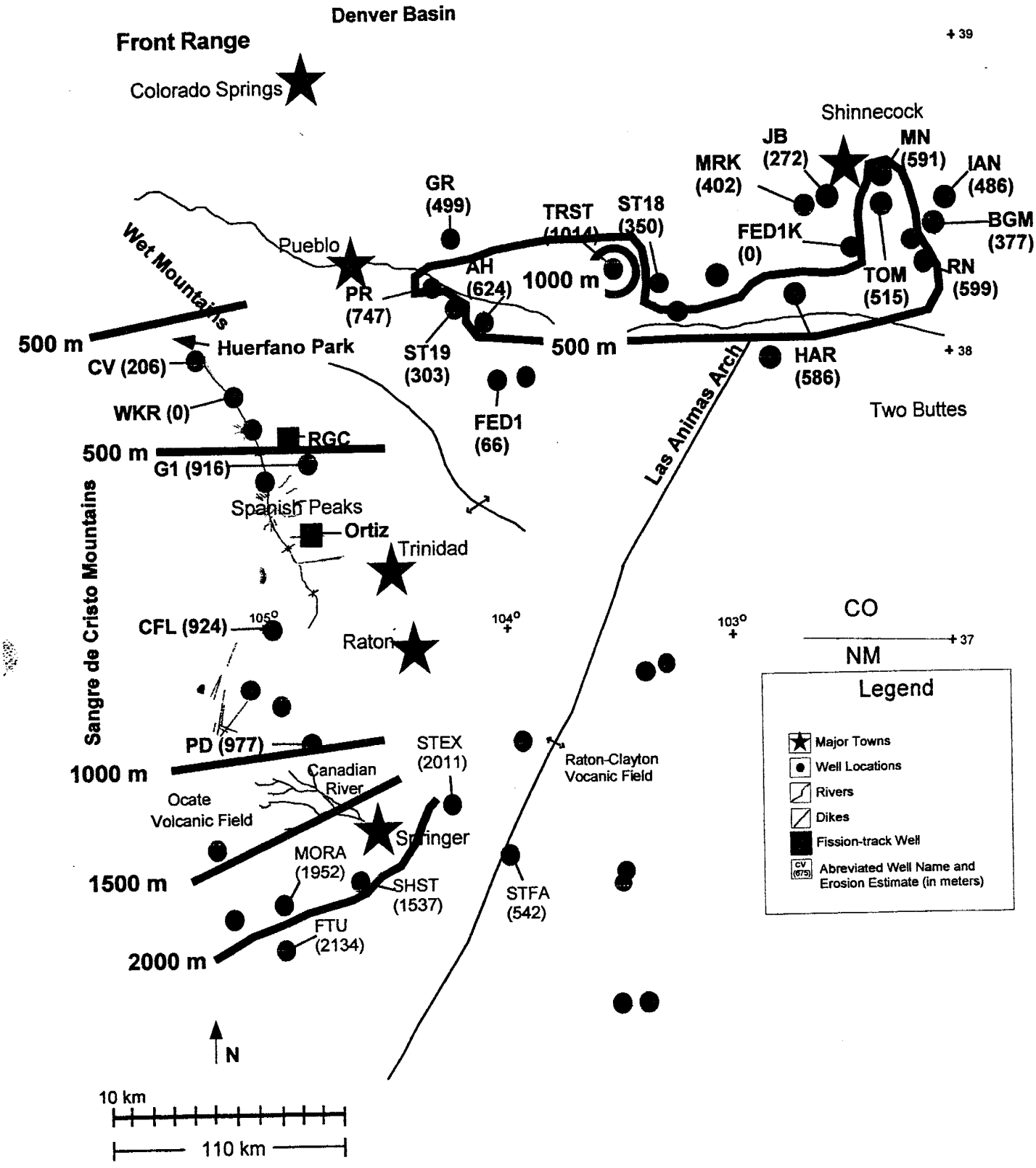

Figure 10. Erosion contours (500 m interval) determined from
a. Dakota Sandstone

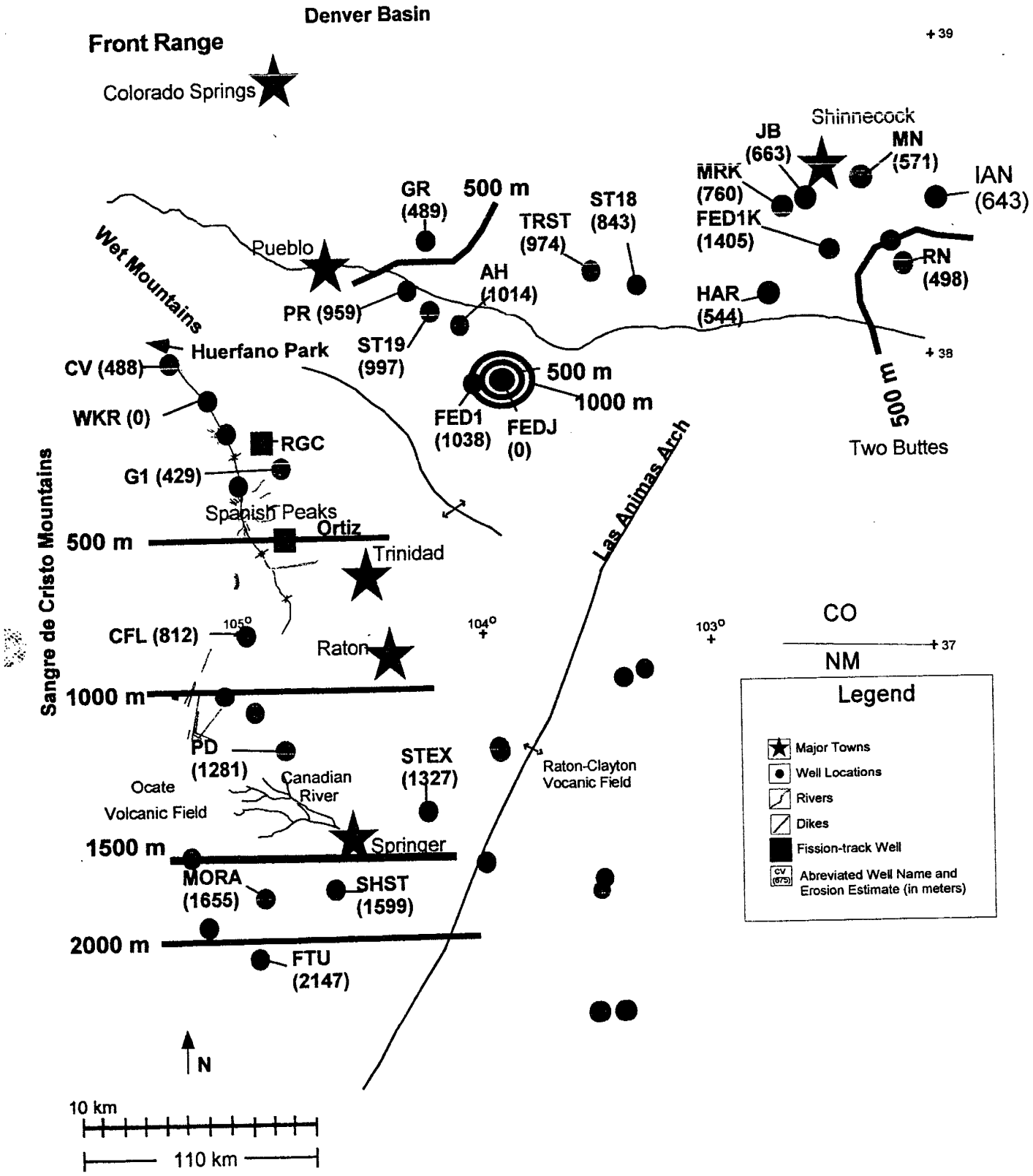

Figure 10. Erosion contours (500 m interval) determined from
b. Graneros Shale

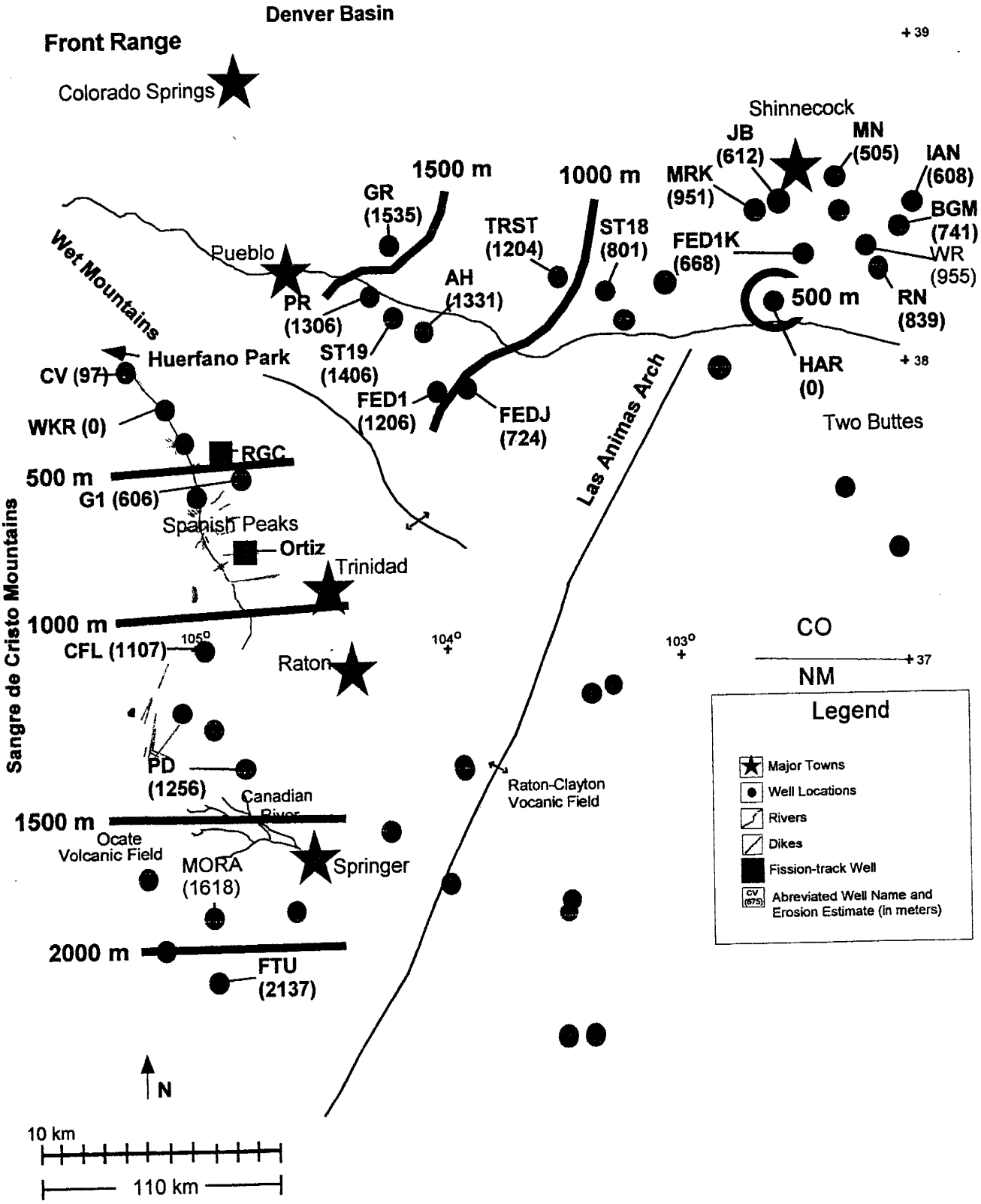

Figure 10. Erosion contours (500 m interval) determined from
c. Greenhorn Shale

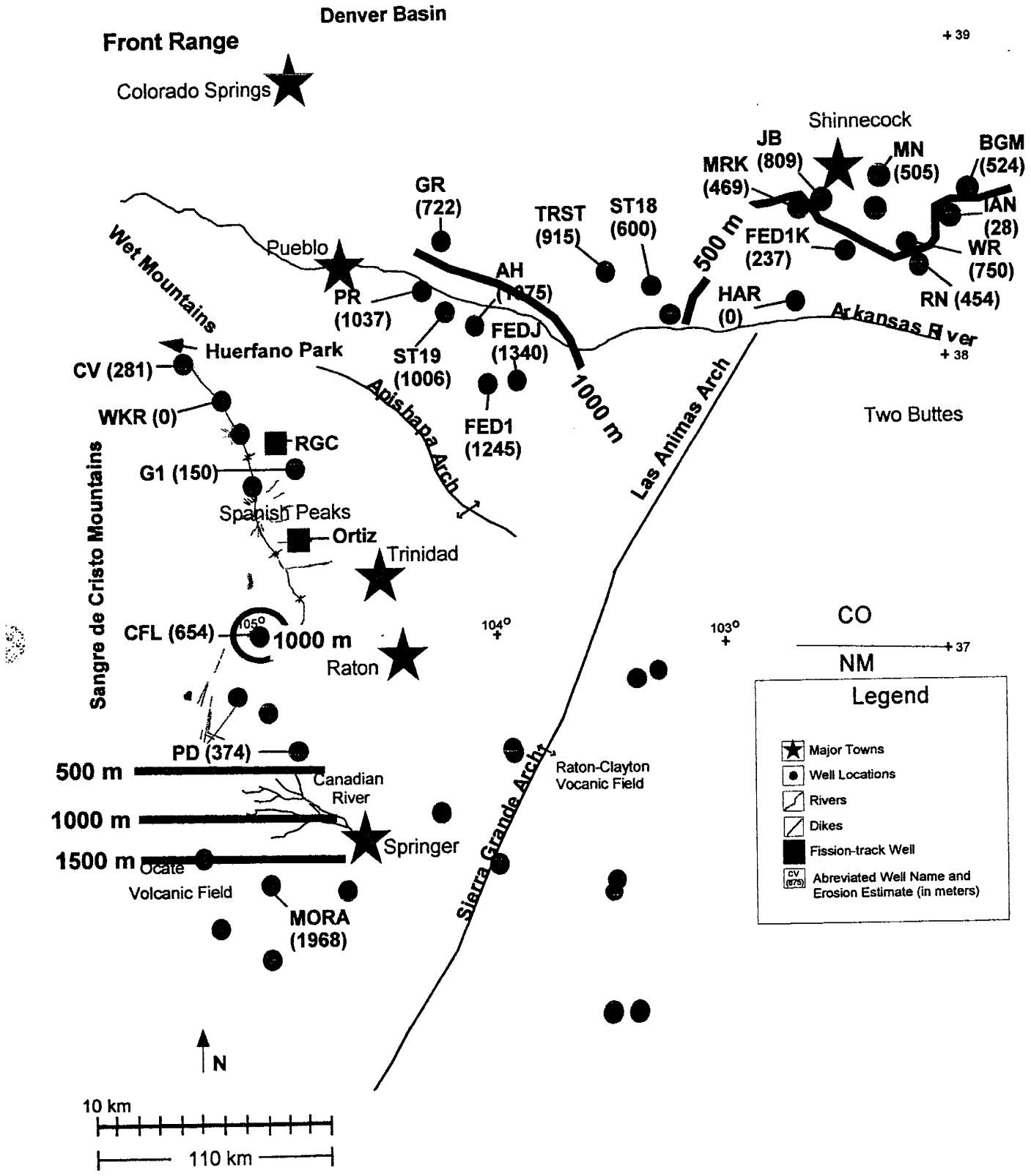

Figure 10. Erosion contours (500 m interval) determined from
d. Greenhorn Limestone

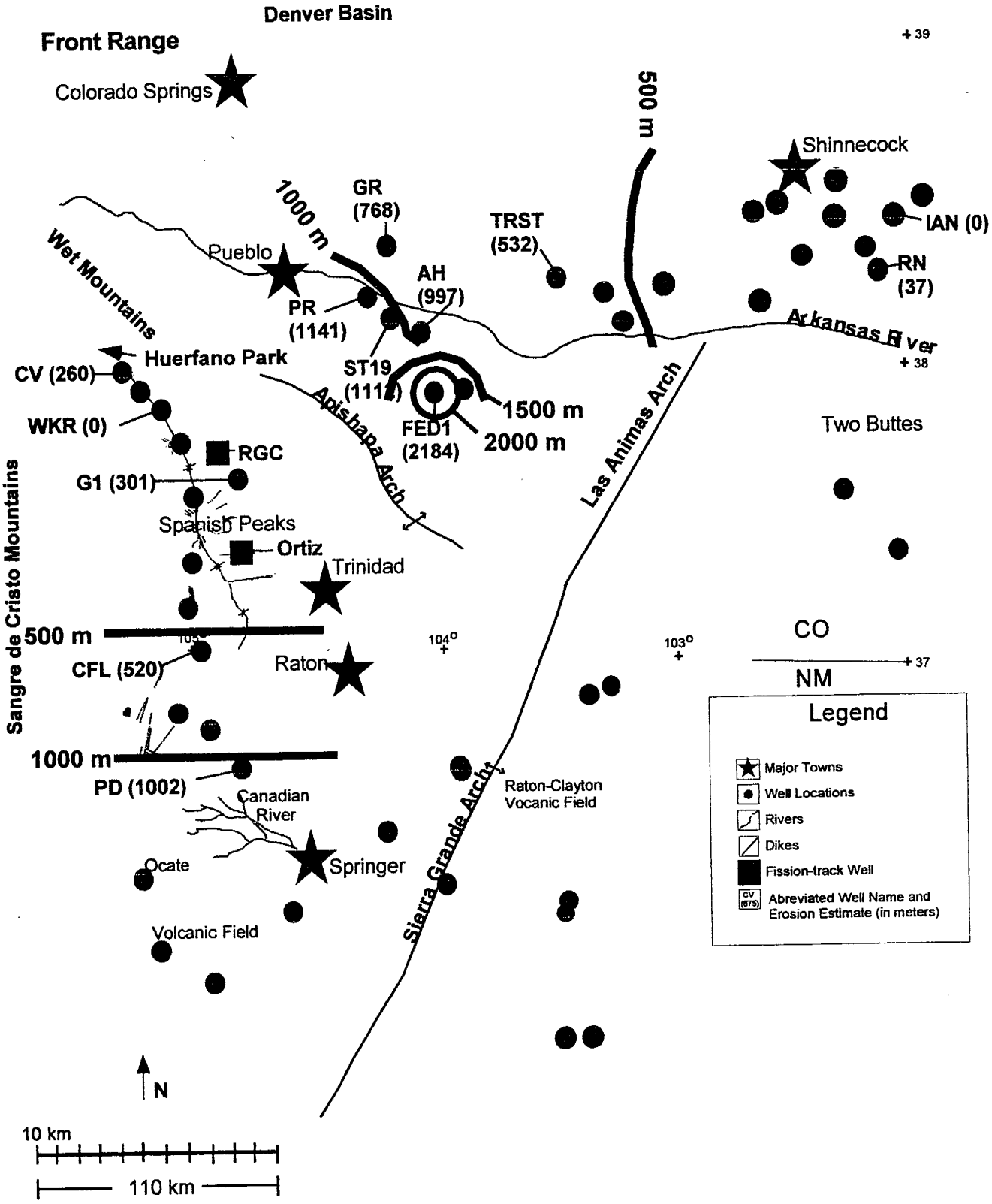

Figure 10. Erosion contours (500 m interval) determined from
e. Niobrara Formation

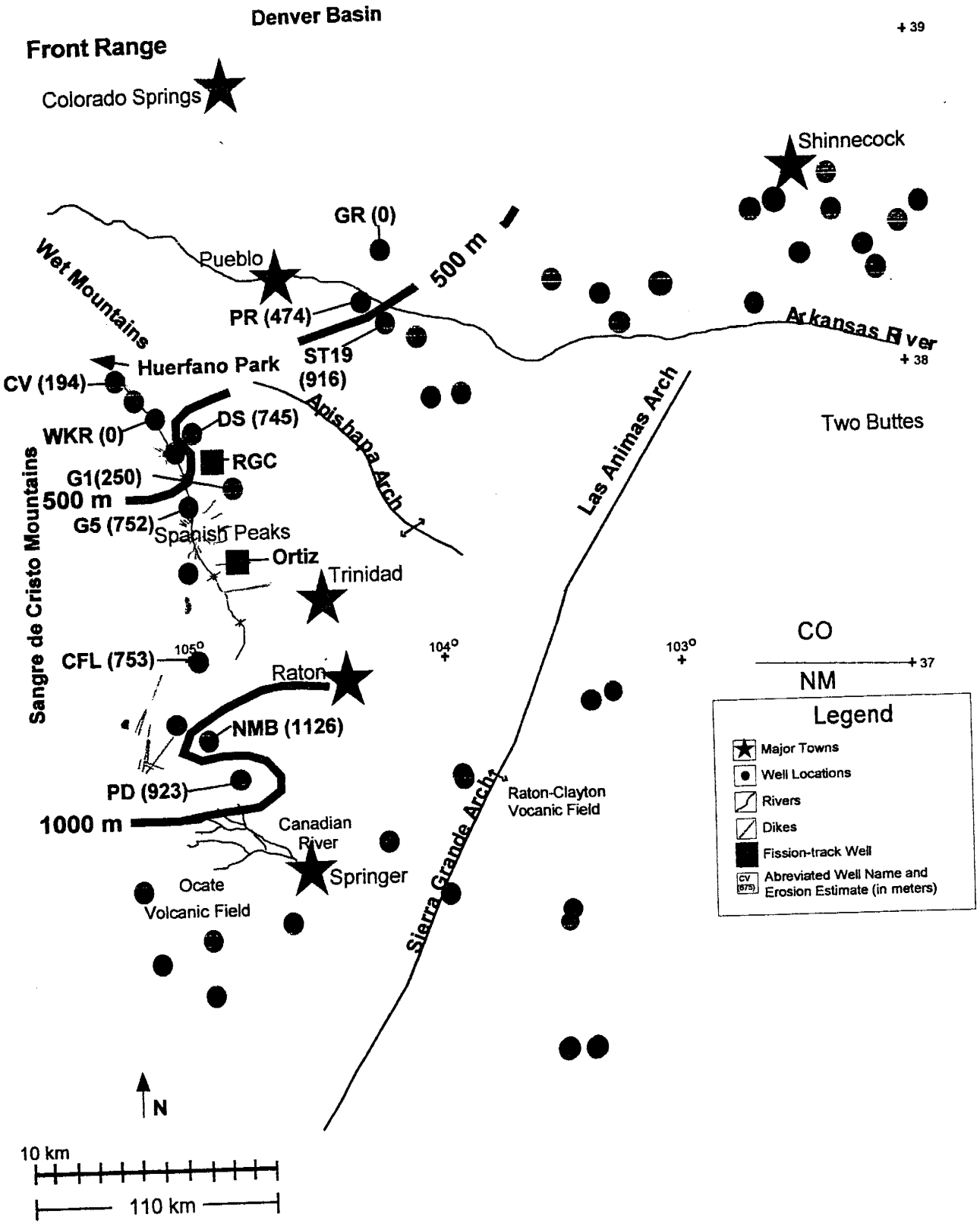

Figure 10. Erosion contours (500 m interval) determined from
f. Pierre Shale

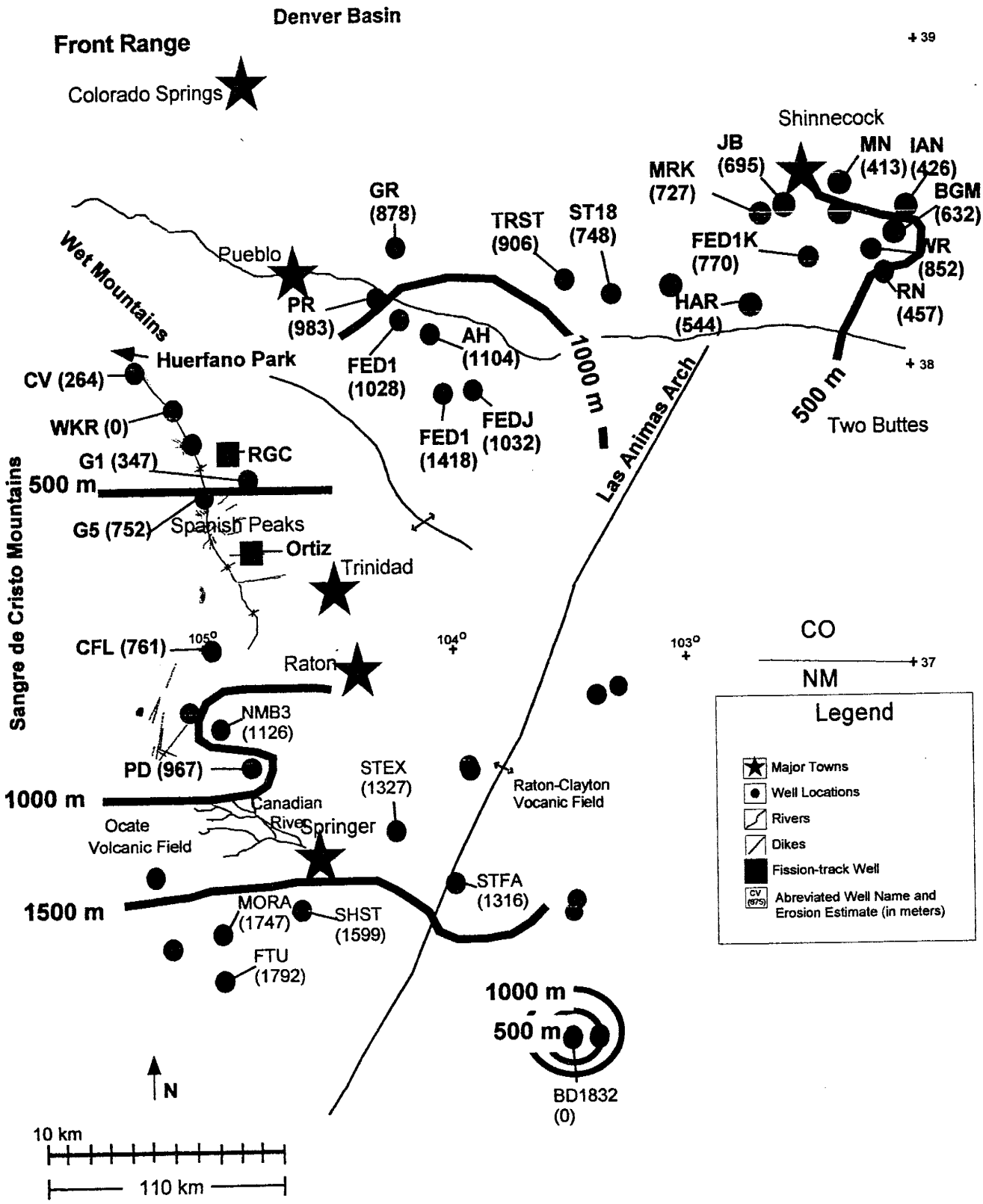

Figure 10. Erosion contours (500 m interval) determined from
g. Average erosion estimates from limestone, shale, and chalk units.

assumption is correct, any significant difference in the erosion values obtained from the different units would be related to depth-independent processes. In order to check the consistency of the erosion estimates between units, the apparent erosion calculated from each unit was plotted against the erosion estimates from the other units (Appendix C). The ideal situation is a one-to-one ratio (R^2 value of 1), where estimates from different units are the same for a given well. Any deviation from the one-to-one line occurs when the erosion estimates are not in full agreement with one another. Hillis (1995), for example, determined correlation coefficients of 0.48 (shale versus chalk), 0.54 (sandstone versus chalk) and 0.83 (sandstone versus shale). Statistically, R^2 calculations measure the linear association between variables (Moore and McCabe, 1993). The higher the R^2 value, the better the correlation. For example, an R^2 value of 0.67 implies that 67% of the time, the variables are associated. Individual points that lie far from the other data will affect the R^2 value most when the data set is small (Moore and McCabe, 1993). The confidence level and accuracy of results depend in part on the number of samples (in this case, wells). A larger sample size produces less variability in the statistics (Moore and McCabe, 1993). A larger sample also enables one to confidently distinguish outlier points. My range of correlation coefficients is very similar to that of Hillis (1995). Exceptions are correlations with the Pierre Shale and Niobrara Shale, which have R^2 values as low as 0.14 (Pierre Shale versus Dakota Sandstone) and 0.33 and 0.36 (Niobrara Formation versus Dakota Sandstone, and Niobrara Formation versus Pierre Shale, respectively).

In Appendix C, the cases where erosion values from a limestone or shale unit are compared to erosion values from another limestone or shale unit, the wells generally follow the one-to-one ratio line. The best examples are plots of the Greenhorn Limestone versus the Greenhorn Shale, the Graneros Shale versus the Niobrara Formation, and the Greenhorn Limestone versus the Graneros Shale. As mentioned above, some exceptions are comparisons with the Pierre Shale, which has the lowest R^2 values, from 0.14 to 0.58. Recall that outlier points will have the most influence when the sample size is small. The Pierre Shale was penetrated in only nine of the wells in this study. The Pierre Shale also has an intra-unit gradient that influences the calculation of the average transit time. The top of the Pierre Shale has high transit time values of approximately 110 to 120 μs/ft that decrease with depth to approximately 90 to 100 μs/ft (Figure 16). With the combination of these factors, it is not surprising that comparisons between estimates obtained from the Pierre Shale and other units have low R^2 values.

The erosion estimates obtained from the Greenhorn Shale and the Greenhorn Limestone are comparable. These two different lithologies from the same unit therefore produce similar erosion estimates. Previous studies have only used shales in their single unit compaction studies (Magara, 1976). The comparison of the Greenhorn Shale and the Greenhorn Limestone from my study offers evidence that limestones may be just as reliable as shales for compaction studies. Consistently, the Greenhorn Shale overestimates erosion values in comparison to all other units. The Greenhorn Limestone tends to estimate

values equivalent to those determined most of the other units. The comparison of the Graneros Shale and both the Greenhorn Shale and the Pierre Shale shows that overall, the shales agree on the estimated erosion. The Niobrara Formation behaves similarly to the chalk in Hillis (1995) study. Hillis (1995) found that the chalk unit he studied had a higher correlation coefficient to the shale unit, and poorest correlation with the sandstone. The Niobrara Formation, primarily a chalk, has an R^2 range of 0.33 (compared to the Dakota Sandstone) to 0.84 (compared to the Graneros Shale), which are similar to Hillis' correlation values. Unfortunately, the Niobrara Formation, like the Pierre Shale, was contained in few wells. Had more wells with the Niobrara Formation been available, I think the R^2 values would have risen, showing more accurate estimates between lithologies. The estimates obtained from the Dakota Sandstone correlated well with those determined from the overlying Graneros and Greenhorn Shales, but overestimated erosion values compared to the younger units (Niobrara Formation and the Pierre Shale). Hillis' (1995) sandstone produced greater erosion values in comparison to the shale and the chalk. The Dakota Sandstone produced similar erosion values to some shales, but produced greater values in other shales.

Multiple Unit Method

For this portion of the study, all of the post-middle Permian stratigraphic units were combined to calculate the magnitude of erosion. Figure 7 shows an example of a well with both the uncorrected exponential equation (Eq. 1) and the

corrected exponential equation (Eq. 2). Notice the significant differences in erosion estimates determined with and without a shift constant. For example, the uncorrected curve provides an erosion estimate of 220 ft (67 m), whereas using the best statistical fit shift constant of 59 significantly changes the estimate to 727 ft (222 m). The uncorrected exponential equations generally underestimate the apparent exhumation; they commonly suggest a negative amount of erosion. In contrast, the corrected equation produces sensible estimates of erosion amounts in most of the wells. The results of this portion of the study are provided in Appendix D and contoured in Figure 11. Overall, there appear to be three areas of maximum erosion, based on this method. Two occur along the western front of the basin, near the Sangre de Cristo Mountains. The other maximum is located along the Arkansas River in the northern portion of the study area. These calculations indicate that erosion has been uneven across the basin, with values as great as 2.5 km. As can be seen from Figure 11, this method had several wells with large differences in erosion estimates within close proximity to other. One problem occurs with the State "EV" well, in the center region of the study area, which had apparent exhumation of 93 m. The BDGDCU 2332 well estimates an erosion value 576m greater than the well next to it, Caroline Gonzales. Similarly, Federal #1 (Otero County) estimates over a 1000m while the Federal Jordan well only indicates 100 m of erosion. In most of the above-mentioned wells, there are only a few feet of sonic data (<2000 ft / 610 m) to evaluate. There is therefore less control on the erosion estimates obtained from these wells in comparison to other wells in the study area.

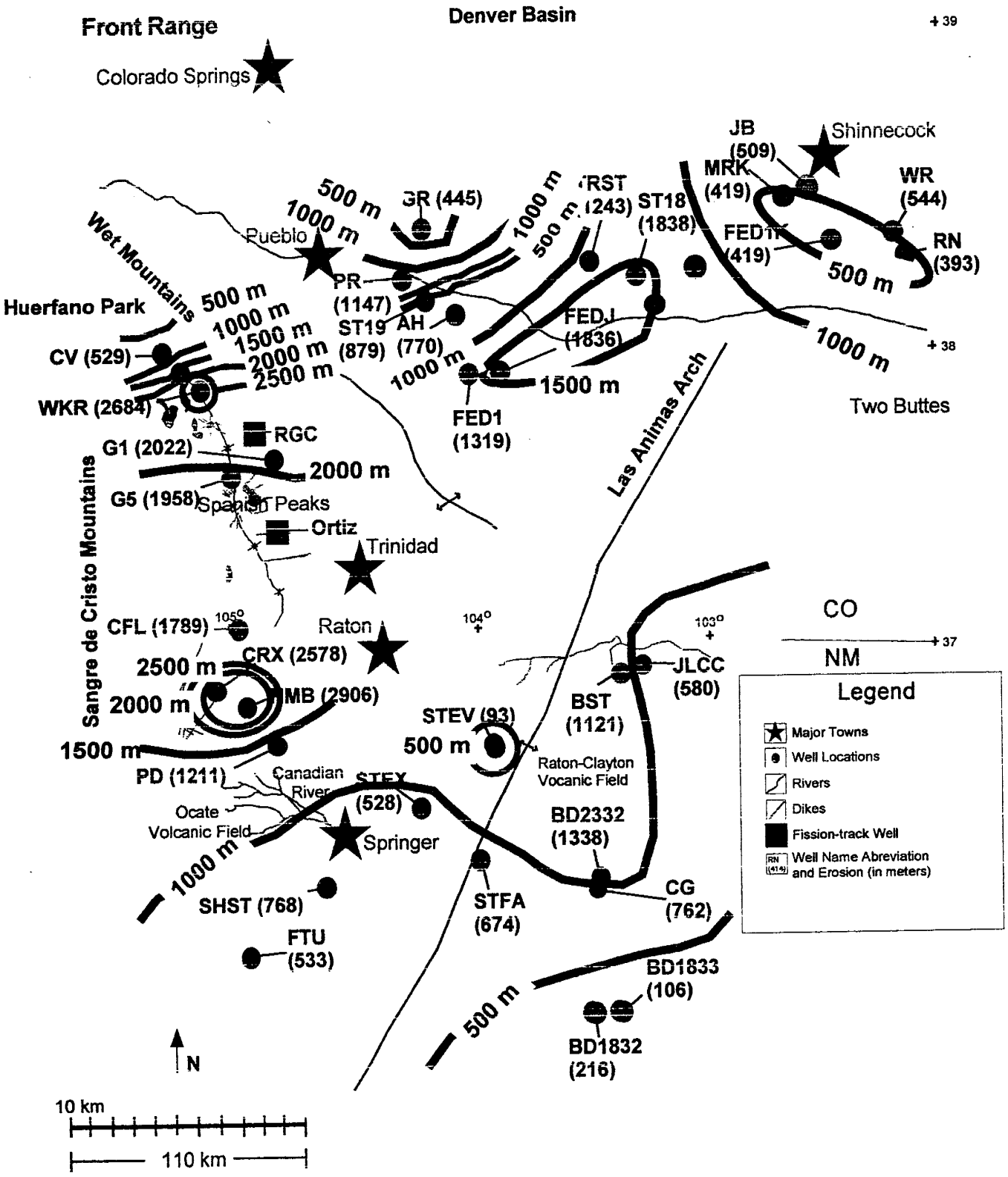

Figure 11. Erosion contours (500 m interval) determined from Multiple Unit Method

Fission-Track Analysis

Examination of the ages and track-length distributions from the dated samples provides a qualitative thermal history for the Raton Basin. Table 2 lists the results for the fission-track analysis. Figure 12 is a plot of fission-track age versus depth for the wells with usable data. For the Logan well, the two shallowest samples have mixed age populations – implying that they are within the fossil PAZ and retain older as well as newer tracks. The deepest sample, however, has a single population. This sample is below the base of the fossil PAZ. Based on these data, the lower boundary of the PAZ must fall between the depths of 767 m and 905 m. Taking the average distance between the two depths puts the base of the fossil PAZ at a modern depth of approximately 838 m below ground surface. To estimate the amount of denudation from the AFT method, the amounts of rock uplift, changes in sea level, and geothermal gradients must all be taken into consideration. Figure 13 the relationship between fission-track age and depth for the Logan well before exhumation (A) and after exhumation (B). Denudation was calculated using the following equation:

Denudation = Rock Uplift – Surface Uplift

For the Logan well, the amount of rock uplift was determined by using the base of the PAZ (110°C) as a marker through time. At the end of Cretaceous time, the distribution of samples is interpreted as shown in Figure 13 (A). Assuming a surface temperature of 20°C and a geothermal gradient of 20°C/km, the base of

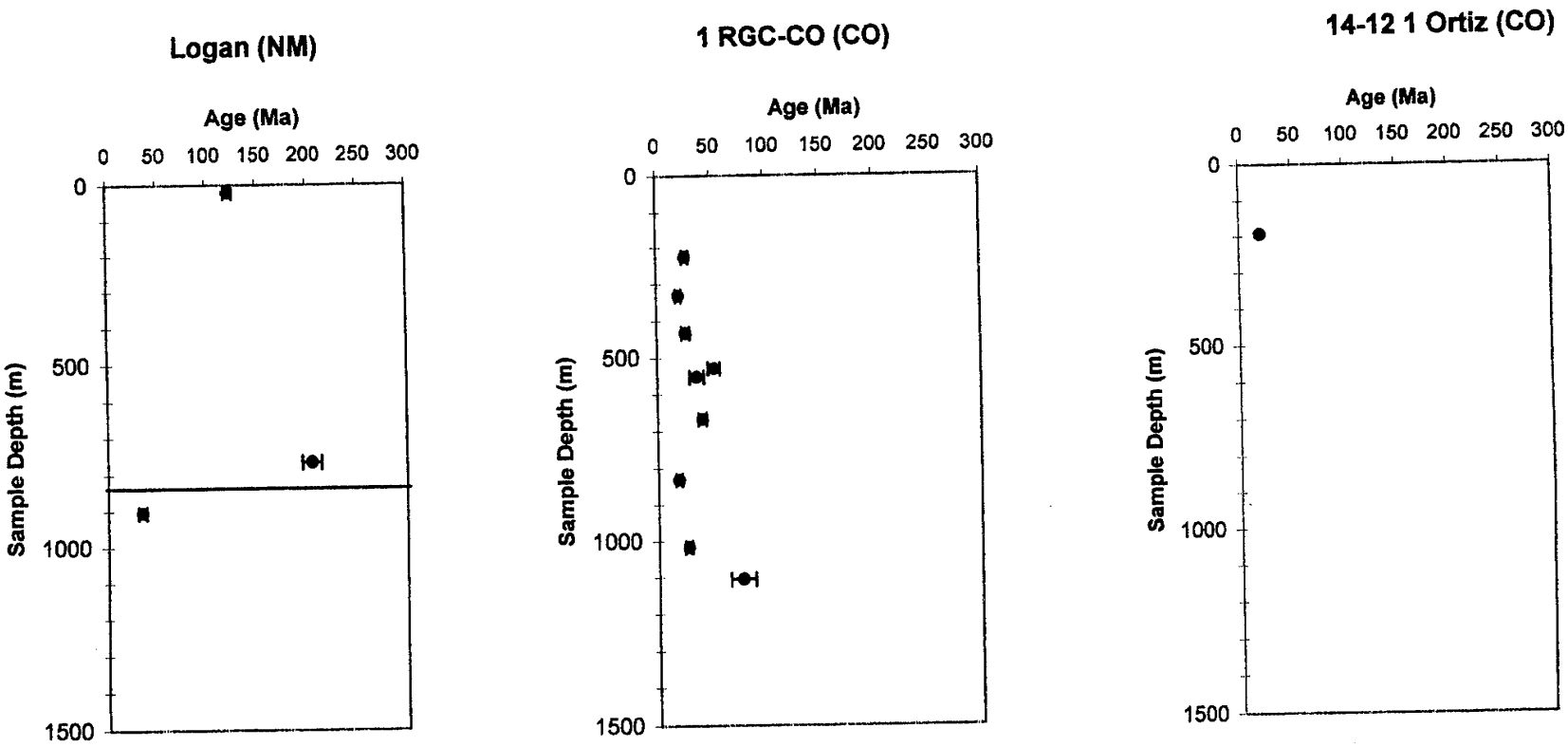

Figure 12. Sample depth versus age for three wells analyzed with the AFT method. Error bars for the age are indicated; where unobservable, the error is smaller than the symbol.

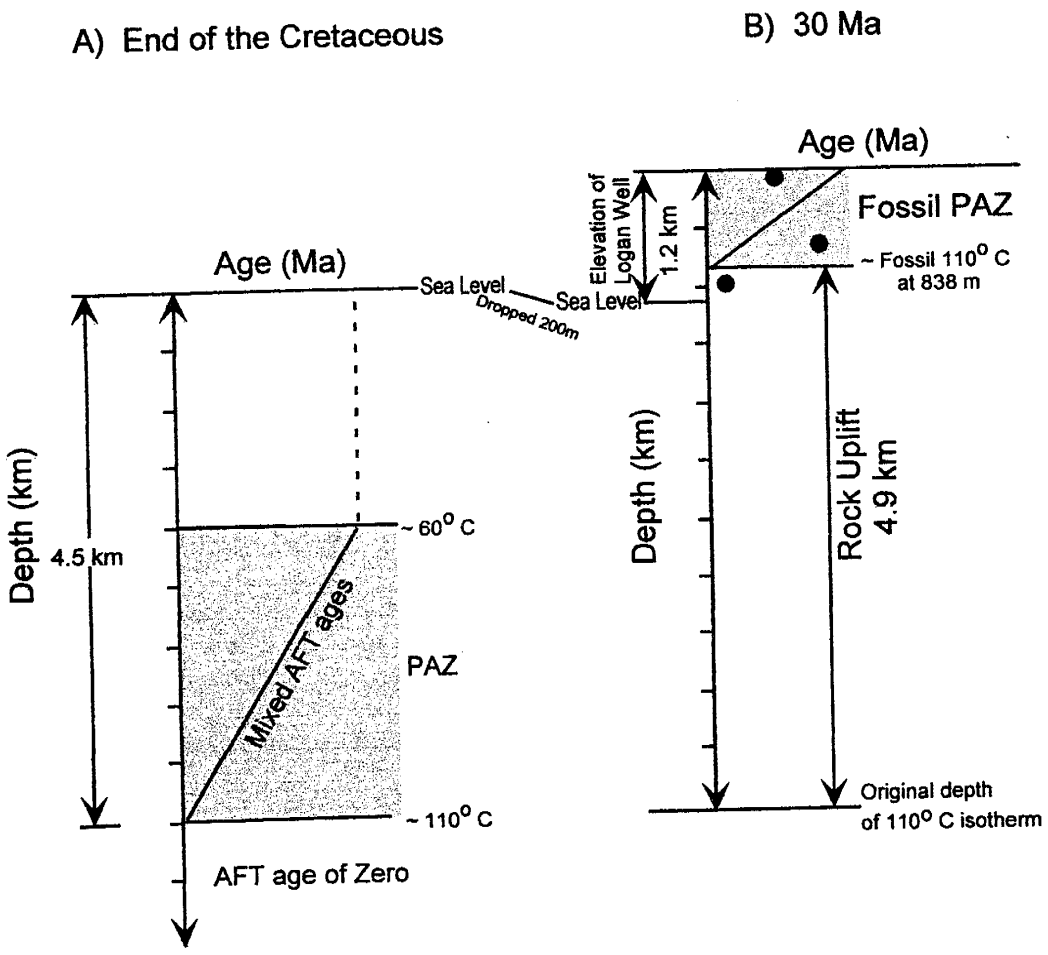

Figure 13. Diagram showing spatial distribution of AFT ages for the Logan well before (A) and after (B) denudation. Depth in km is on the vertical axis and age in Ma is on horizontal axis. The samples from the Logan well are shown as solid circles.

the PAZ would have been at a depth of 4.5 km at that time. Today sea level has dropped 200m with respect to Cretaceous time and the Logan well is at an modern elevation of 1 km, representing a total surface uplift of 1.2 km. The base of the fossil PAZ is at a depth of 838m (.84 km) below ground surface . Thus, the total amount of rock uplift can be calculated by:

Rock Uplift = Original PAZ Depth + (Elevation of Well – Depth of Fossil)
Above Sea Level PAZ

Or Rock Uplift = 4.5 km + (1.2km - .84km)

So the total amount of rock uplift for the Logan well is 4.9 km. Substituting this value into the equation for total denudation results in the following:

denudation = 4.9 km – 1.2 km = 3.7km

This calculation is based on two assumptions. The first assumption is that heat flow remained constant over time in this area. The second assumption is that the geothermal gradient was 20°C/km. This temperature gradient would indicate that the tectonic conditions of the region were stable during this time. The same calculation can be run for different geothermal gradients. A tectonically unstable regime might have a geothermal gradient of 35°C/km. An intermediate tectonic regime would be best represented by a gradient between those two values. Edwards et al. (1978) published heat flow and geothermal gradients for the Raton Basin. According to their study, the modern geothermal gradient for the Raton Basin ranges from 19.81 to 31.91^{0}C/km, but averages around 26^{0}C/km. For comparison in this study, the calculation was run at 20^{0}C/km and at 30^{0}C/km, since these values characterize the spread of modern-day gradients in the Raton

Basin. For a 30^{0}C/km gradient, the resulting amount of rock uplift is 3.4 km and the total denudation is 2.2 km.

The 1 RGC-CO well, in contrast to the Logan well, does not contain a fossil PAZ. The samples analyzed all yielded Late Oligocene to Miocene ages, except for the sandstone at 1017 m. Since all samples have single populations of grains (except for sample RGC 1017, which contains chlorine-rich grains), the fossil PAZ should be located above the shallowest sample. The base of the fossil PAZ could be at a maximum of 213 m deep within the well, but most likely it has been eroded away.

The one sample from at a depth of 194 m in the 14-12 1 Ortiz well provided an age of 20.8 Ma. This sample passed the X^2 test (single age population) and confirms that the fossil PAZ is not present in this well. This agrees with the findings from the RGC well; the PAZ is not present in the northwestern Raton Basin.

The PAZ is therefore deeper in the subsurface in the east but is increasingly shallow to the west. Unpublished AFT data from drill holes in the Texas and Oklahoma panhandles (S.A. Kelley, unpublished) indicate that the fossil PAZ is at ~2600 m in the subsurface. Figure 14 is a schematic cross section summarizing the relationship between the fossil PAZ and the current topographic surface.

The AFTSolve© modeling program can be used to models thermal histories that best describe the observed FT track-length and age data. At least two constraints are necessary for the AFTSolve© program to model the data, one at either end of the age spectrum. Other independent geologic constraints

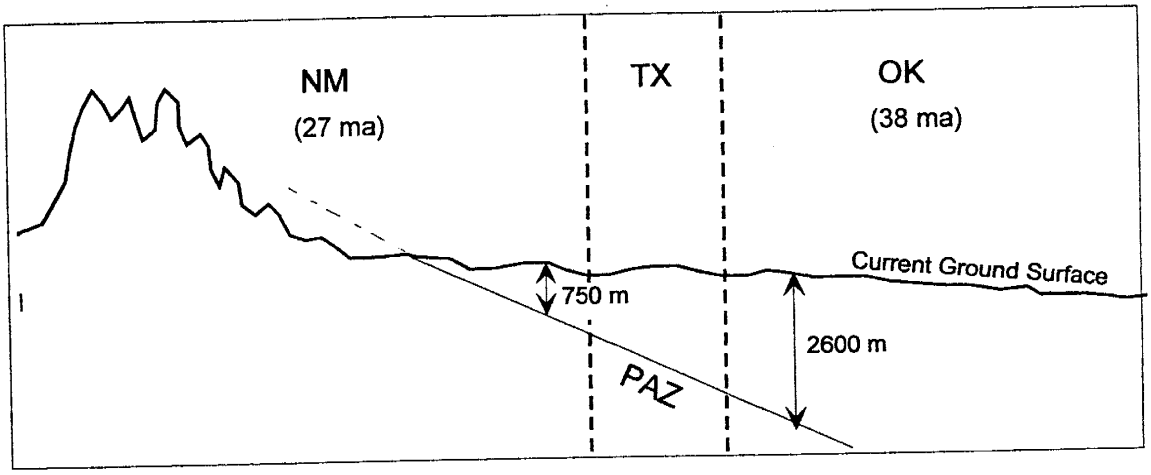

Figure 14. From Oklahoma to New Mexico, the base of the PAZ is found at progressively decreasing depths. The fission-track ages of samples from the Anadarko Basin in OK indicate that by 38 ma the base of the PAZ was brought to 2600m depth. In New Mexico, the fission-track data suggest that by 27 Ma the base of the PAZ was as shallow as 750 m and father west, it is missing altogether. Not to scale.

can be incorporated into the modeling program to direct the model to honor known thermal constraints. Unfortunately, only one sample contained sufficient track-length numbers for the analysis, Log 73. Independent knowledge of the geologic history for Log 73 was unavailable for this study. Therefore, the model was run using a general and very broad constraint that spanned from 180^0 C to 30^0 C at 230 Ma and a more defined constraint from 70^0C to 20^0C at 0 Ma. Ten thousand thermal history paths were generated (Figure 15).

The model suggests that the sample remained at temperatures greater than 120^0 C until the onset of cooling at 133 Ma. The sample cooled gradually, staying in the PAZ for almost 100 Ma. It was not until 35 Ma that the rate of cooling increased and the sample cooled rapidly.

Discussion

Data Analysis

Single Unit Method

The erosion estimates obtained from the single unit method support two separate trends in the magnitude of erosion across the study area. As mentioned previously, the Huerfano Park region (northern study area) contains the most complete stratigraphic section. The fact that the single unit method consistently estimated significantly less erosion for this region substantiates the accuracy of the method and the resulting erosion trends.

The erosion estimates derived from the limestone and shale groups using the single unit method correlated relatively well with one another. The correlation

Logan 73

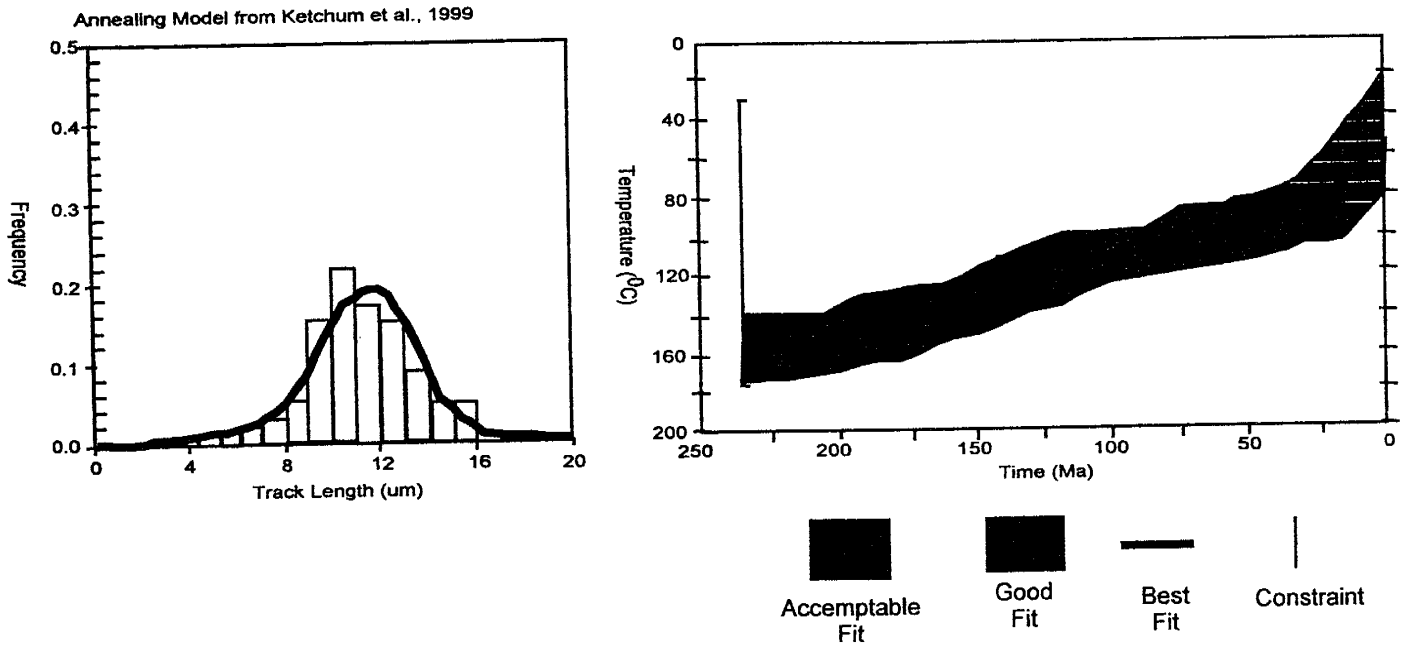

Figure 15. AFT model graphs for the sample with track length data. The black line represents the "best" fit prediction and the green shaded area outlines an "acceptable" fit. The model did not define a "good" fit to the track length data. The vertical lines are broad, very general geologic constraints necessary for the model to run.

of the crossplots supports the assumption that depth-controlled compaction is indeed the primary control on porosity in the units studied. In a similar study, Hillis (1995) compared exhumation estimates determined from shale, sandstone, and chalk units in the North Sea, United Kingdom. His results show that the shale, sandstone, and chalk all provide similar erosion estimates. The fact that in both his study and mine different lithology types yield statistically similar erosion estimates validates the use of the single unit method as an accurate indicator of compaction. Hillis' sandstone unit consistently produced higher erosion estimates than the chalk and the shale units, suggesting that the values obtained from the sandstone overestimated erosion. The chalk and the shale, however, produced similar erosion estimates (Hillis, 1995). In my study area, the Greenhorn Shale is interpreted to consistently provide overestimates of apparent exhumation, but values obtained from the Dakota Sandstone only occasionally overestimated the erosion. Both Hillis (1995) and my study document that lithologies other than shales can provide accurate exhumation values. The difference between the studies is that for the case of the Raton Basin – High Plains, several different shales and limestones could be compared directly to each other. Careful examination of the table in Appendix B reveals that there are no consistent patterns in erosion estimate as a function of stratigraphic level in wells containing several of the evaluated units. Some wells show decreasing amounts of erosion upsection, but other wells show the opposite trend or no pattern at all. Hillis (1995) had similar results.

When the erosion estimates from the single unit method are viewed spatially, values obtained from a given well agree with those of the surrounding wells (Figure 10). One exception occurs with the Federal Jordan well, which is a control well, but is located next to the Federal #1 well, which has an erosion estimate of over 1000 m (Figure 10b,e). These same two wells show a similar "bullseye" effect of erosion estimates determined from the Niobrara Formation. The difference is not as great in values calculated from the Niobrara Formation as it is in values calculated from the Graneros Shale, but it is still pronounced. Three possible explanations of the difference between the two wells were considered. The first possibility was the potential of structural influence; the well exhibiting higher erosion values might be located on a structural high. Tweto (1979), however, did not map any structure in the vicinity of either of these wells, including extensions of Apishapa arch or the Las Animas arch. The stratigraphic units in the Federal Jordan well are ~61 m higher than the equivalent units in Federal 1, indicating a minor difference in structural position but not enough to explain the difference in erosion estimates. The second possibility is that local sedimentological and/or diagenetic mechanisms could have produced an *apparent* exhumation difference. If diagenesis or cementation of the pore space occurred, then the sediment would appear to be under- or overcompacted. There was no sign of alteration to the sediments in either the Federal #1 well or the Federal Jordan well; there are no surface outcrops of the units in question, nor core samples available to petrographically substantiate the condition of the units. Finally, the calibration of the logs was re-examined to insure that the

difference in erosion values was not due to scaling issues. Both sonic logs were calibrated in the same way and were accurate. It is clear that more subsurface data are needed in this local area in order to fully understand why these two wells, so close in location, show such an extreme variation in apparent exhumation.

One shortcoming of the well log analysis portion of this study is the fact that most of the wells that include sonic velocity data are located on the border instead of in the center of the study area. This spatial distribution occurred for two reasons. First, few wells have been drilled in the center of the basin. Second, the wells that are available are generally either too shallow (915 m) for the sonic log analysis to be done accurately or the log suite available does not include sonic logs. The single unit method was affected the most by the geographically limited number of wells, since not all the wells contain every unit examined in this study. The younger units like the Pierre Shale have been stripped away and thus the data base is smaller. For example, only 14 wells contain the Niobrara Formation. The Pierre Shale is only sampled in nine of the wells. The oldest units have not been removed by erosion, so these units (e.g. Dakota Sandstone) are found in the most wells and hence have more data for the older units. The Pierre Shale also exhibits an internal transit time gradient that makes it challenging to calculate the average transit time. In light of the lack of wells, and the strong internal transit time gradient of the Pierre Shale, the poor correlation between the Pierre Shale and the other units is not surprising.

Multiple Unit Method

The multiple unit sonic log analysis allowed an evaluation of the sensitivity of the sonic logs to mixed lithologies. Heasler and Kharitonova (1996) determined that mixed lithologies provided reasonable erosion estimates when compared to single lithologies.

The multiple unit method has more instances of "bullseye" contours than the single unit method. The "bullseyes" occur around the wells with the greatest erosion estimates; with erosion values as high as 2.5 km (Figure 11). The erratic erosion contours indicate that for my study, there is greater uncertainty associated with the multiple unit method. One possible explanation for the dissimilar erosion values derived from the multiple unit analysis is related to the fact that some units, in particular the Pierre Shale, have a strong, characteristic transit time signature (intra-unit gradient) that controls the calculation of the erosion estimate.

Figure 16 is a plot of the digitized sonic log for the No. 1 Walker Ranch well with depth on the vertical axis and interval transit time on the horizontal axis. Superimposed on this plot are the locations of different ages and stratigraphic units. All units are undifferentiated except for the Pierre Shale. Note that the top of the Pierre Shale coincides with a significant increase in the internal transit time compared to the overlying sandstones and shales of the synorogenic Tertiary sedimentary rocks and the latest Cretaceous nearshore units. Also note the pronounced transit time gradient as a function of depth for the Pierre Shale, which can be seen in other wells where the Pierre Shale is present (see

No. 1 Walker Ranch

Twp 27S Rng 70W Sec 1
Huerfano, CO

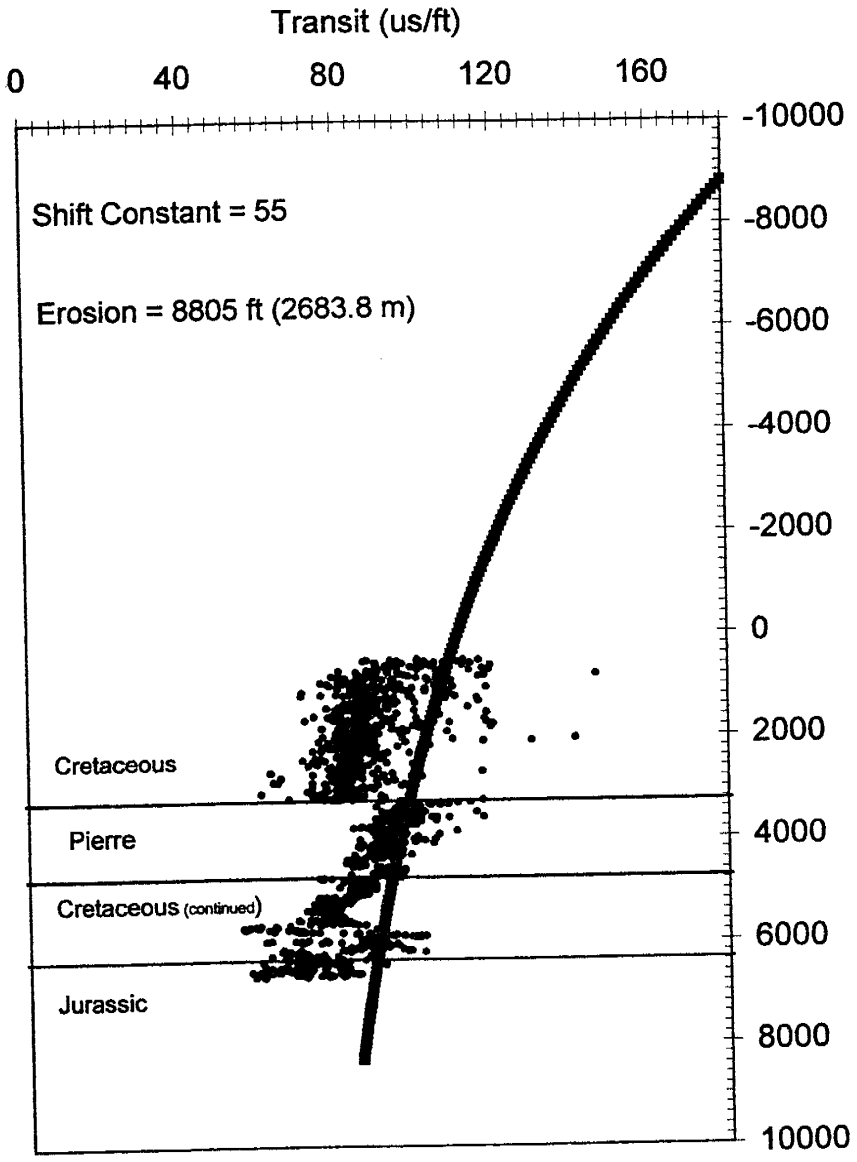

Figure 16. Scatter plot of sonic log data from the No. 1 Walker Ranch well. Stratigraphic units were determined from log suites. All units are undifferentiated except the Pierre Shale. Note the "jump" in transit time values found above the Pierre Shale.

Appendix D). The depth of the Pierre Shale within a given well is thus an important factor controlling the shape of the upper portion of the exponential curve that forms the basis of the multi-unit technique. Recall that the upper portions of the exponential curve are the most important for determining erosion amounts. If the Pierre Shale is close to the surface, its high transit time velocities and sharp gradient will act as a proxy for uncompacted sediments and skew the estimated compaction trend to predict lower erosion amounts. In contrast, if the Pierre Shale is located relatively deep in a given well, its high transit time values will be countered by the rest of the data (e.g. No. 1 Walker Ranch). The younger units above the Pierre Shale control the shape of the exponential curve, which explains why the Walker Ranch is a control well for the single unit method, but the multiple unit method estimates over 2 km of erosion. The impact of intra-unit compaction gradients on erosion estimates is beyond the scope of the current study, but these affects can be considered using the techniques of Magara (1976). Finally, the use of a surface value for transit time of 180 μs/ft, estimated from marine sediments, as the velocity of zero compaction with terrestrial sediments such as those filling the Raton Basin during Laramide deformation, has not been examined.

Comparison of Sonic Log Methods

The single unit method strongly suggests decreased erosion toward the north, along the west side of the study area. The fact that this trend can be seen in all five of the single units but is difficult to see in the values obtained through

the multiple unit method substantiates the validity of separating lithologies. The most likely reason the multiple unit method yielded more variable erosion estimates in this study area as compared, for example, to Heasler and Kharitonova's (1996) study area lies in the differences in completeness of the stratigraphic column. In the Wyoming basin they studied, the stratigraphy is more consistently preserved throughout the area. For the Raton Basin and vicinity, the stratigraphic section is more complete in the northern and western regions but has been eroded in the southern and eastern regions. The multiple unit method has to be applied carefully – meaningful data can be extracted when comparing similar sections (e.g. Arkansas River transect) but as seen in Figure 11, will result in widely varying estimates of erosion where the sedimentary section preserved is not consistent throughout the area of study.

The single unit method is thus a much better method for obtaining accurate erosion estimates, as has been suggested by numerous workers (Magara, 1976; Hillis, 1995), especially if the erosional history of the study area is poorly understood and poorly constrained. However, previous workers have suggested that the method be applied only to shales (Magara, 1976). My work demonstrates that the single unit method works with lithologic units other than shale.

Thermal History

The AFT method adds the time/temperature component for this study area that is lacking in the sonic log methods. The observations and interpretations

from my AFT samples are compared to published vitrinite reflectance data for the same area as an additional thermal gauge.

The AFT ages of the 1 RGC-CO and Ortiz well samples all fell roughly within the range of the timing of magmatic activity in the northern Raton Basin (approximately 35 to 25 Ma; Woodward, 1987b; Miggins et al., 1999). The contours of vitrinite reflectance from coal ranks place the maximum values, not at the Spanish Peaks intrusive center, but instead along the Purgatoire River (Scott et al., 1990). The values increase toward the Colorado/New Mexico state line but decrease abruptly after crossing into New Mexico (Close and Dutcher, 1990; Scott et al., 1990). The coal ranks record a heating event - that, based on the AFT data from RGC-CO and the 14-21 Ortiz wells in Colorado, died away approximately 20-30 Ma. The AFT samples are recording cooling following the last heating event that reset the fission-track clock, which happens to coincide with the emplacement of the dikes and plutons in the northern Raton basin. The overlap of the timing of the Spanish Peaks intrusion and the AFT ages makes it difficult to determine if cooling ages in 1 RGC-CO are related to denudation or cooling following the heating event. Miggins et al. (1999) obtained widespread ages of 25 Ma for dikes and sills throughout the Raton Basin; Close and Dutcher (1990) link Spanish Peaks and Mt. Maestas as well as the numerous dikes and sills to the same Cenozoic event. Recall that the plutons in the Spanish Peaks were intruded and then the surrounding sediment was eroded. The combination of the vitrinite reflectance data and the AFT data substantiate that the northwestern study area has experienced elevated temperatures (and

subsequent cooling) as well as erosion, as determined from previous studies of the Eocene strata found on the Spanish Peaks.

While the RGC-CO and 14-21 Ortiz wells indicate influence from the Spanish Peaks intrusions, there is no evidence, surface or subsurface, that Cenozoic volcanics influenced the cooling history of the Logan well. Neither the Raton-Clayton nor the Ocate volcanic fields influenced any of the samples, otherwise, the AFT ages would have been significantly younger, <8 Ma. Thus the heat from these fields is highly localized.

The deepest sample in the Logan well cooled at ~35 Ma. However, the vitrinite reflectance data indicate that coal ranks in the southern Raton Basin have not been baked to the same extent as in the northern portion (Scott et al., 1990) Therefore, the exhumation amounts determined from the Logan sample can be taken as denudation resulting from uplift without the component of heating and subsequent cooling. Determination of the amount of denudation compared to rock uplift and sea level changes (calculated previously in this paper) provides a denudation estimate of 2.2 km for a tectonically intermediate geothermal gradient. Unpublished AFT data from S.A. Kelley (pers. comm., 2001) puts the fossil PAZ at around 2600 m in wells in the Texas and Oklahoma panhandles. These data collectively record nearly 2 km of removed material between the Logan well in New Mexico and wells in Oklahoma.

Tectonic Analysis

The purpose of this investigation was to use sonic well log velocities as well as apatite fission-track (AFT) thermochronology to evaluate the denudational and thermal history of the transition between the Southern Rocky Mountains and the High Plains. The three mechanisms proposed earlier to explain previous AFT results are 1) relaxation of isotherms following a heating event with affects extending hundreds of kilometers east of the Rio Grande rift; 2) regional epeirogenic surface uplift, which triggered denudation of the High Plains; or 3) some combination of the latter two mechanisms.

The single unit sonic log analysis yielded two erosion trends: northward decreasing erosion and westward increasing erosion. Ideally, data from additional wells from the center region would confirm these trends. The trends from the sonic log data strictly record denudation values related to uplift and erosion of the sediments. The AFT technique was incorporated in order to add a thermal component to the study.

The AFT data from the Logan well in NE New Mexico provided a cooling age of 34.7 Ma. Because vitrinite reflectance data (Scott et al., 1990) does not indicate extensive heating in the area of the Logan Well, the results from the Logan samples provide an estimate of denudation related to uplift and erosion. The RGC-CO and 14-21 Ortiz AFT data coupled with the vitrinite data indicate that the denudation values are related to cooling after a Cenozoic heating event, although there has been a component of uplift and erosion. Based on the results of my study, the third proposed mechanism has the most merit. The AFT data

from the Logan well in NE New Mexico indicate rock uplift values of 4.9 km and surface uplift of 1.2 km, which triggered denudation at 34.7 Ma. However, because the 1 RGC-CO samples reflect cooling after the Cenozoic heating event in the northern Raton basin, the relaxation of isotherms after a heating event is also supported. Therefore, the Raton Basin and Southern High Plains have experienced a combination of localized relaxation of isotherms after heating as well as denudation brought on by regional surface and rock uplift. The northern portion of the basin experienced a larger component of cooling following the heating event, while the southern areas have a greater component of denudation following uplift. The latter resulted in removal of nearly 2.5 km of sediment from the southern and western stratigraphic column, but left the northern and eastern sediments somewhat unaffected. The removal of 2.5 km is no small task.

Recently, several workers have correlated changes in climate with landscape features over the Cenozoic Period (Stroud and McIntosh, 1996; Galloway et al., 2000). By collecting well, seismic, and other published data, Galloway et al. (2000) were able to interpret the Cenozoic depositional history of the Gulf of Mexico. Their findings strongly indicate that the Southern Rocky Mountains and vicinity were responsible for massive amounts of deposition into the Gulf of Mexico during the middle to late Cenozoic. Their study identified the Rio Grande River system as one of the largest contributors of sediment to the Gulf of Mexico. It is unlikely the Rio Grande River was solely responsible for the removal of 2 km of sediment from the Raton Basin – High Plains region. However, the Arkansas River, the Colorado River in Texas, and several smaller

tributaries flow through the area as well. Although they are not mentioned by name, Galloway et al. (2000) indicated that most smaller river systems in this area eventually joined one of the several larger river systems and inevitably deposited sediment into the Gulf of Mexico.

Conclusions

Sonic log data can now be added to the long list of evidence that indicates that the Southern High Plains experienced significant post-Cretaceous denudation. Although previous sonic log studies only used shales, my work shows that the single unit method can be applied effectively to different lithologies to estimate erosion values. The shales, limestones, sandstones, and chalks of this study all indicate that the southern portion of the area underwent more erosion, nearly 2.5 km more than the northern region, which has an almost complete stratigraphic column. The multiple unit method did not estimate erosion as precisely as the single unit method because the stratigraphic column varied so greatly across the basin. The sonic logs substantiate a denudation history resulting from uplift for the wells analyzed.

The AFT data from across the study area coupled with AFT data from Texas and Oklahoma show that the fossil PAZ resides deeper in the subsurface in wells in the east, but becomes increasingly shallow and is not observed in surface exposures in the eastern Sangre de Cristo mountains near Las Vegas (Kelley and Chapin, 1995). Vitrinite reflectance data (Scott et al., 1990) coupled

with the AFT data for the Colorado portion of the study area record locally elevated temperatures during the Cenozoic. The sediments did not cool from this event until approximately 30 Ma. In contrast, AFT data from New Mexico show no sign of influence from volcanic sources. Similarly, the vitrinite data indicate through coal ranks that the New Mexico portion of the study area did not experience the same amount of heating as the Colorado portion. The Cenozoic history of the Raton Basin – High Plains area has therefore two tectonic elements: denudation due to uplift (dominant in the southern part of the region) and elevated heat flow (dominant in the northern part of the study area).

References

Allen, M.S., and E. McLemore, 1991. Geological, geochemical, and isotopic characteristics of the Lincoln County porphyry belt, New Mexico: implications for regional tectonics and mineral deposits: NM Geol. Soc. Guidebook 42, p. 97-102.

Applegate, J.K., and P.R. Rose, 1985. Structure of the Raton Basin from a regional seismic line, *in* Dyer, R.C., ed., Seismic exploration of the Rocky Mountain region: Rocky Mountain Association of Geologist and Denver Geophysical Society, p. 259-265.

Athy, L.F., 1930. Density, porosity, and compaction of sedimentary rocks: AAPG Bulletin, v. 14, p. 1-24.

Baltz, E. H., 1965. Stratigraphy and history of the Raton Basin and notes on San Luis Basin, Colorado-New Mexico: AAPG Bulletin, v. 49, p. 2041-2075.

Carlson, W.D., 1990. Mechanisms and kinetics of apatite fission-track annealing: American Mineralogist, v. 75, p. 1120-1139.

Carter, L.S., S.A. Kelley, D.D. Blackwell, and N.D. Naeser, 1998. Heat flow and thermal history of the Anadarko Basin, Oklahoma: AAPG Bulletin, v. 82, p. 291-316.

Clair, J. R., and R.W. Volk, 1968. Pre-Permian Paleozoic Rocks of the Las Animas Arch - A new oil province: The Mountain Geologist, v. 5, p. 95-107.

Clarkson, G., and M. Reiter, 1984. Analysis of terrestrial heat-flow profiles across the Rio Grande rift and southern Rocky Mountains in Northern New Mexico *in* Baldridge, W.S., P.W. Dickerson, R.E. Riecker, J. Zidek, eds., Rio Grande Rift: Northern New Mexico: NM Geol. Soc. 35th Field Conf. Guidebook, p. 39-44.

Cline, L. M., 1953. Raton Region Preliminary Statement, Field Trip of the Raton Basin Region and the Sangre de Cristo Mountains of New Mexico: Panhandle Geological Society, p. 5-8.

Close, J.C., and R.R. Dutcher, 1990. Update on Coalbed Methane Potential of the Raton Basin, Colorado and New Mexico: Society of Petroleum Engineers Special Paper 20667, p. 497-512.

Dane, C.H., and G.O. Bachman, 1965. Geologic map of New Mexico: U.S. Geological Survey Special Geologic Map, scale 1:500,000.

Davis, L.L., D. Smith, F.W. McDowell, N.W. Walker, and L.E. Borg, 1996. Eocene potassic magmatism at Two Buttes, Colorado, with implications for Cenozoic tectonics and magma generation in the western United States: Geol. Soc. Am. Bulletin, v. 108, p. 1567-1579.

Edwards, C.L, M. Reiter, C. Shearer, and W. Young, 1978. Terrestrial heat flow and crustal radioactivity in northeastern New Mexico and southeastern Colorado: Geol. Soc. of Am. Bulletin, v. 89, p. 1341-1350.

Galbraith, R.F., 1981. On statistical models for fission track counts: Math. Geol., v. 13, p. 471-478.

Galloway, W.E., P.E. Ganey-Curry, X. Li, and R.T. Buffler, 2000. Cenozoic depositional history of the Gulf of Mexico basin: AAPG Bulletin, v. 84, p. 1743-1774.

Gibson, A.A., R.N. Thompson, P.T. Leat, M.A. Morrison, G.L. Hendry, A.P. Dickin, and J.G. Mitchell, 1993. Ultrapotassic magmas along the flanks of the Oligo-Miocene Rio Grande rift, USA: Monitors of the zone of lithosphereic mantle extension and thinning beneath a continental rift: Journal of Petrology, v. 34, p. 187-228.

Haun, J. D., 1968. Stratigraphy of the Dakota Group and relationship to petroleum occurrence, northern Denver Basin: Rocky Mountain Association of Geologists 14th Field Conference Guidebook, v. 14, p. 119-134.

Hawley, J.W., 1984. The Ogallala Formation in eastern New Mexico *in* Proceedings of the Ogallala Aquifer Symposium II, Lubbock, TX, p. 157-176.

Hayes, P.T., 1957. Possible igneous origin of Turkey Mountain dome, Mora County, New Mexico: AAPG Bulletin, v. 41, p. 953-956.

Heasler, H.P., and N.A. Kharitonova, 1996. Analysis of Sonic well logs applied to erosion estimates in the Bighorn Basin, Wyoming: AAPG Bulletin, v. 80, p. 630-646.

Hillis, R.R., 1995. Quantification of Tertiary Exhumation in the United Kingdom Southern North Sea using Sonic Velocity Data: AAPG Bulletin, v. 79, p. 130-152.

Jacob, A. F., 1983. Mountain front thrust, Southeastern Front Range and Northeastern Wet Mountains, Colorado: Rocky Mountain Association of Geologists, v. 83, p. 229-244.

Kelley, S.A., C.E. Chapin, and J. Corrigan, 1992. Late Mesozoic to Cenozoic cooling histories of the flanks of the northern and central Rio Grande rift, Colorado and New Mexico: New Mexico Bureau of Mines and Mineral Resources Bulletin 145, p. 1-39.

Kelley, S.A., and C.E. Chapin, 1995. Apatite fission-track thermochronology of the Southern Rocky Mountains – Rio Grande rift – Western High Plains provinces: NM Geol. Soc. Guidebook 46, p. 87-96.

Ketchum, R.A., R.A. Donelick, and W.D. Carlson, 1999. Variability of apatite fission track annealing kinetics III: Extrapolation to geological time scales: American Mineralogist, v. 84, p. 1235-1255.

Ketchum, R.A., R.A. Donelick, and M.B. Donelick, 2000. AFTSolve: A program for multi-kinetic modeling of apatite fission-track data: Geological Materials Research, v.2, p. 87-96.

Liu, G., and E. Roaldset, 1994. A new decompaction model and its application to the North Sea: First Break, v. 12, p. 81-89.

Magara, K., 1976. Thickness of removed sedimentary rocks, paleopore pressure, and paleotemperature, southwestern part of Western Canada basin: AAPG Bulletin, v. 60, p. 554-566.

Magara, K., 1980. Comparisons of porosity/depth relationships of shale and sandstone: Journal of Petroleum Geology, v. 3, p. 92-102.

Mallory, W. W., 1977. Oil and gas from fractured shale reservoirs in Colorado and northwestern New Mexico: Rocky Mountain Association of Geologists Special Publication 1, p. 1-38.

Miggins, D.P., L.W. Snee, C.L. Pillmore, J.R. Budahn, M.J. Kunk, and C.R. Stern, 1999. $^{40}AR/^{39}AR$ Geochronology and Geochemistry of sills within the cretaceous Pierre Shale near the Spanish Peaks in South Central Colorado: Geol. Soc. Am. Abstracts with Programs, v. 31, p. 158.

Miller, J. P., A. Montomery, and P.K. Sutherland., 1963. Geology of part of the Southern Sangre de Cristo Mountains, New Mexico: New Mexico Bureau of Mines and Mineral Resources Memorandum Mem. 11, p. 1-106.

Moore, D.S., and G. P. McCabe, 1993. Introduction to the Practice of Statistics: W.H. Freeman and Company, New York, NY. Second Edition, p. 117-147, 638-686.

Naeser, C.W., 1979. Fission-track dating and geologic annealing of fission tracks, *in* Jager, E., and J.C. Hunziker, eds., Lectures in isotope geology: Springer-Verlag, New York, p. 154-169.

O'Neill, J.M., and H.H. Mehnert, 1988. Petrology and physiographic evolution of the Ocate volcanic field, north-central New Mexico: U.S. Geological Survey Professional Paper 1478-A, p. 1-30.

Penn, B.S., and D. A. Lindsey, 1996. Tertiary igneous rocks and Laramide structure and stratigraphy of the Spanish Peaks region, south-central Colorado: Road Log and description from Walsenburg to La Veta (first day) and Le Veta to Aguilar (second day): Colorado Geological Survey: Open-File Report 96-4, p. 9.

Penn, B.S., L.W. Snee, and R.F. Wendlandt, 1992. $^{40}Ar/^{39}Ar$ geochronologic constraints on the intrusive history of the Spanish Peaks area in south-central Colorado: American Geophysical Union, EOS, v. 73, p. 657.

Pilione, L.J., D.P. Gold, and E.W. Kreiger, 1977. Fission-track age of apatite from a lamprophyre dike in the Two Buttes igneous complex, southeastern CO: Geol. Soc. Am. Abstracts with Programs, v. 9, p. 641-642.

Rascoe, B., Jr., 1978. Late Paleozoic structural evolution of the Las Animas arch, *in* Pruit, J.D., and P.E. Coffin, eds., Energy resources of the Denver basin symposium: Rocky Mountain Association of Geologists, Denver, p. 237-244

Scott, G.R., R.E. Wilcox, and H.H. Mehnert, 1990. Geology of Volcanic and Subvolcanic Rocks of the Raton-Springer Area, Colfax and Union Counties, New Mexico: U.S. Geological Survey Professional Paper #1507, p. 1-58.

Scott, A.R., and W.R. Kaiser, 1991. Coalbed Methane Potential of the Greater Green River, Piceance, Powder River, and Raton Basin: Gas Research Institute Topical Report # 0315, p. 1-275.

Selley, R.C., 1978. Porosity gradients in the North Sea oil-bearing sandstones: Journal of Geological Society of London, v. 135, p. 119-132.

Speer, W.R., 1976. Oil and gas exploration in the Raton Basin: NM Geol. Soc. 27th Field Conf. Guidebook, p. 217 – 226.

Stroud, J.R., 1997. The Geochronology of the Raton-Clayton volcanic field, with implications for volcanic history and landscape evolution: M.S. Thesis, New Mexico Institute of Mining and Technology, Socorro, NM, p. 1-51.

Stroud, J.R., and W.C. McIntosh, 1996. The volcanic history and landscape evolution of the Raton-Clayton volcanic field, New Mexico: Geol. Soc. Am. Abstracts with Programs 28, p. 260.

Tweto, O., 1979. Geologic map of Colorado: U.S. Geological Survey Special Geological Map, scale 1:500,000.

Viele, G.W., and W.A. Thomas, 1989. Tectonic synthesis of the Ouachita Orogenic Belt *in* The Appalachian-Ouachita Orogen in the United States: Geol. Soc. Am. DNAG F-2, p. 695-728.

Weimer, R. J., 1980. Recurrent movement on basement faults, a tectonic style for Colorado and adjacent areas *in* Kent, H.C., and K.W. Porter, eds., Colorado Geology: Rocky Mountain Association of Geologists, p. 23-35.

Woodward, L.A., 1984. Potential for significant oil and gas fracture reservoirs in Cretaceous rocks of Raton Basin, New Mexico. The Am. Assoc. of Pet. Geol. Bulletin, v. 68, p. 628-636.

Woodward, L.A., 1987a. Oil and Gas Potential of the Raton Basin, New Mexico. NM Geological Society 38th Field Conf. Guidebook, p. 331-337.

Woodward, L.A., 1987b. Tectonic Framework of Northeastern New Mexico and Adjacent parts of Colorado, Oklahoma, and Texas: NM Geol. Soc. Guidebook 38th Field Conf., p. 67-71.

Woodward, L.A., and D.O. Snyder, 1976. Structural Framework of the Southern Raton Basin, New Mexico: NM Geol. Soc. 27th Field Conf. Guidebook, p. 125-127.

Appendix A: Root Mean Squared (RMS) and Average Absolute Value (AAV)

Root Mean Square (RMS) and Average Absolute Value (AAV) are two statistical methods used to evaluate the closeness of calculated data to observed data. In the case of this study, the two were paired in order to determine the most accurate shift constant for each well. Each shift constant and the corresponding transit time curve was assessed with both RMS and AAV. The lower the RMS and AAV, the closer the calculated data are to the actual data. In the case where RMS and AAV error predictions are very close, the one with the lowest AAV is chosen since AAV is less influenced by errors and thus taken to be the more accurate. The equations are explained below.

$$RMS = \sqrt{1/N \, \Sigma(D_i - C_i)^2}$$

Where D_i are the measured values, C_i are the corresponding calculated values, and N is the shift constant in question.

$$AAV = 1/N \, \Sigma|D_i - C_i|$$

Where D_i are the measured values, C_i are the corresponding calculated values, and N is the shift constant in question.

Appendix B: Single Unit Erosion Estimates

Unit		Dakota			Graneros				Greenhorn Shale			
Well	Ave TT	Midpt	EA (ft)	EA (m)	Ave TT	Midpt	EA (ft)	EA (m)	Ave TT	Midpt	EA (ft)	EA (m)
BDCDGU 1833												
BDCDGU 1832												
Medina												
State "FA"	93.8	373	1777	542								
Earl "B"												
Castle Rock												
State 1-5												
State 1-18	95.6	613	1150	350	120.3	473	2764	843	110.4	390	2629	801
AP Tanner												
Federal 1 (K)	100.9	595	C	0	101.7	500	4609	1405	112.9	430	2190	668
Phelps Dodge	73.9	3275	3207	977	80.0	3098	4203	1281	83.8	3060	4120	1256
Cuerno Verde	87.5	2855	674	206	109.5	2720	1602	488	110.8	2640	318	97
Sam Taylor	59.9	3788	5729	1746	68.5	3635	4828	1472	73.6	3533	5230	1594
CF & L No. 1	68.4	4650	3031	924	81.6	4480	2664	812	79.1	4400	3504	1068
Reinhert	89.5	1130	1967	599	125.9	1030	1633	498	106.0	945	2751	839
John Brown	95.8	815	892	272	123.4	745	2176	663	112.6	663	2008	612
Walker	75.3	6205	C	0	87.0	6110	C	0	90.9	6045	C	0
Geommer 5												
Goemmer 1	64.1	5605	3004	916	84.3	5460	1408	429	82.3	5422	1988	606
State "EX"	70.5	620	6598	2011	104.7	450	4355	1327				
NM "B" #3												
Shell State	76.3	903	5044	1537	93.4	705	5248	1599				
Ft. Union	66.9	998	7002	2134	73.6	905	7045	2147	80.0	750	7012	2137
Merrick	93.3	935	1318	402	119.2	850	2494	760	104.8	765	3121	951
Parsons	58.4	3350	6490	1978	89.2	3245	3131	954	63.3	3060	7310	2228
21-4 True State	83.4	1080	3328	1014	111.1	965	3194	974	98.8	870	3952	1204
Arnold Harriman	89.9	948	2048	624	108.5	1100	3327	1014	95.3	1018	4365	1331
Federal Jordan					145.8	663	C	0	110.8	573	2375	724
Federal 1 (O)	98.4	948	216	66	109.9	878	3406	1038	99.3	795	3957	1206
11-31 Green	82.8	2905	1638	499	108.7	2800	1605	489	80.2	2695	5034	1535
Porter	84.1	1810	2450	747	104.2	1714	3145	959	91.7	1645	4286	1306
State 1-19	92.0	1550	995	303	105.7	1440	3270	997	91.6	1345	4613	1406
BDCDGU 2332												
Caroline												
Jolla Land												
Union "B" St.												
State "EV"												
Will Rose									105.8	602	3132	955
Mora	70.4	846	6404	1952	91.9	672	5429	1655	92	582	5309	1618
Baughman	93.5	980	1237	377					109.5	725	2431	741
Iannitti	90.7	1230	1596	486	120.4	1112	2110	643	110.3	1037	1994	608
Hardy 1	92.1	600	1922	586	129.5	517	1786	544	126.7	470	C	0
Meek-Newsom	90.2	995	1940	591	125.0	885	1873	571	114	795	1658	505
Thomas	92.9	660	1688	515								
Dog Spring												

Unit	Greenhorn Limestone				Niobrara				Pierre Shale			
Well	Ave TT	Midpt	EA (ft)	EA (m)	Ave TT	Midpt	EA (ft)	EA (m)	Ave TT	Midpt	EA (ft)	EA (m)
BDCDGU 1833												
BDCDGU 1832												
Medina												
State "FA"												
Earl "B"												
Castle Rock												
State 1-5												
State 1-18	94.3	345	1967	600								
AP Tanner												
Federal 1 (K)	101.7	360	777	237								
Phelps Dodge	82.4	2975	1226	374	76.4	2155	3288	1002	85.7	1750	3028	923
Cuerno Verde	86.9	2575	923	281	100.6	1900	853	260	104.5	1150	636	194
Sam Taylor	56.5	3475	4844	1477	62.7	2650	4317	1316	96.6	1400	1655	504
CF & L No. 1	68.1	4330	2146	654	77.4	3625	1707	520	88.6	1850	2470	753
Reinhert	94.0	875	1488	454	120.0	480	121	37				
John Browm	88.5	588	2654	809								
Walker	71.1	5990	C	0	77.3	5320	C	0	89.1	4350	C	0
Geommer 5									67.1	5260	2466	752
Goemmer 1	71.9	5375	494	150	73.8	4750	987	301	90.8	3150	819	250
State "EX"												
NM "B" #3									90.3	358	3694	1126
Shell State												
Ft. Union												
Merrick	94.9	685	1538	469								
Parsons	59.2	2950	4945	1507	92.0	2245	1461	445				
21-4 True State	85.0	795	3000	915	105.9	425	1745	532				
Arnold Harriman	80.7	945	3527	1075	91.7	475	3272	997				
Federal Jordan	78.0	500	4397	1340								
Federal 1 (O)	78.6	723	4083	1245	59.1	200	7164	2184				
11-31 Green	77.4	2640	2368	722	83.6	2125	2520	768	110.0	925	C	0
Porter	77.6	1575	3401	1037	82.5	1030	3742	1141	102.5	550	1556	474
State 1-19	80.0	1280	3301	1006	86.0	735	3648	1112	94.0	450	3005	916
BDCDGU 2332												
Caroline												
Jolla Land												
Union "B" St.												
State "EV"												
Will Rose	90	540	2460	750								
Mora	65	510	6458	1968								
Baughman	93.9	662	1719	524								
Iannitti	102.2	972	91	28	120.3	562	C	0				
Hardy 1	106.3	412	C	0								
Meek-Newsom	101	722	532	162								
Thomas												
Dog Spring									80.7	3127	2444	745

Unit Well	Average (ft) Shale/Lmst	Average (m) Shale/Lmst	Average (ft) All	Average (m) All
BDCDGU 1833				
BDCDGU 1832				
Medina				
State "FA"			1777	542
Earl "B"				
Castle Rock				
State 1-5				
State 1-18	2454	748	2128	648
AP Tanner				
Federal 1 (K)	2526	770	2526	770
Phelps Dodge	3173	967	3179	969
Cuerno Verde	866	264	834	254
Sam Taylor	4175	1273	4434	1351
CF & L No. 1	2498	761	2587	789
Reinhert	1498	457	1592	485
John Browm	2280	695	1933	589
Walker	0	0	0	0
Geommer 5	2466	752	2466	752
Goemmer 1	1139	347	1450	442
State "EX"	4355	1327	5476	1669
NM "B" #3	3694	1126	3694	1126
Shell State	5248	1599	5146	1568
Ft. Union	7029	2142	7020	2140
Merrick	2384	727	2118	645
Parsons	4212	1284	4667	1423
21-4 True State	2973	906	3044	928
Arnold Harriman	3623	1104	3308	1008
Federal Jordan	3386	1032	3386	1032
Federal 1 (O)	4653	1418	3765	1148
11-31 Green	2882	878	2633	803
Porter	3226	983	3097	944
State 1-19	3568	1087	3139	957
BDCDGU 2332				
Caroline				
Jolla Land				
Union "B" St.				
State "EV"				
Will Rose	2796	852	2796	852
Mora	5732	1747	5900	1798
Baughman	2075	632	1796	547
Iannitti	1399	426	1448	441
Hardy 1	1786	544	1854	565
Meek-Newsom	1354	413	1501	457
Thomas			1688	515
Dog Spring	2444	745	2444	745

Appendix C: Crossplots

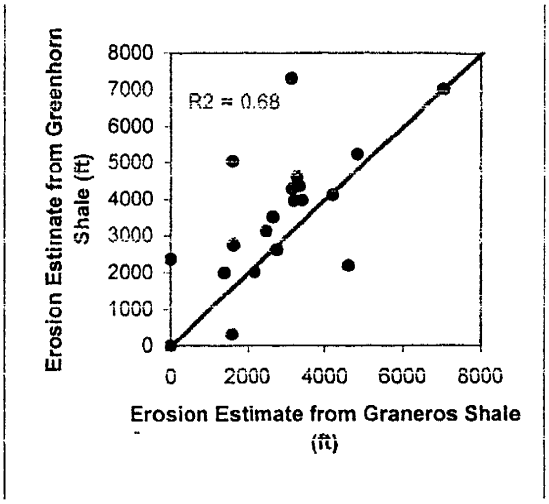
Erosion Estimate from Greenhorn Shale (ft)
R2 = 0.68
Erosion Estimate from Graneros Shale (ft)
0
1000
2000
3000
4000
5000
6000
7000
8000
0
2000
4000
6000
8000

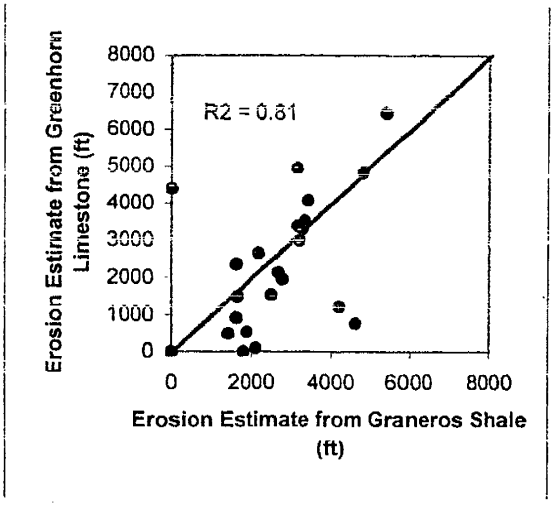
Erosion Estimate from Greenhorn Limestone (ft)
R2 = 0.61
Erosion Estimate from Graneros Shale (ft)
0
1000
2000
3000
4000
5000
6000
7000
8000
0
2000
4000
6000
8000

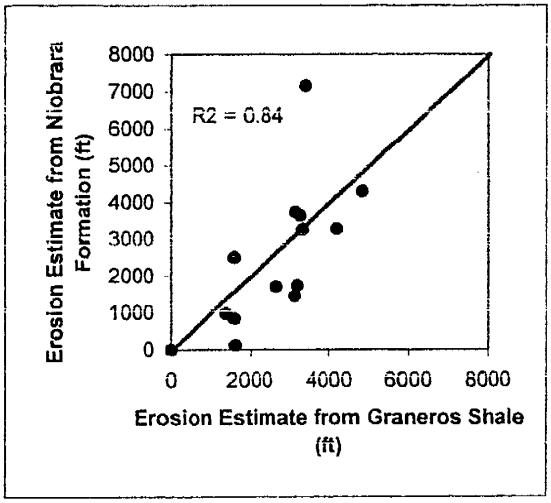
Erosion Estimate from Niobrara Formation (ft)
R2 = 0.64
Erosion Estimate from Graneros Shale (ft)
0
1000
2000
3000
4000
5000
6000
7000
8000
0
2000
4000
6000
8000

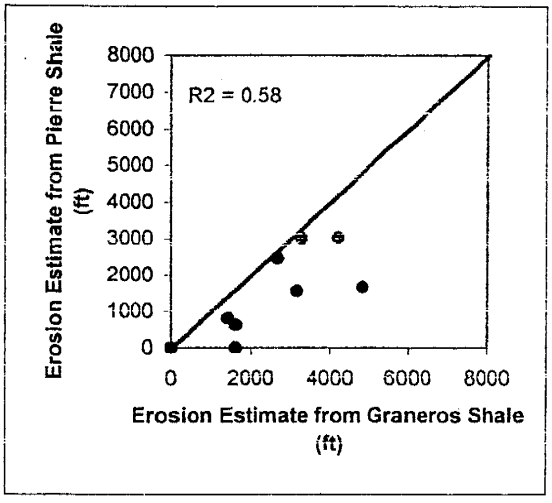
Erosion Estimate from Pierre Shale (ft)
R2 = 0.58
Erosion Estimate from Graneros Shale (ft)
0
1000
2000
3000
4000
5000
6000
7000
8000
0
2000
4000
6000
8000

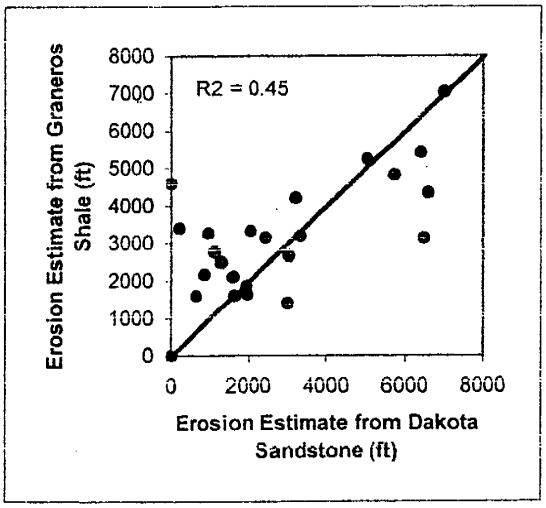
Erosion Estimate from Graneros Shale (ft)
R2 = 0.45
Erosion Estimate from Dakota Sandstone (ft)
0
1000
2000
3000
4000
5000
6000
7000
8000
0
2000
4000
6000
8000

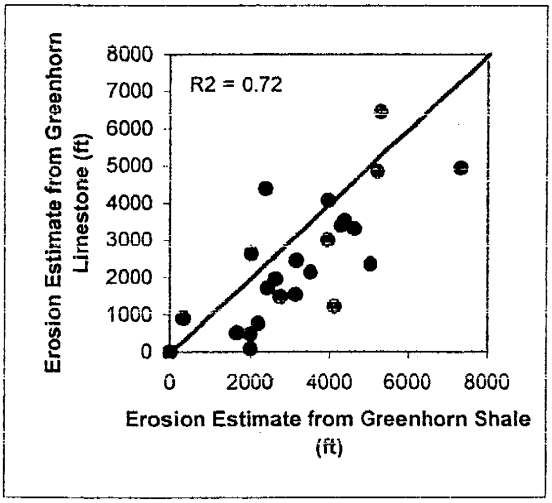
Erosion Estimate from Greenhorn Limestone (ft)
R2 = 0.72
Erosion Estimate from Greenhorn Shale (ft)
0
1000
2000
3000
4000
5000
6000
7000
8000
0
2000
4000
6000
8000

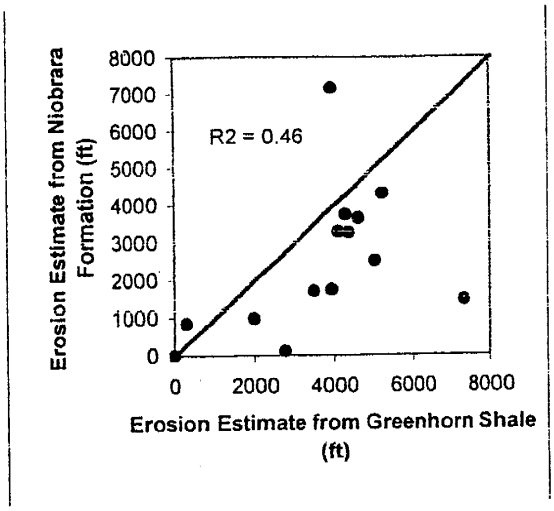
Erosion Estimate from Niobrara Formation (ft)
R2 = 0.46
Erosion Estimate from Greenhorn Shale (ft)
0
1000
2000
3000
4000
5000
6000
7000
8000

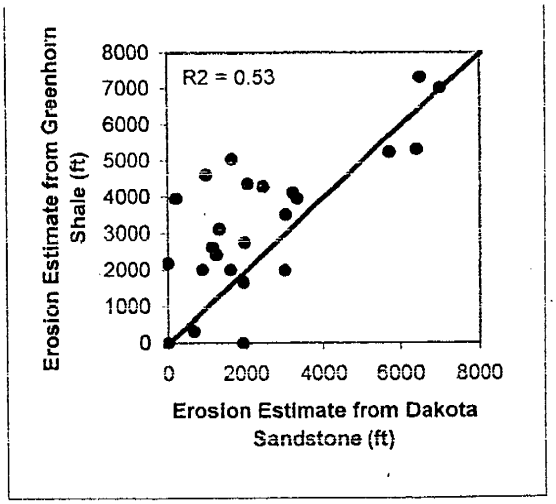
Erosion Estimate from Greenhorn Shale (ft)
R2 = 0.53
Erosion Estimate from Dakota Sandstone (ft)
0
1000
2000
3000
4000
5000
6000
7000
8000

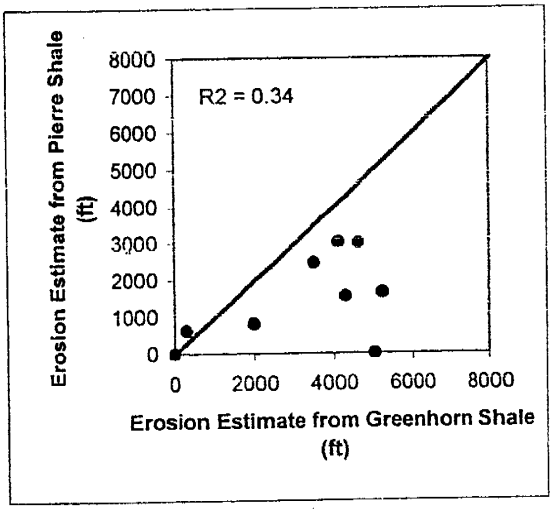
Erosion Estimate from Pierre Shale (ft)
R2 = 0.34
Erosion Estimate from Greenhorn Shale (ft)
0
1000
2000
3000
4000
5000
6000
7000
8000

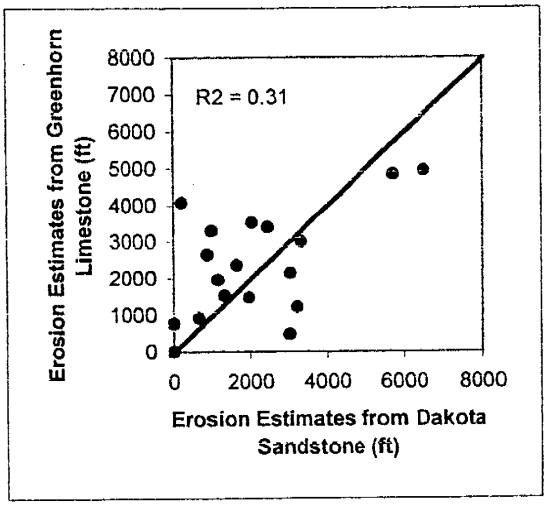
Erosion Estimates from Greenhorn Limestone (ft)
R2 = 0.31
Erosion Estimates from Dakota Sandstone (ft)
0
1000
2000
3000
4000
5000
6000
7000
8000

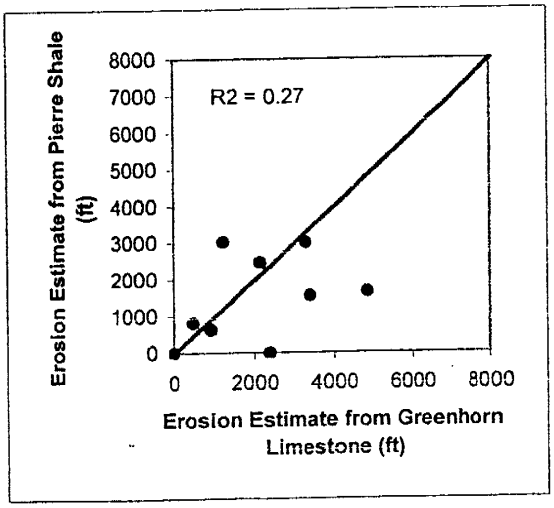
Erosion Estimate from Pierre Shale (ft)
R2 = 0.27
Erosion Estimate from Greenhorn Limestone (ft)
0
1000
2000
3000
4000
5000
6000
7000
8000

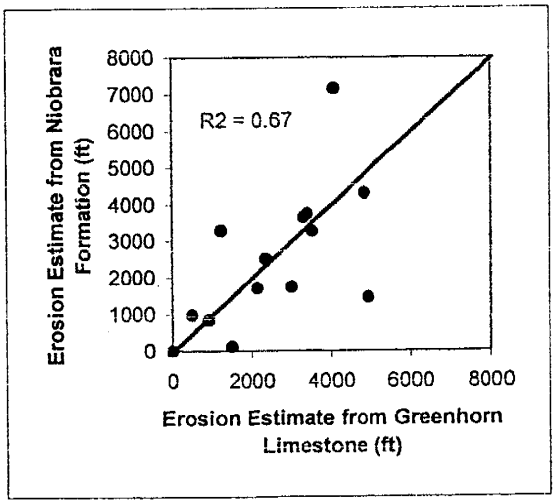
Erosion Estimate from Niobrara Formation (ft)
R2 = 0.67
Erosion Estimate from Greenhorn Limestone (ft)
0
1000
2000
3000
4000
5000
6000
7000
8000

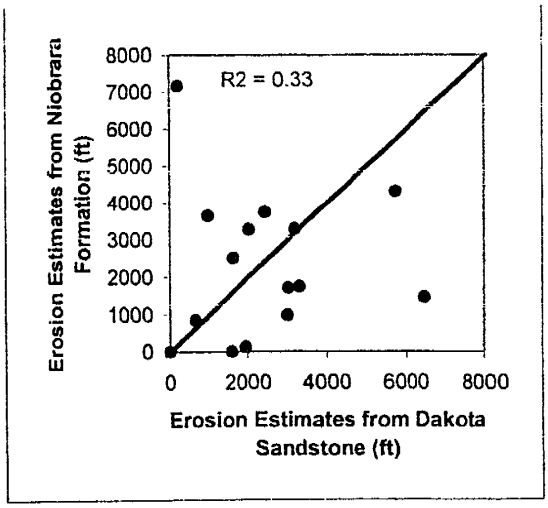
Erosion Estimates from Niobrara Formation (ft)
8000
7000
6000
5000
4000
3000
2000
1000
0
R2 = 0.33
0
2000
4000
6000
8000
Erosion Estimates from Dakota Sandstone (ft)

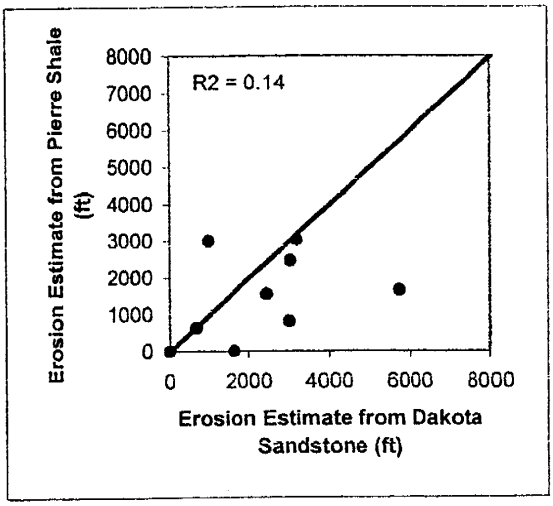
Erosion Estimate from Pierre Shale (ft)
8000
7000
6000
5000
4000
3000
2000
1000
0
R2 = 0.14
0
2000
4000
6000
8000
Erosion Estimate from Dakota Sandstone (ft)

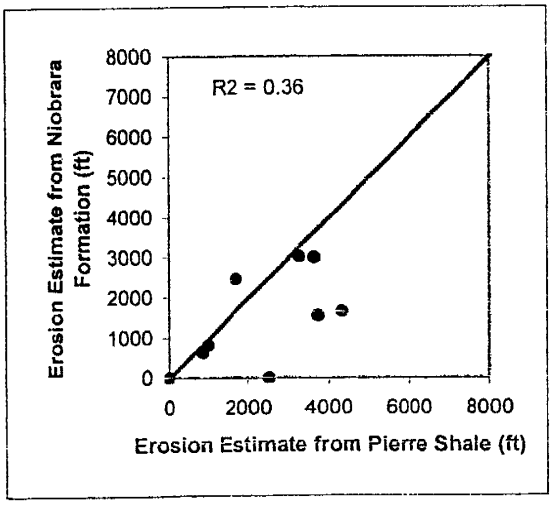
Erosion Estimate from Niobrara Formation (ft)
8000
7000
6000
5000
4000
3000
2000
1000
0
R2 = 0.36
0
2000
4000
6000
8000
Erosion Estimate from Pierre Shale (ft)

Appendix D: Multiple Unit Erosion Estimates (Transit Time Versus Depth Plots)

Appendix D contains the graph for each well used in the entire well method. The vertical axis is depth within the well in feet, and the horizontal axis is the corresponding sonic transit time reading in microseconds per foot (μs/ft). Points were taken from the sonic log every five feet. The shift constant chosen and the resulting predicted magnitude of erosion are listed in the upper left-hand corner of each graph. The dashed line represents the corrected exponential curve.

There are several cases where the scatter of points ends abruptly, forming a vacant, vertical space. This occurs where the sonic log that was digitized did not have continuous wrap-around or the copy of the sonic log had been cut off or taped over.

Porter No. 1-28

Twp 21S Rng 61W Sec 28

Pueblo, CO

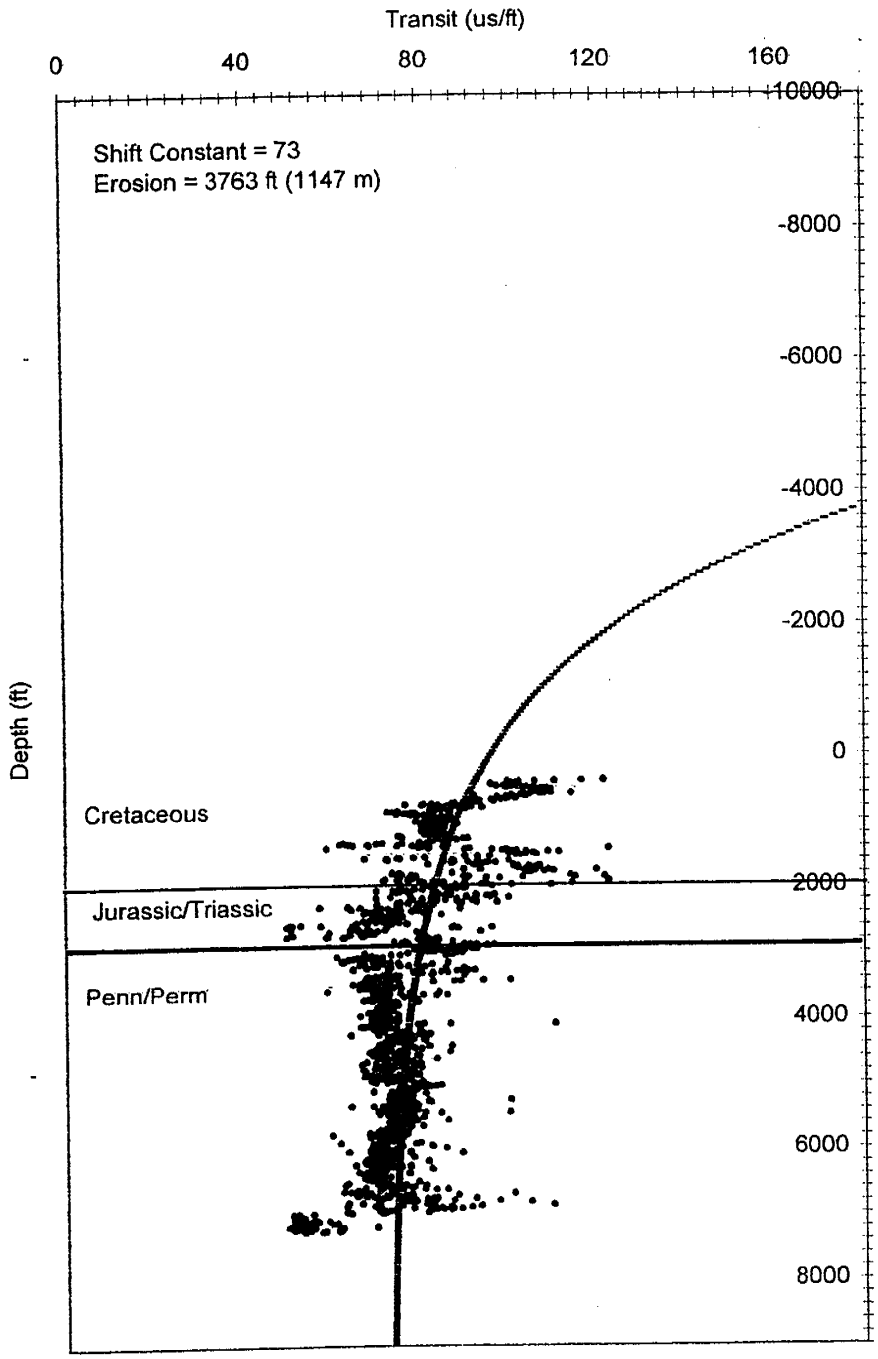

State No. 1-19

Twp 22S Rng 60W Sec 19

Pueblo, CO

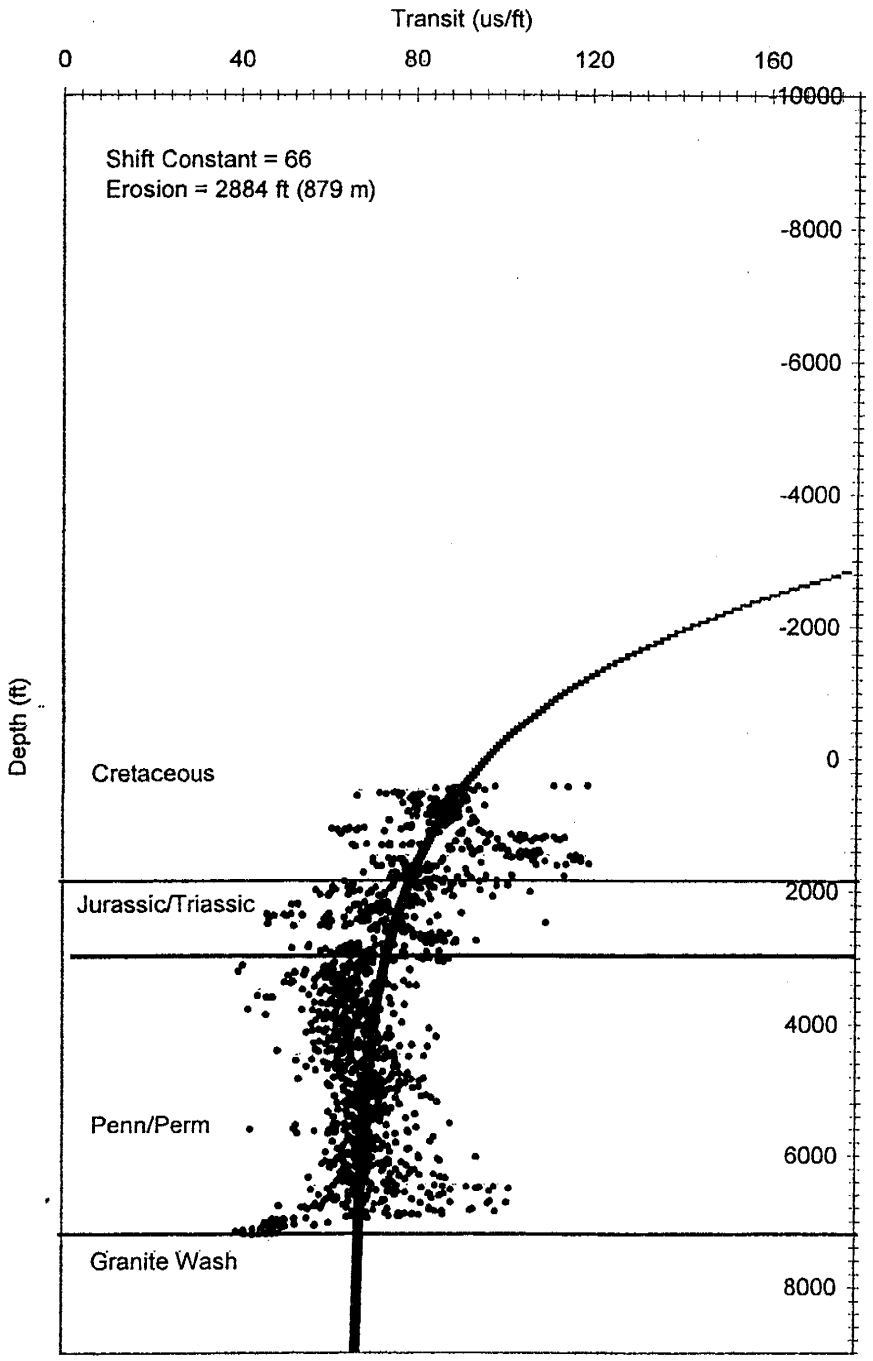

11-31 Green

Twp 19S Rng 60W Sec 31

Pueblo, CO

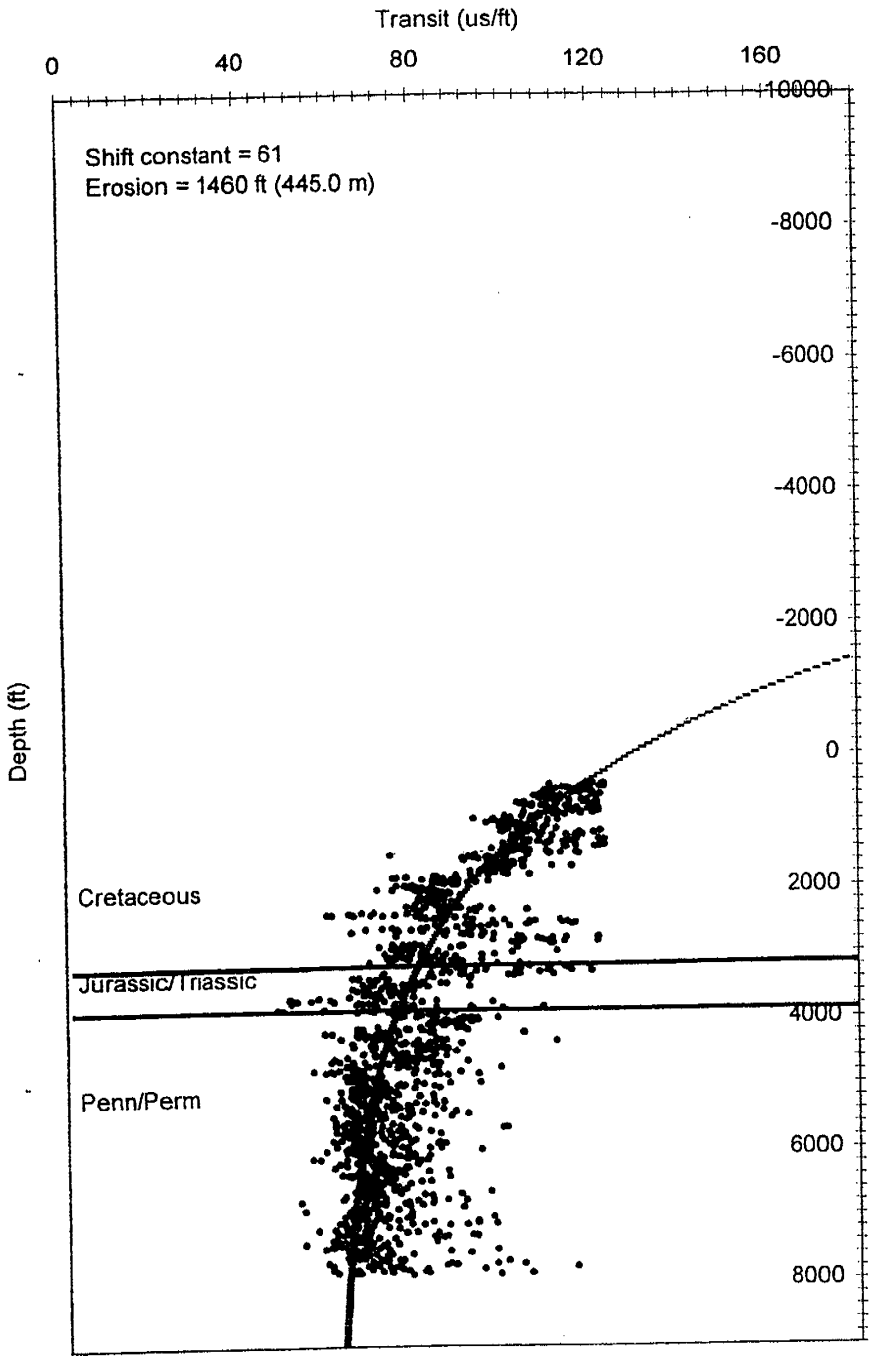

Federal No. 1

Twp 25S Rng 59W Sec 11

Otero, CO

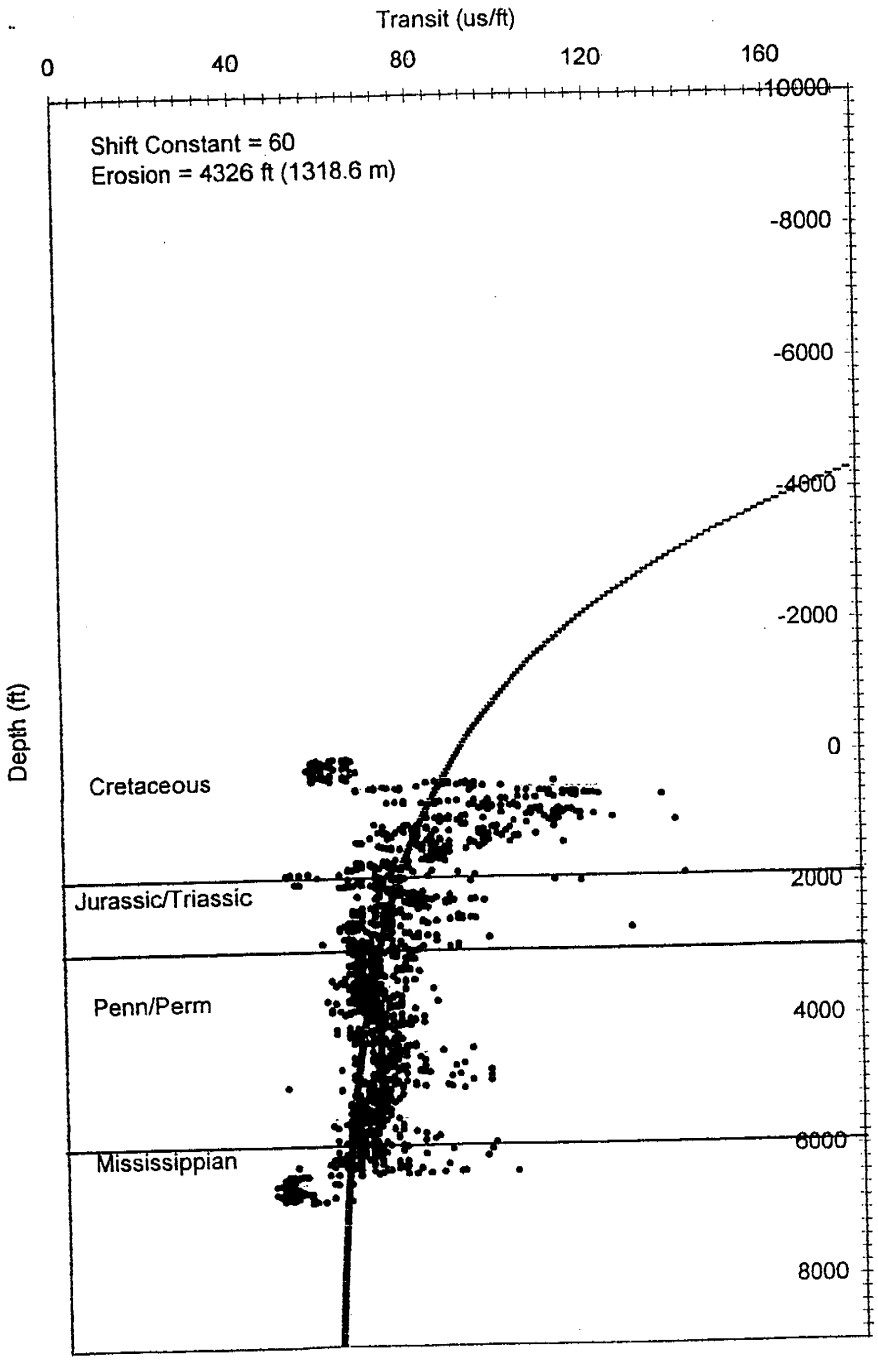

Arnold-Harriman Co. #1

Twp 23S Rng 59W Sec 5

Otero, CO

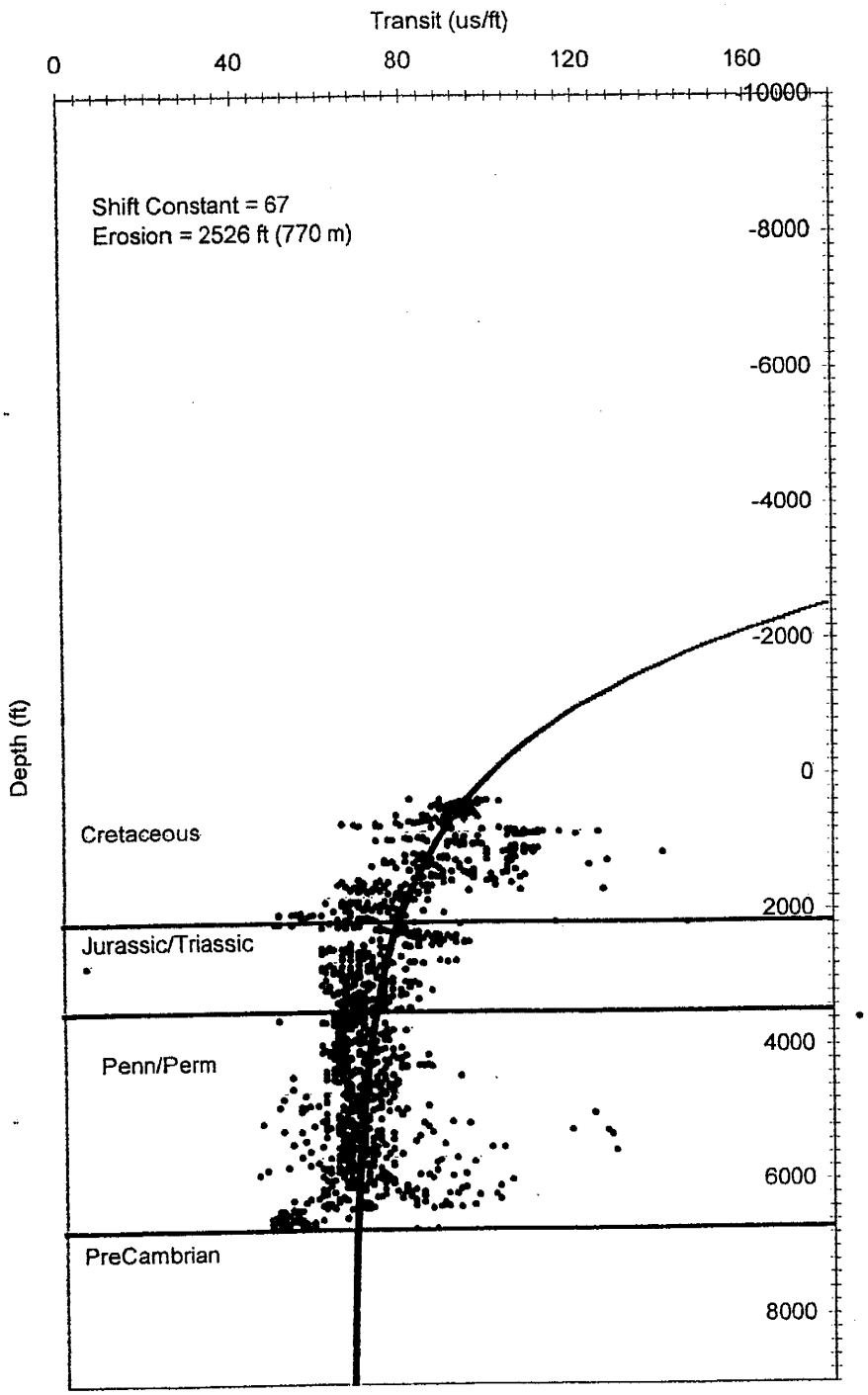

State "EX" No. 1

Twp 25N Rng 25E Sec 14

Colfax, NM

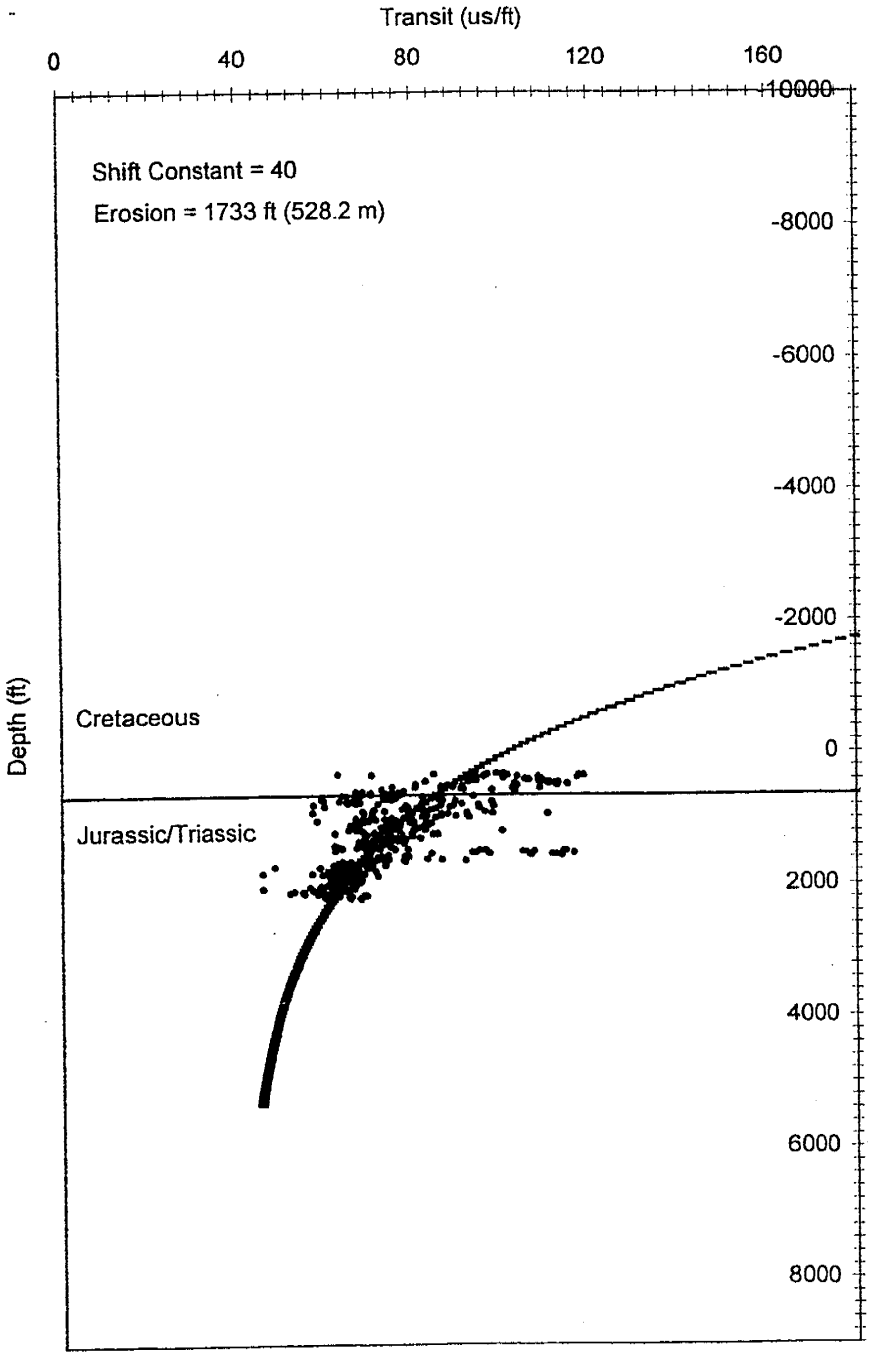

New Mexico "B" No. 3

Twp 30N Rng 13E Sec 22

Colfax, NM

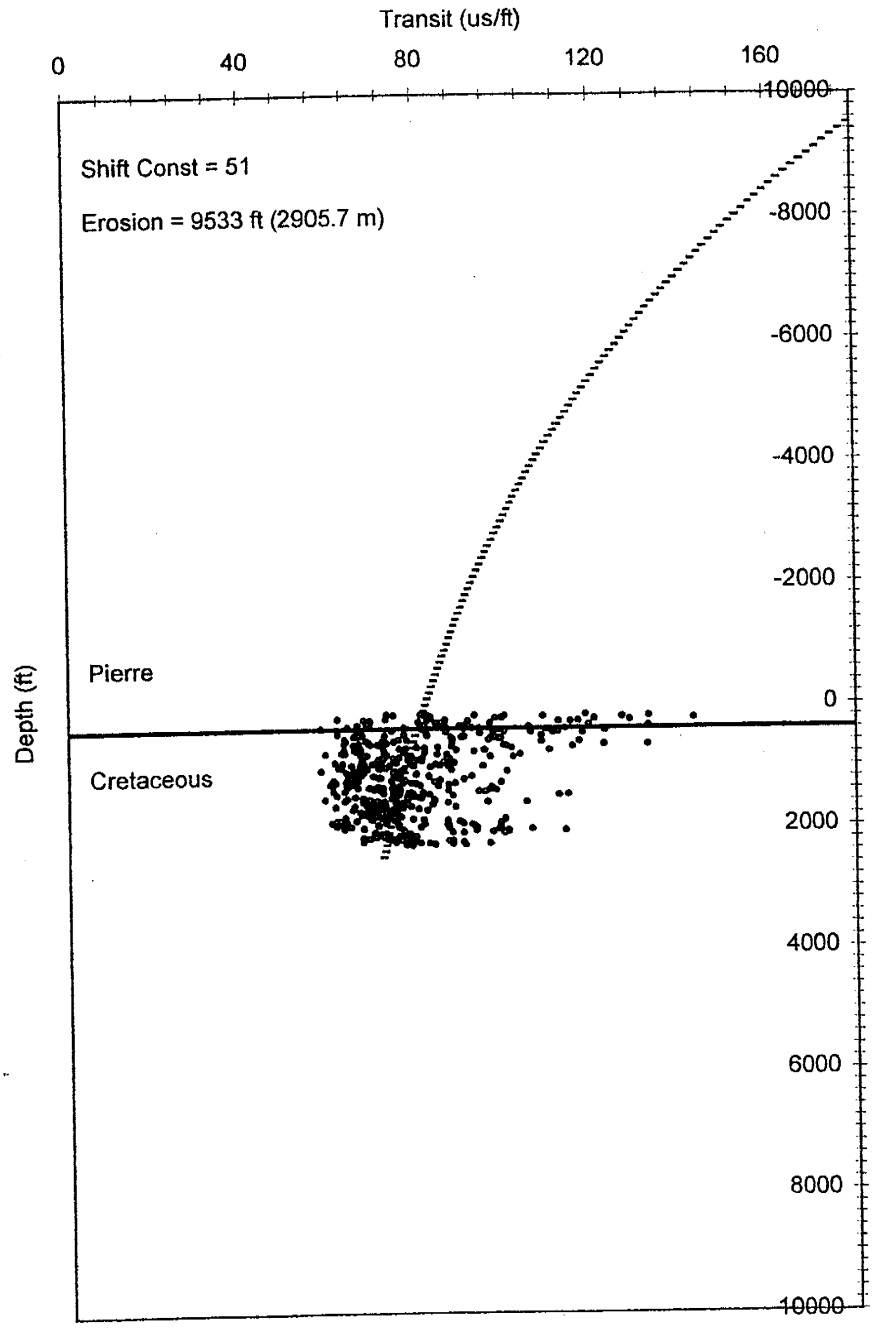

#1 Shell State

Twp 23N Rng 22E Sec 35

Mora, NM

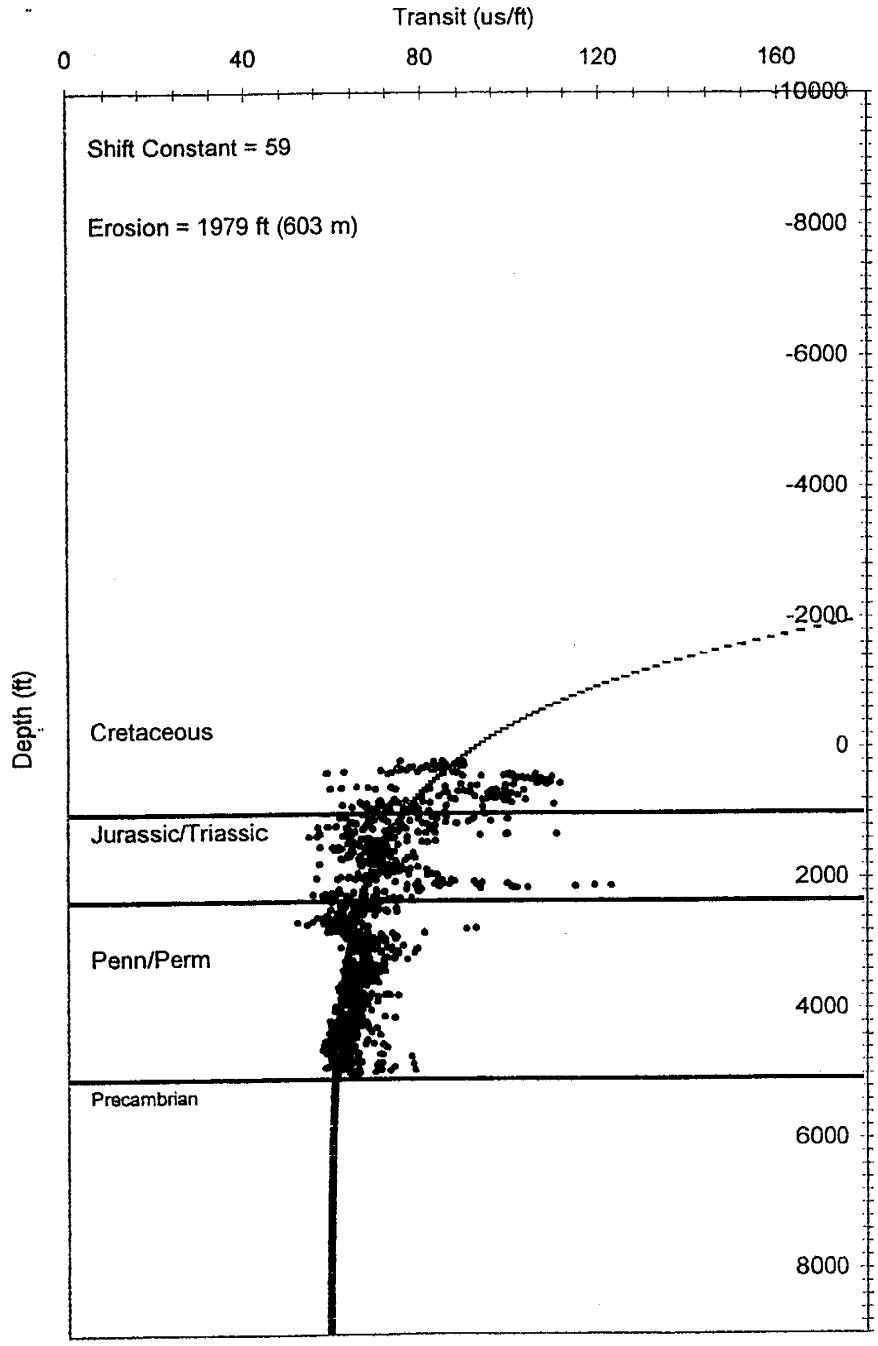

Parsons #1

Twp 32S Rng 68W Sec 18

Las Animas, CO

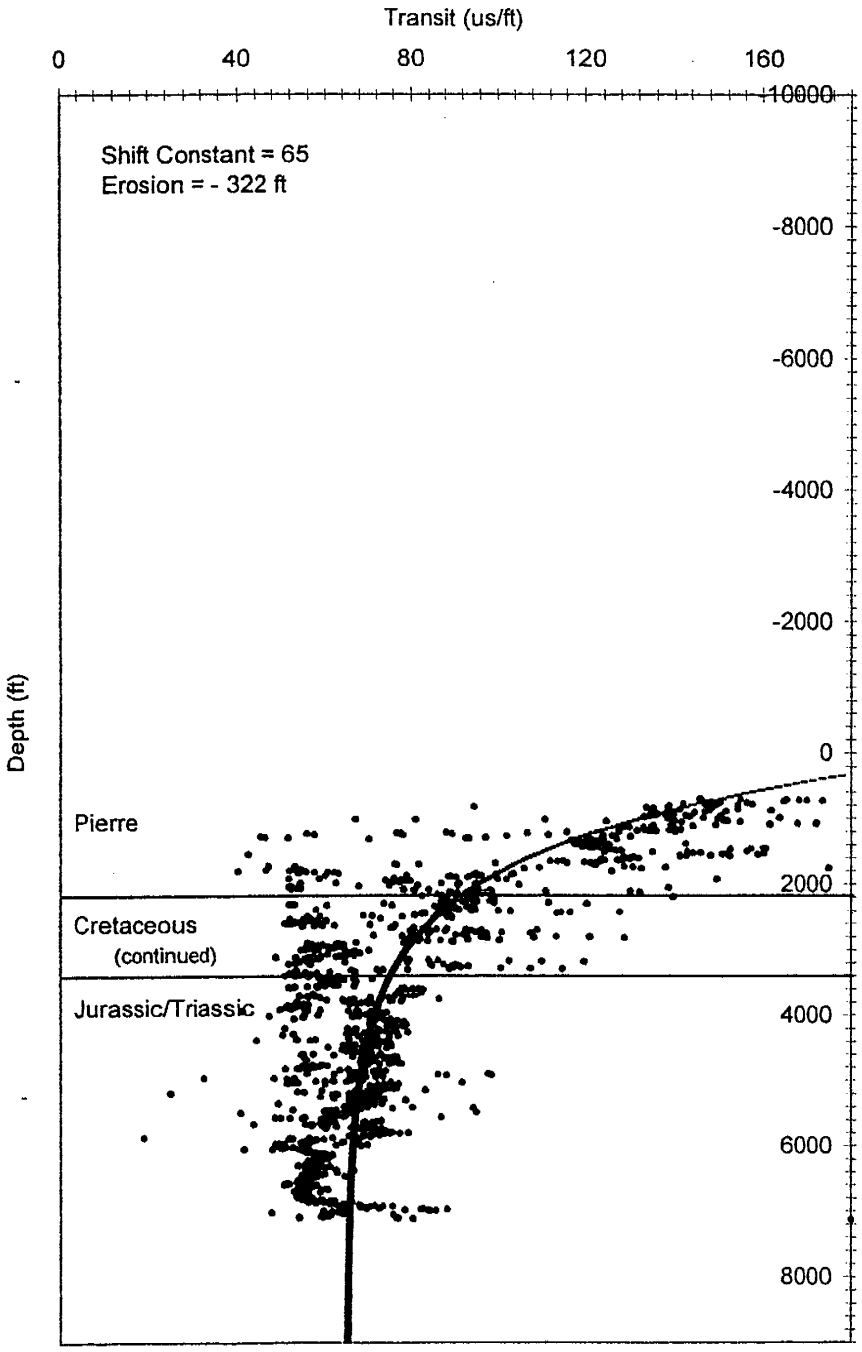

#1 Ft. Union

Twp 20N Rng 19E

Mora, NM

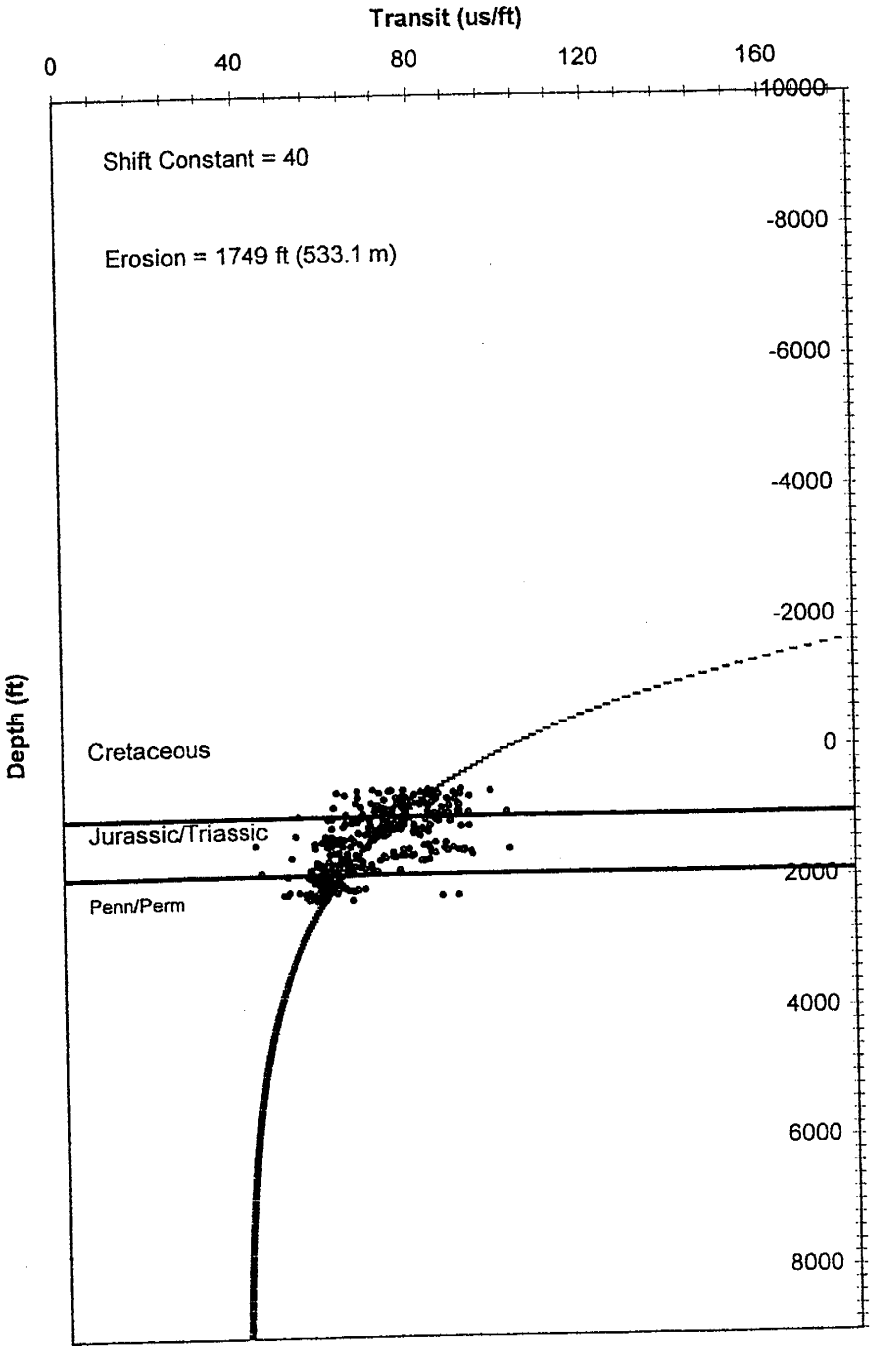

CF and L No. 1

Twp 35S Rng 68W Sec 16

Las Animas, CO

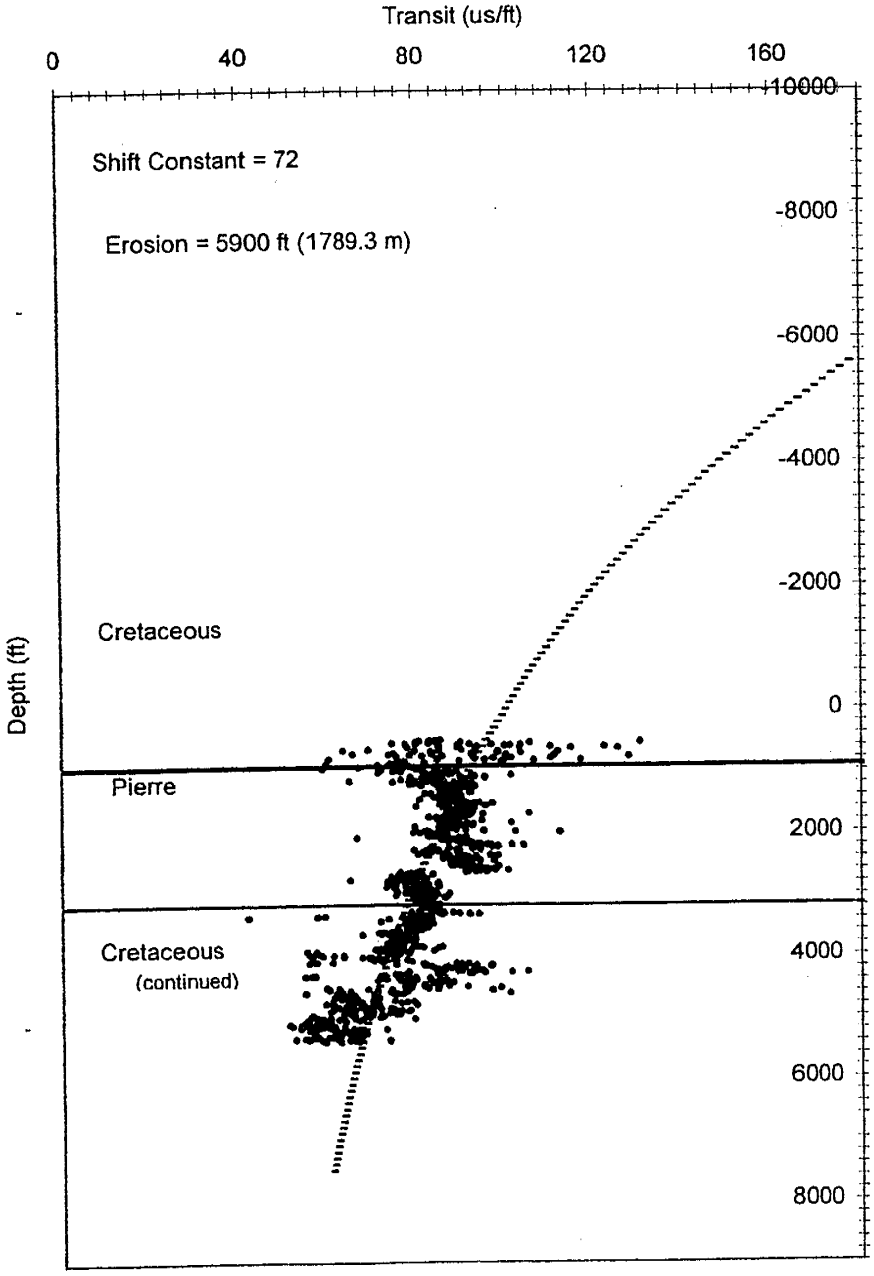

Reinert No. 1-20

Twp 20S Rng 42W Sec 20

Kiowa, CO

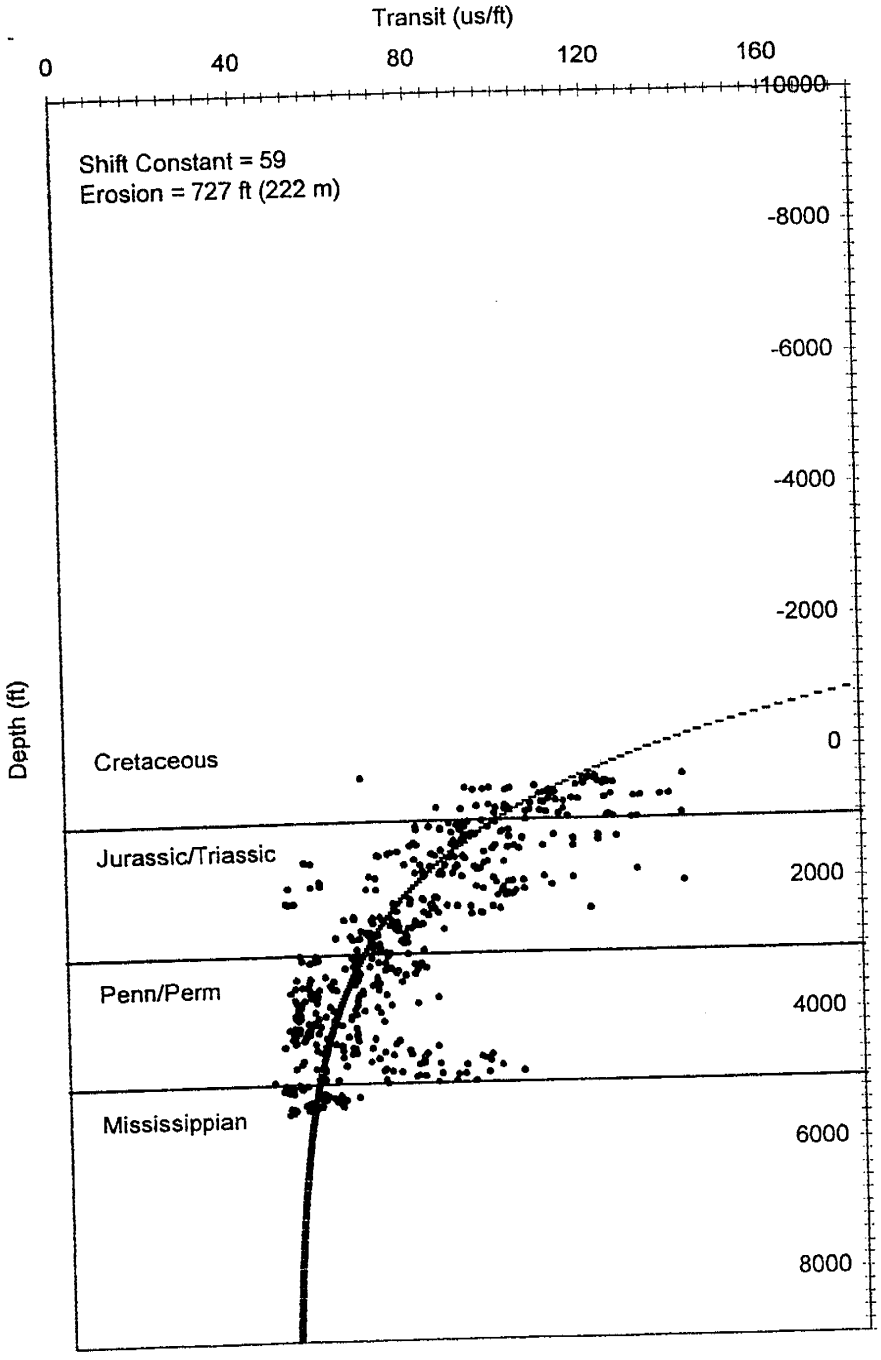

21-4 True State

Twp 21S Rng 54W Sec 4

Otero,CO

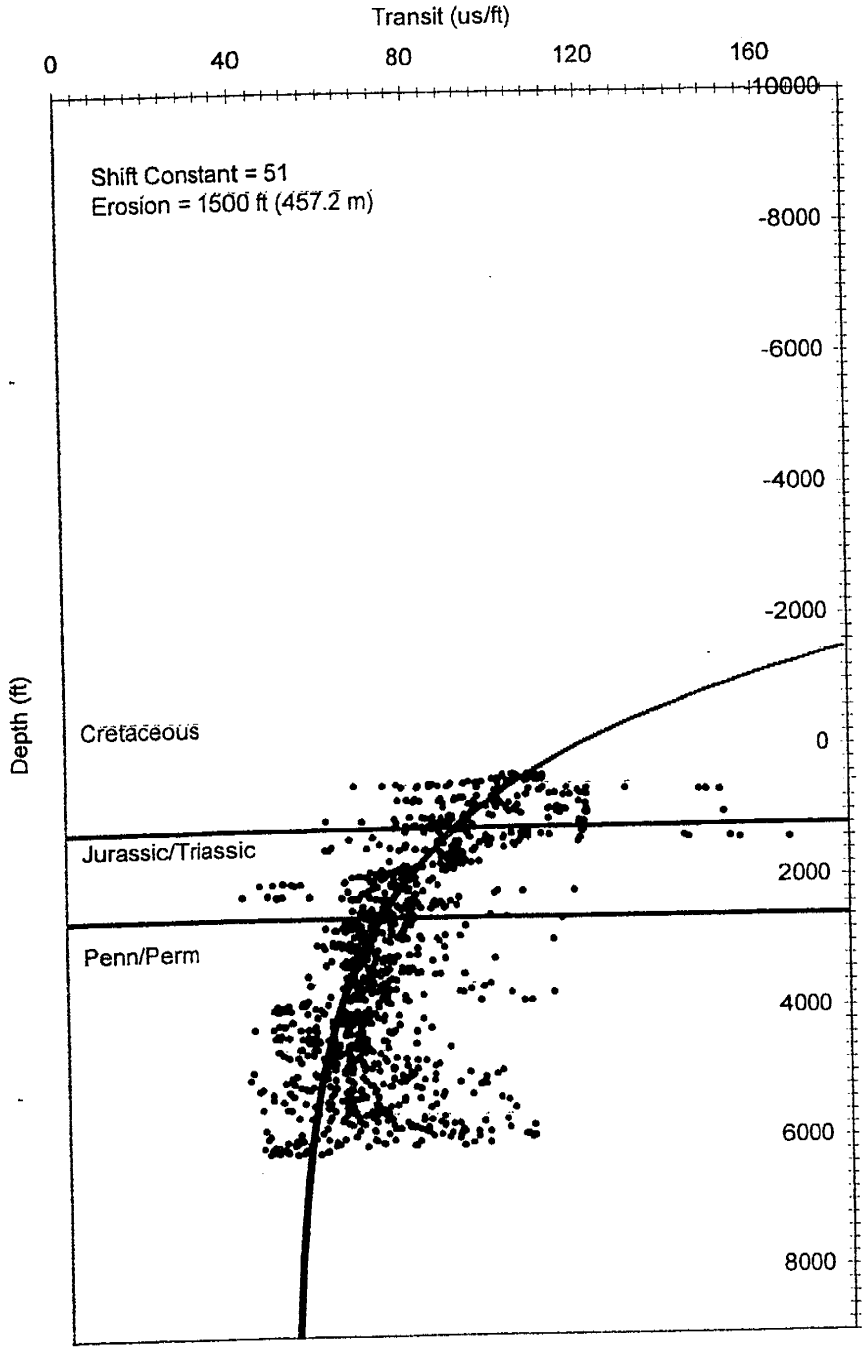

Merrick

Twp 18S Rng 47W Sec 33

Kiowa, CO.

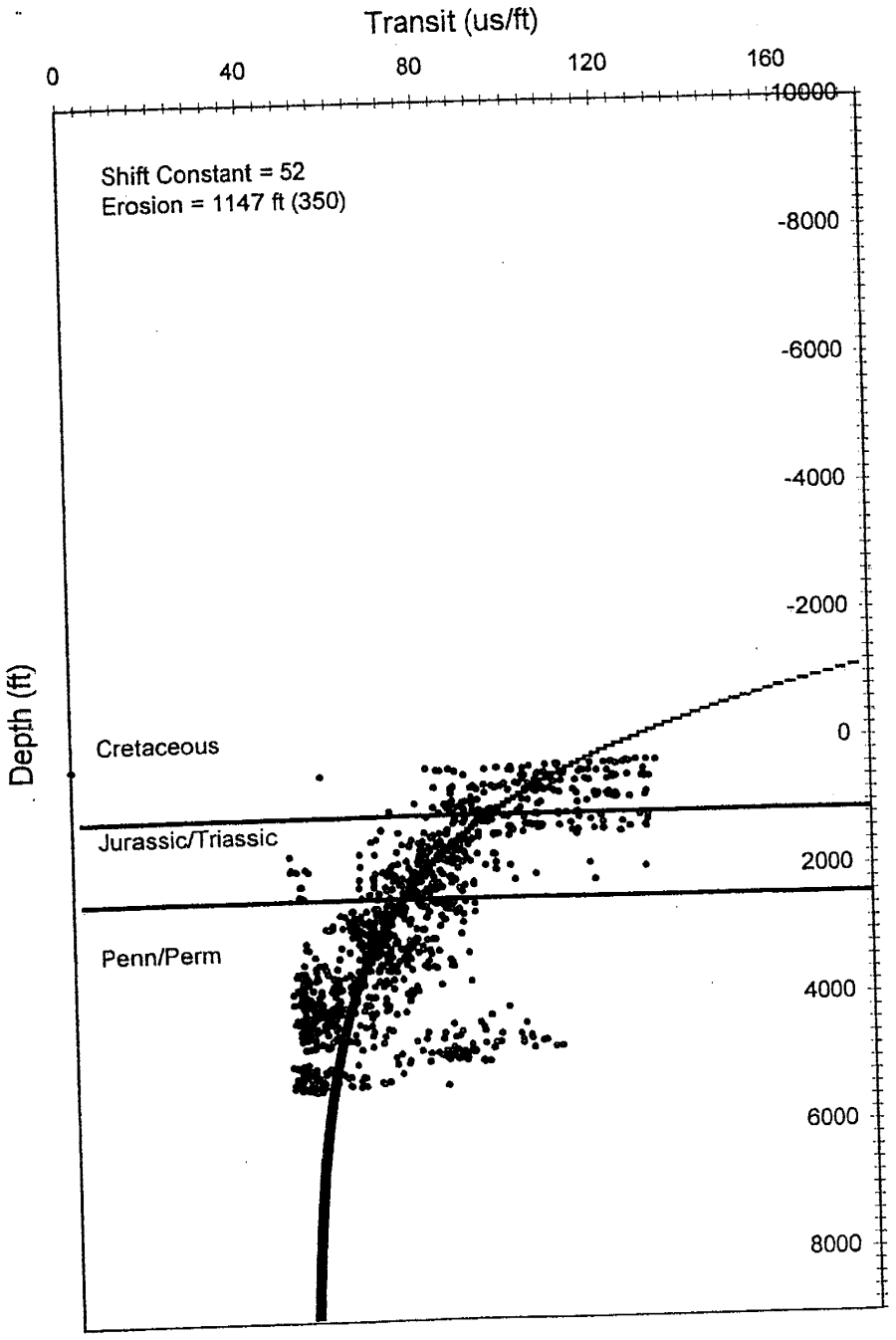

Federal Jordan

Twp 25S Rng 58W Sec 2

Otero, CO

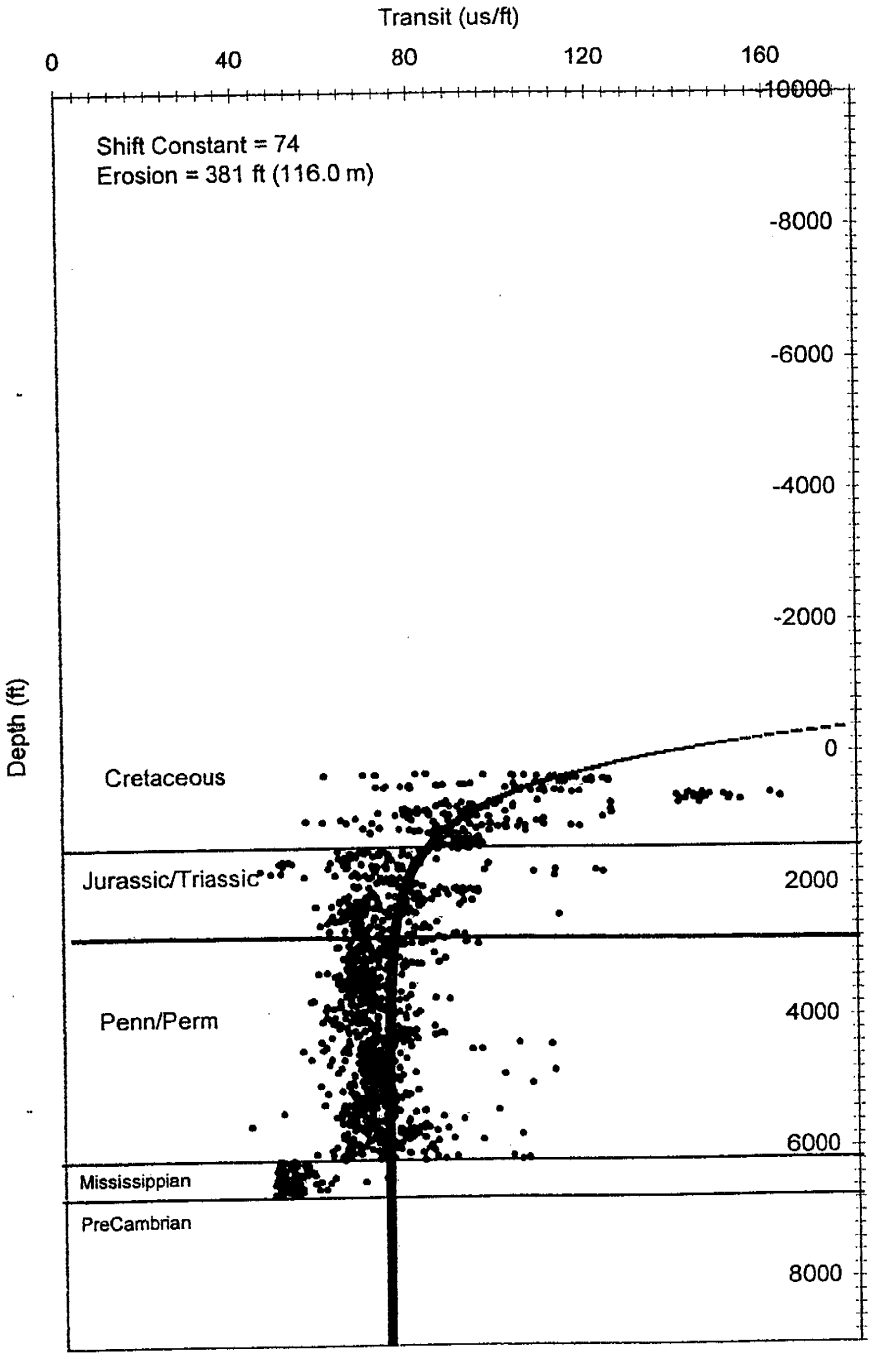

John Brown

Twp 18S Rng 47W

Kiowa, CO

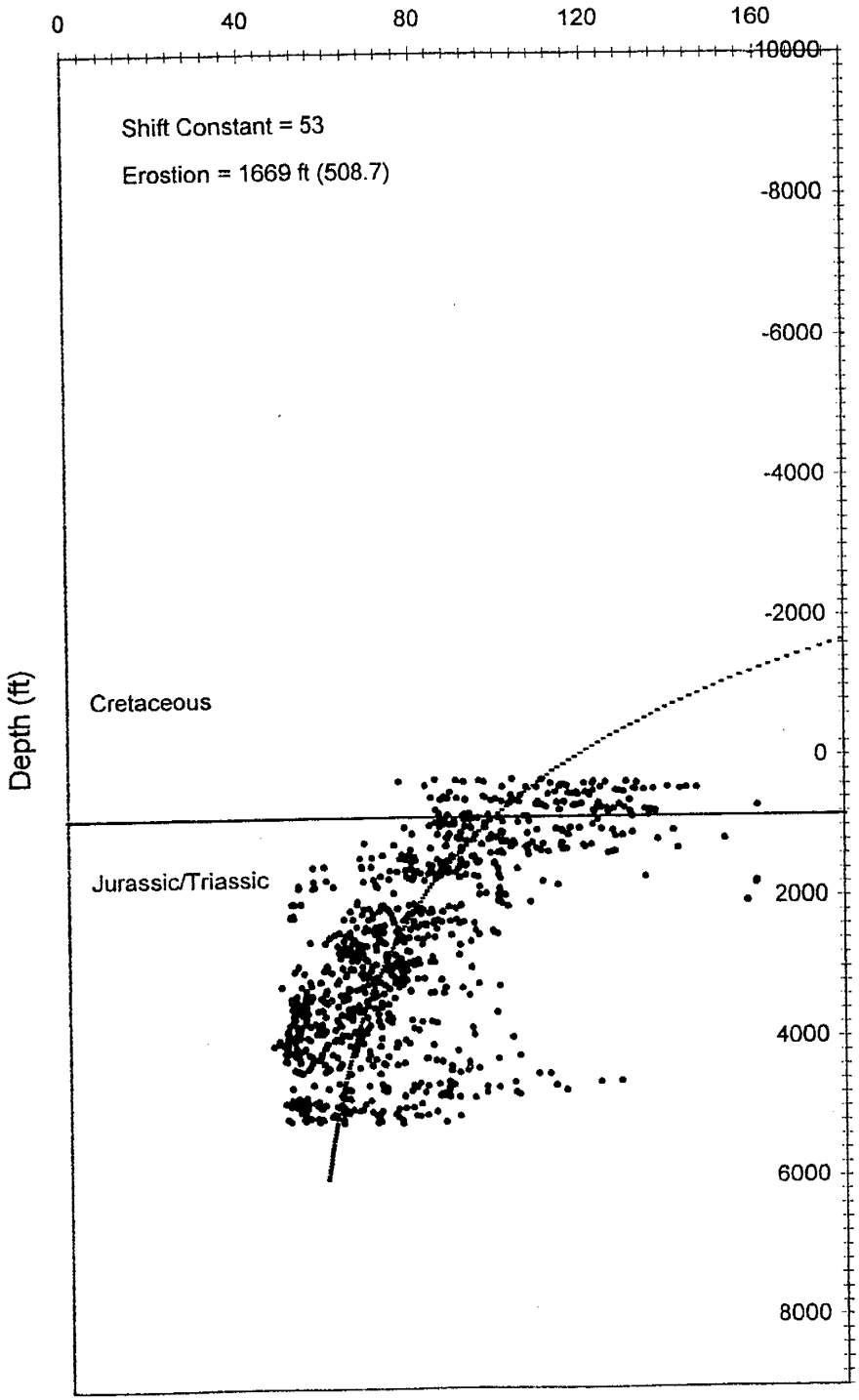

No. 1 Walker Ranch

Twp 27S Rng 70W Sec 1
Huerfano, CO

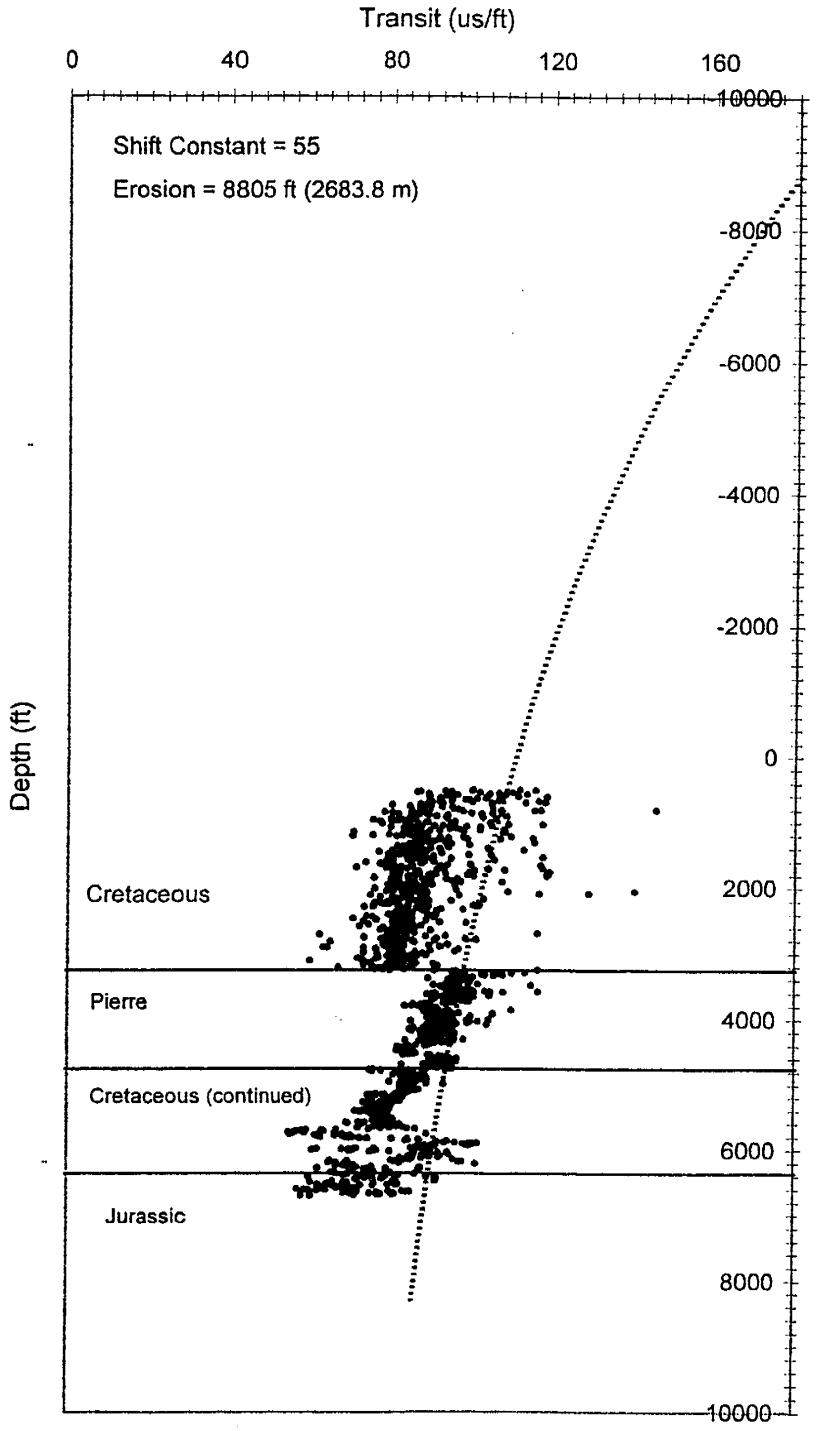

No. 5 Goemmer

Twp 30S Rng 68W Sec 5

Huerfano, CO

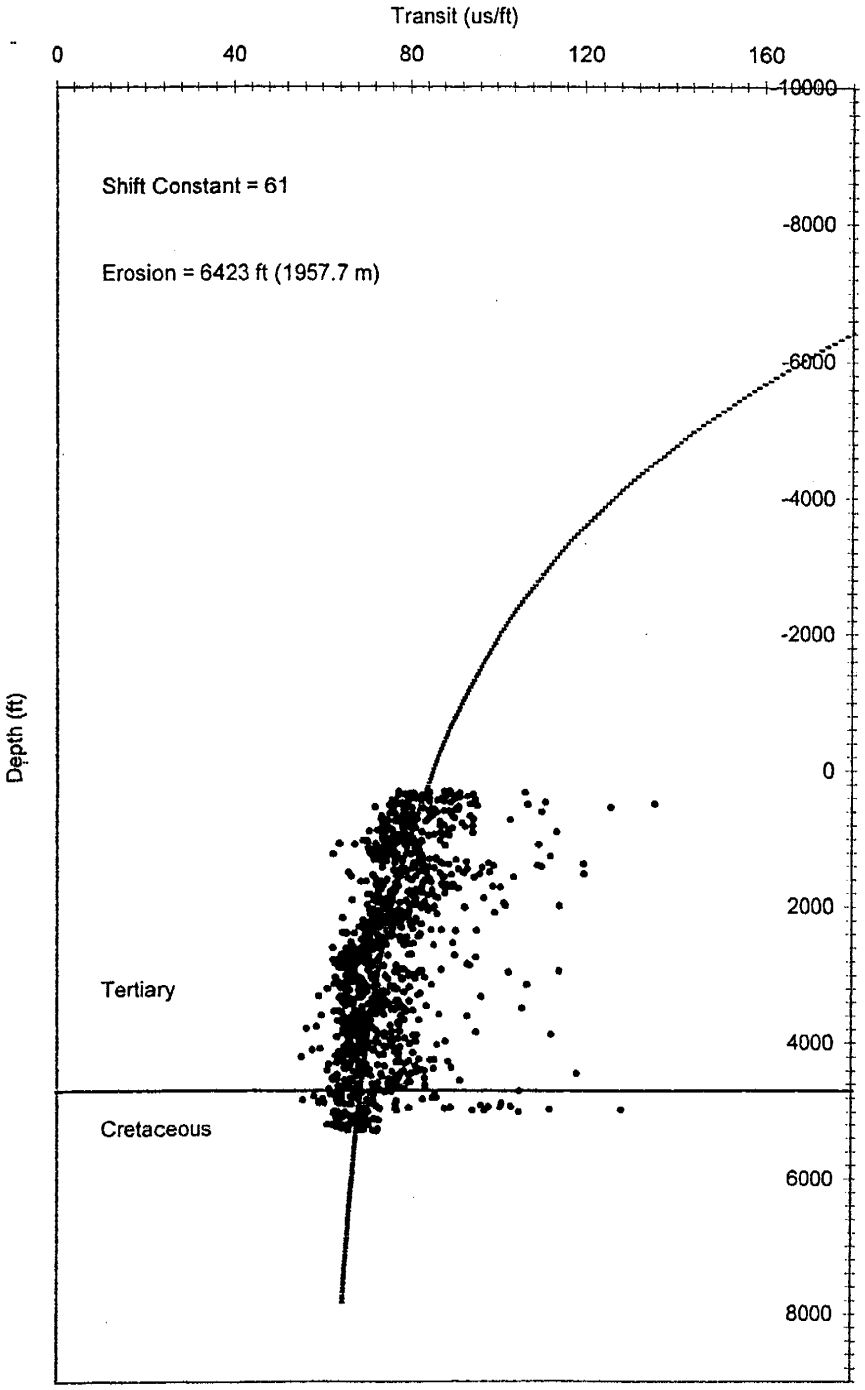

Goemmer Land Co. 1

Twp 29S Rng 67W Sec 11

Huerfano, CO

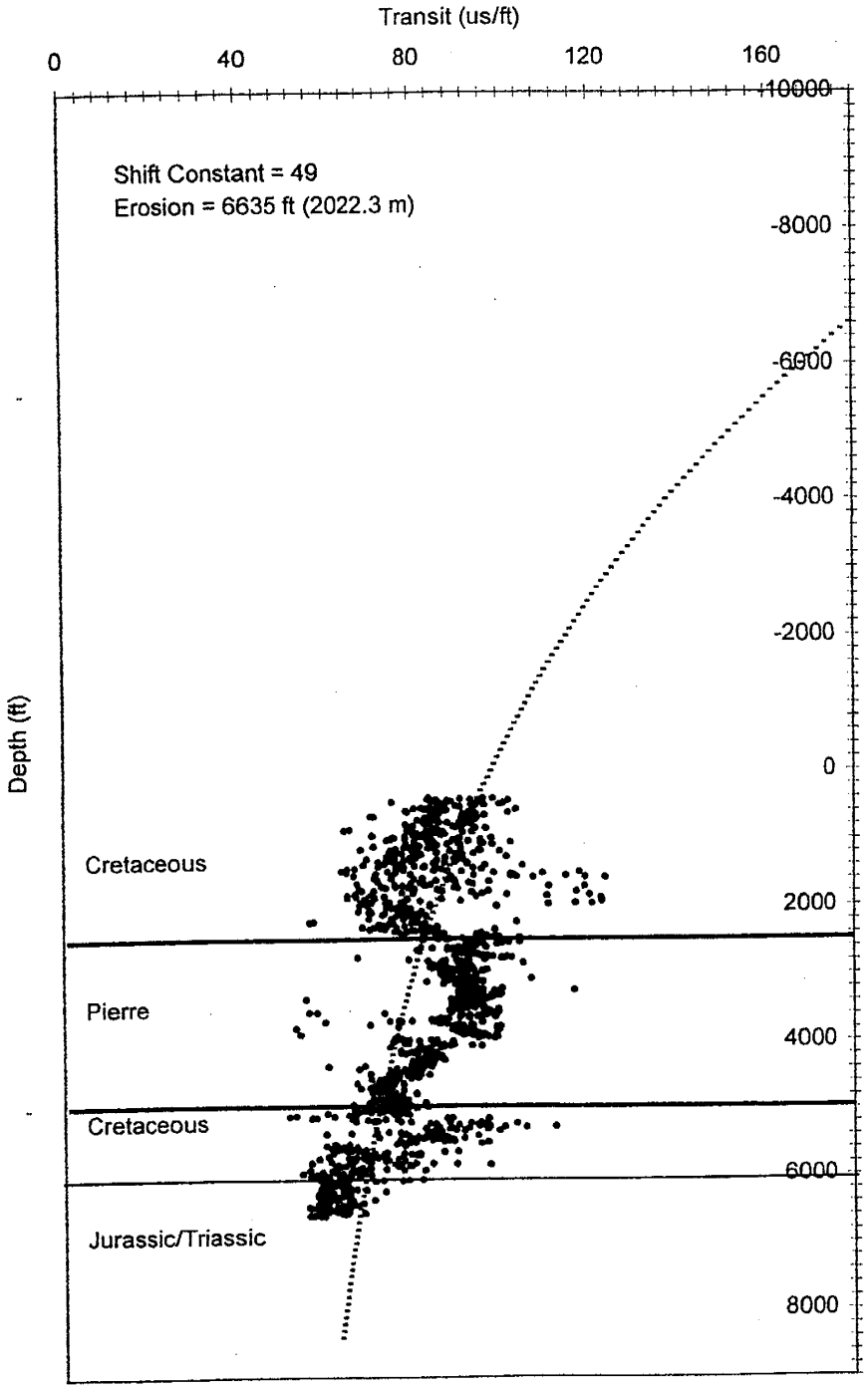

Cuerno Verde Ranch

Twp 25S Rng 71W Sec 21

Huerfano, CO

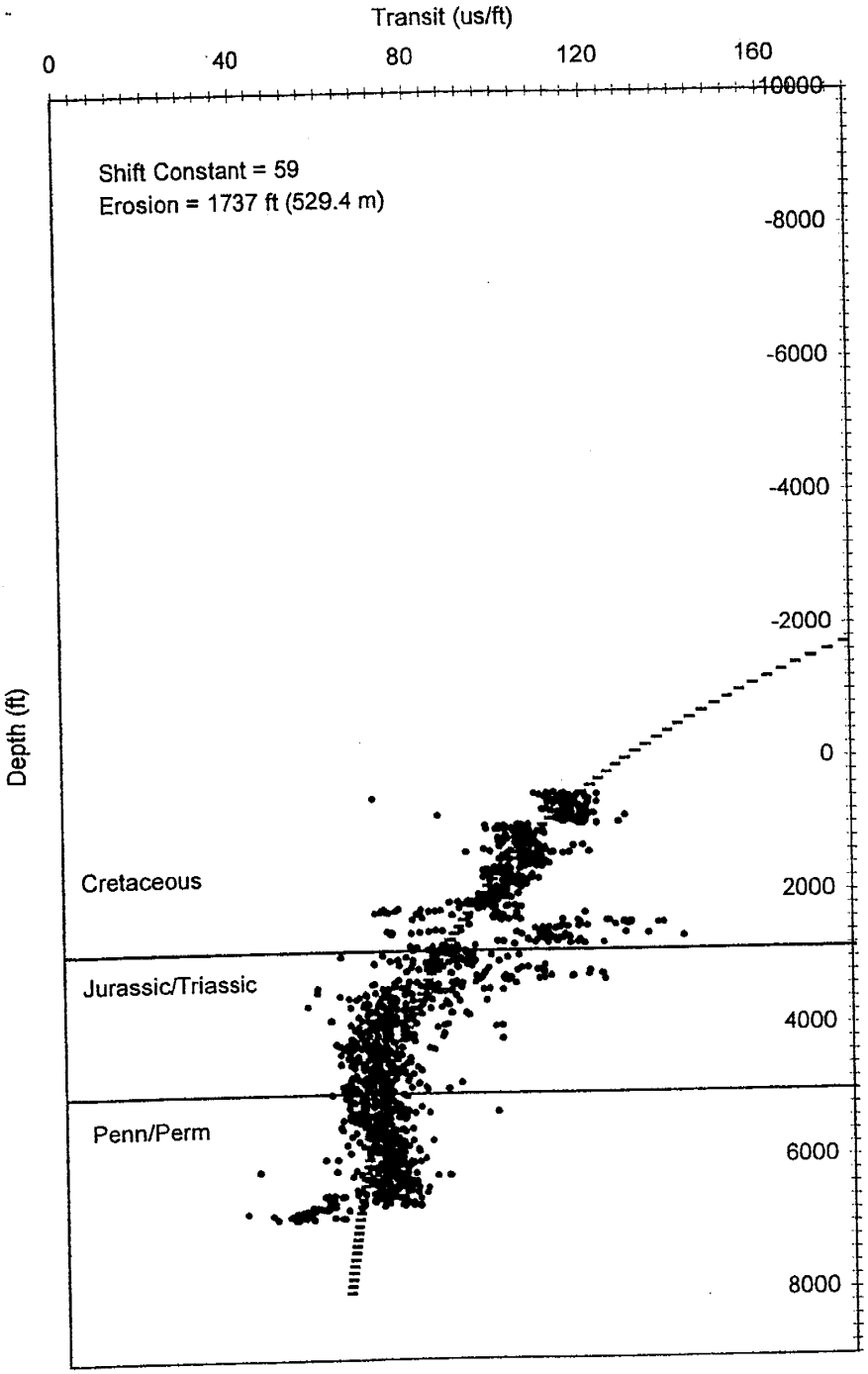

BDCDGU #051 1833

Twp 18N Rng 33E

Harding, NM

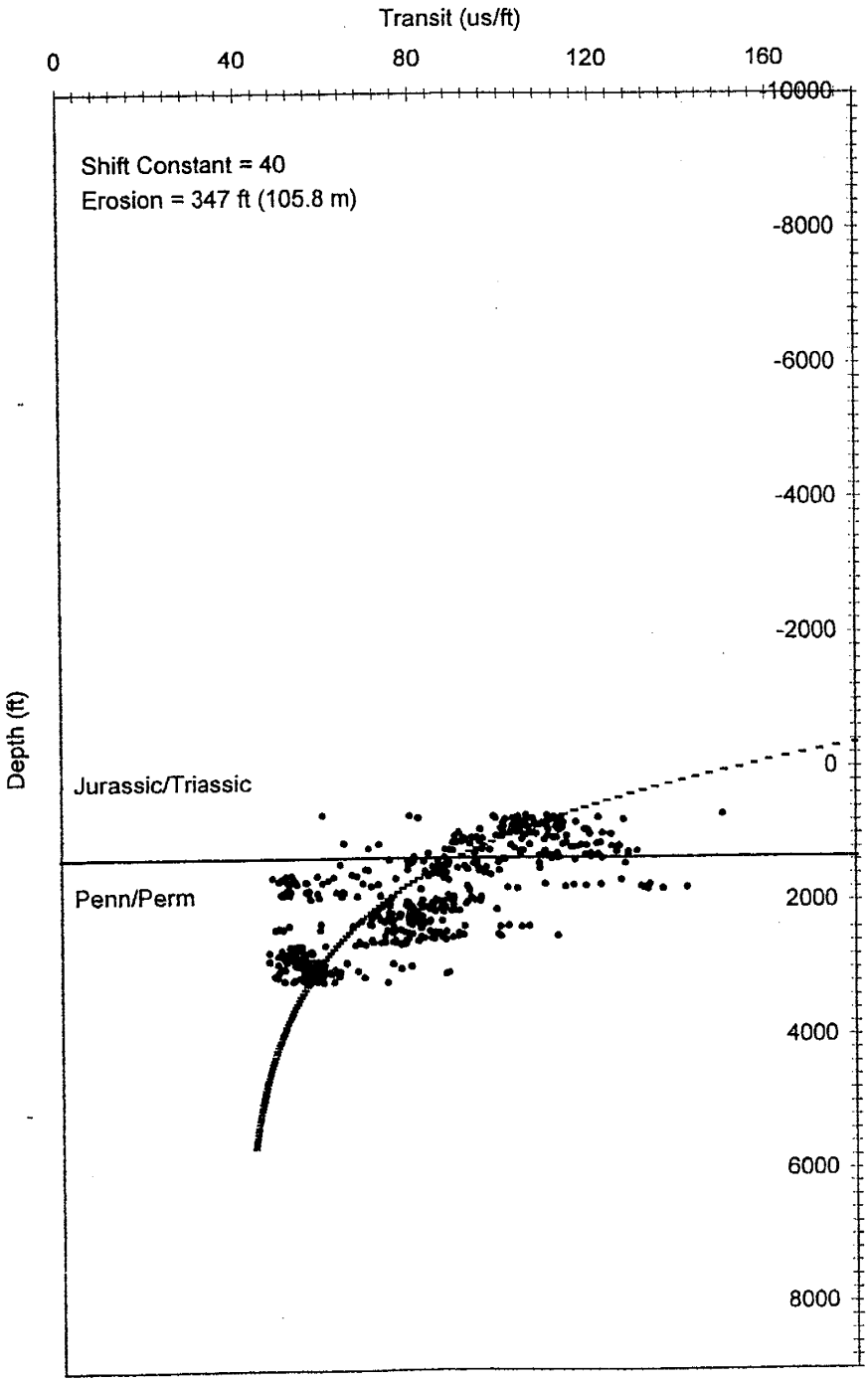

BDCDGU #251G 1832

Twp 18N Rng 32E

Harding, NM

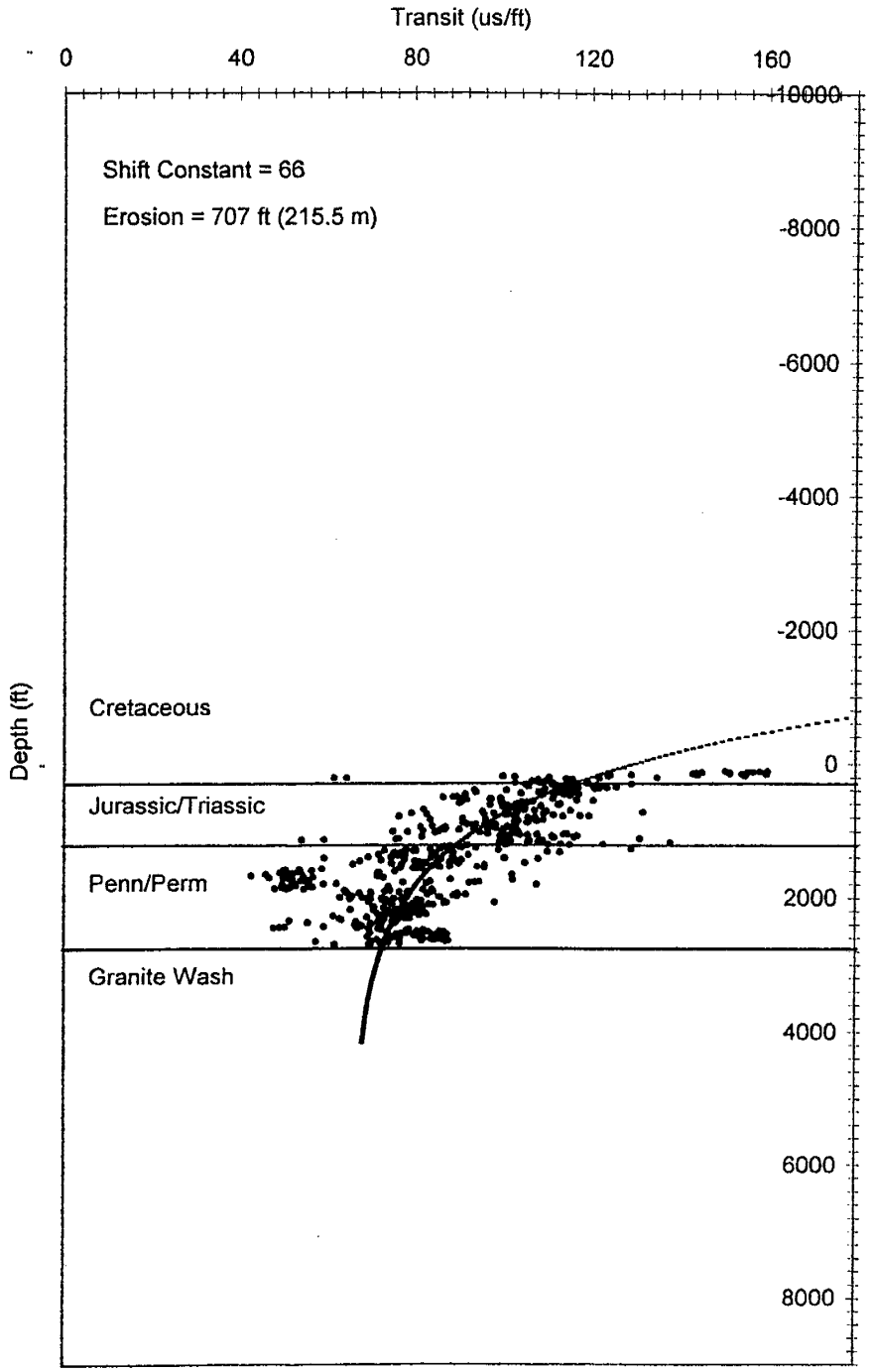

#271G Castle Rock

Twp 31N Rng 17E Sec 27

Colfax, NM

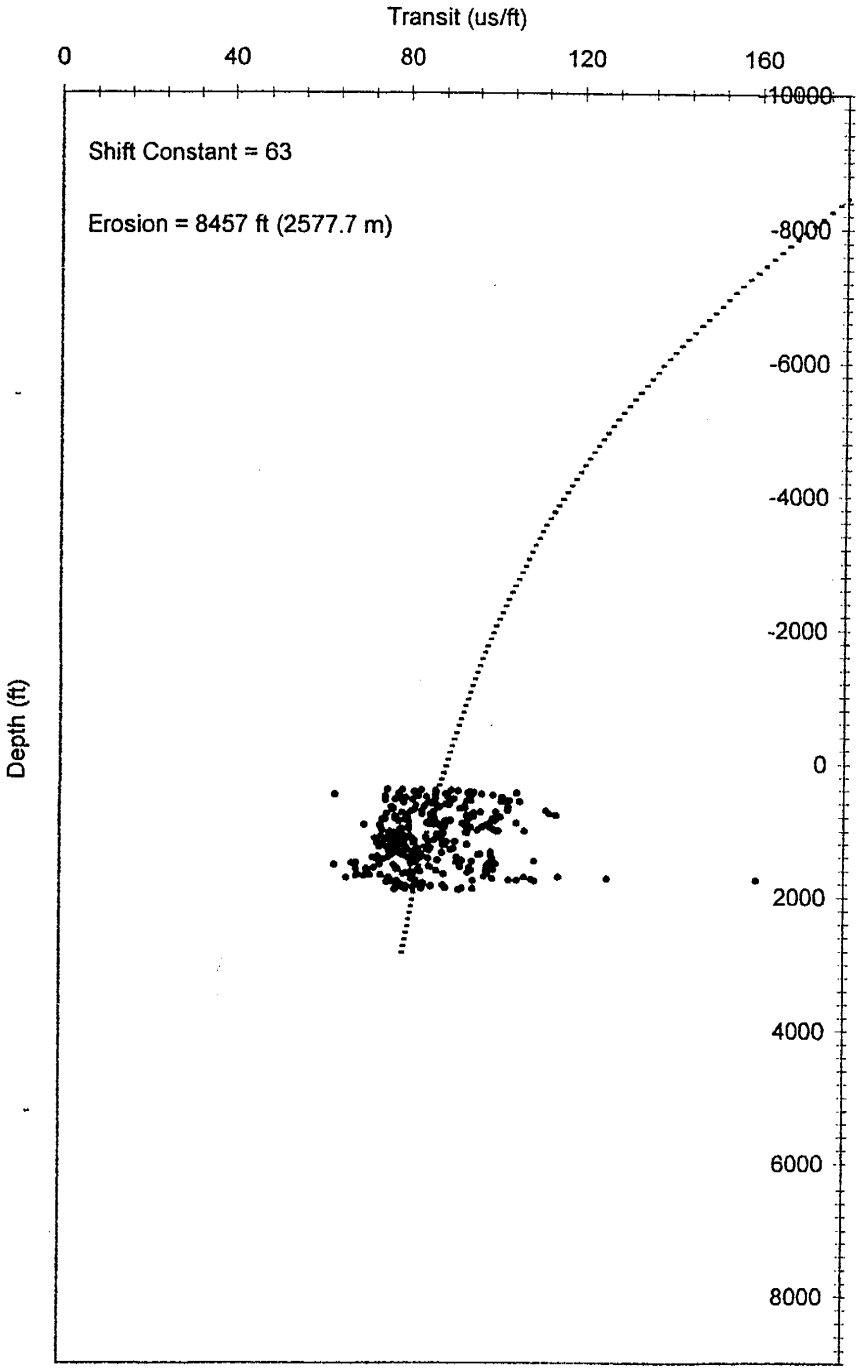

Armstrong No. 1

Twp 24S Rge 48W Sec 5

Bent, CO

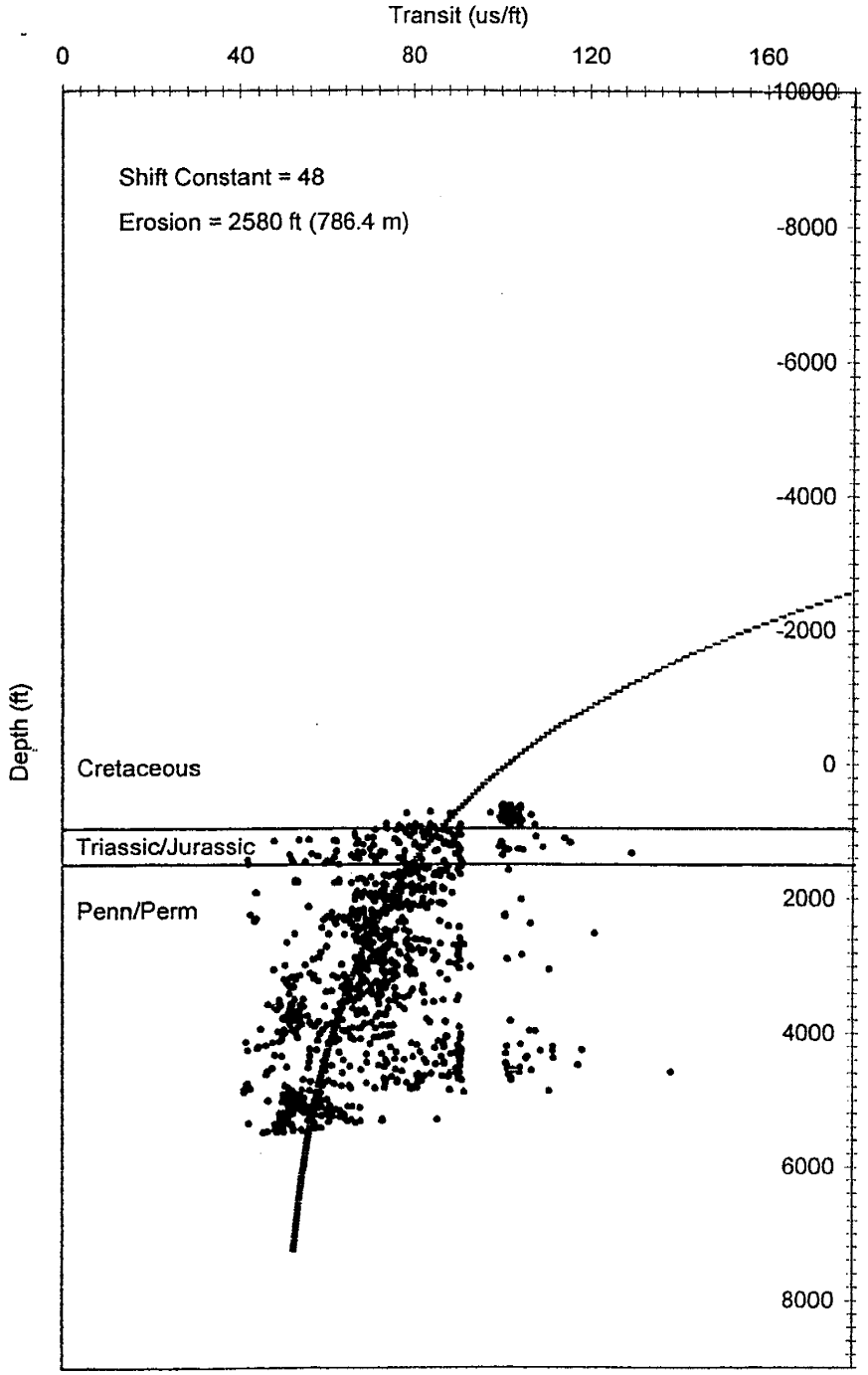

Phelps Dodge #1

Twp 28N Rng 20E Sec 11

Colfax, NM

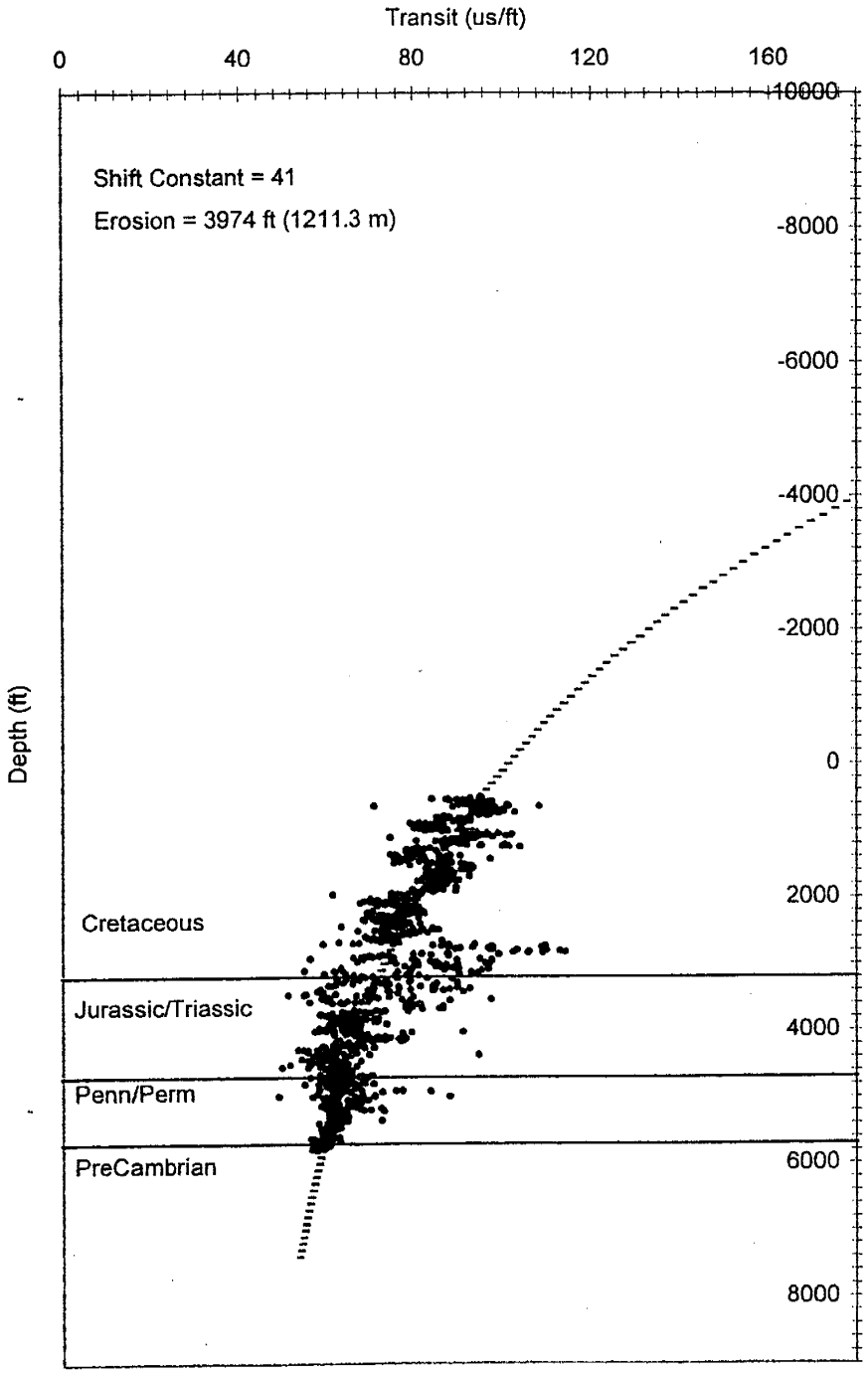

W.E. Niles Estate Unit #1

Twp 29S Rge 44W Sec 2

Baca, Co

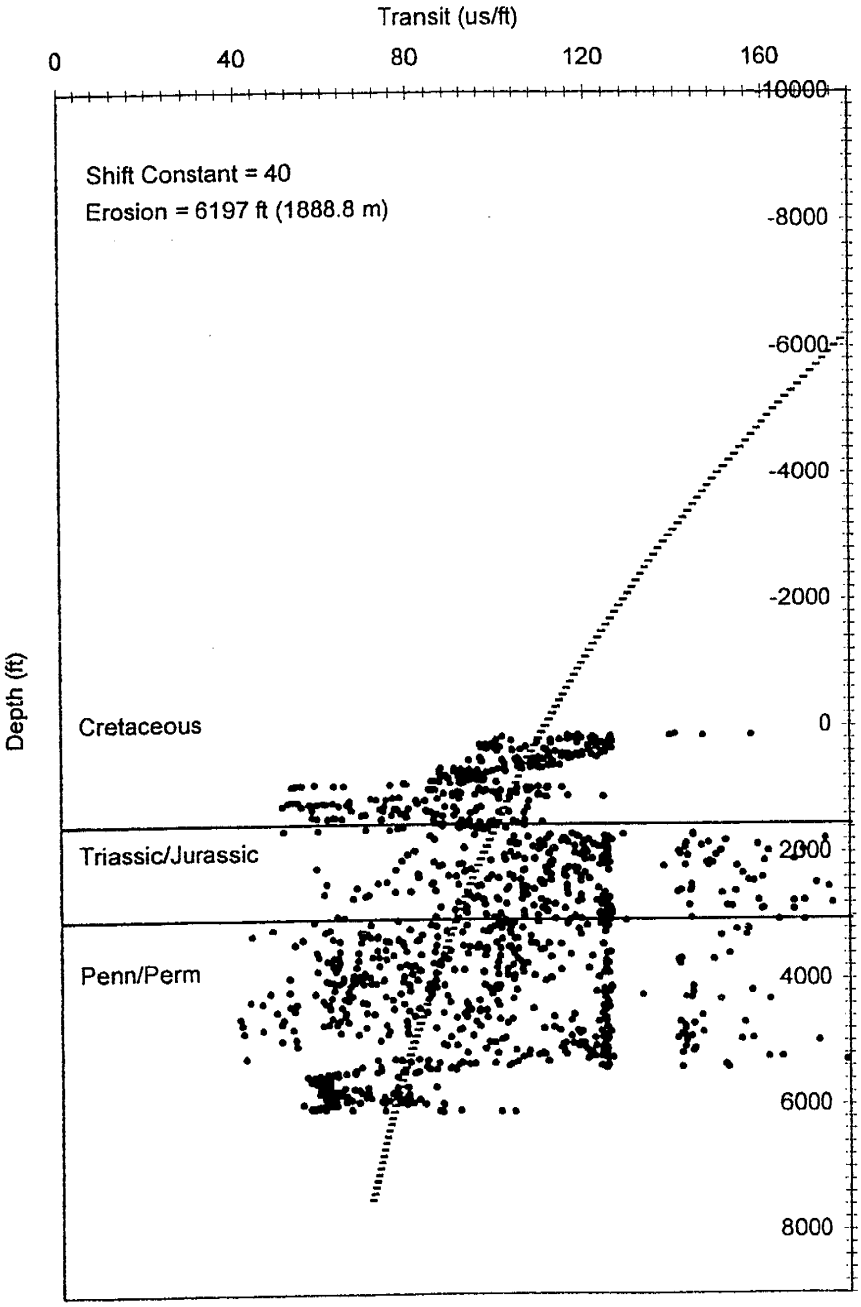

State 1-18

Twp 21S Rng 52W Sec 18

Bent, CO

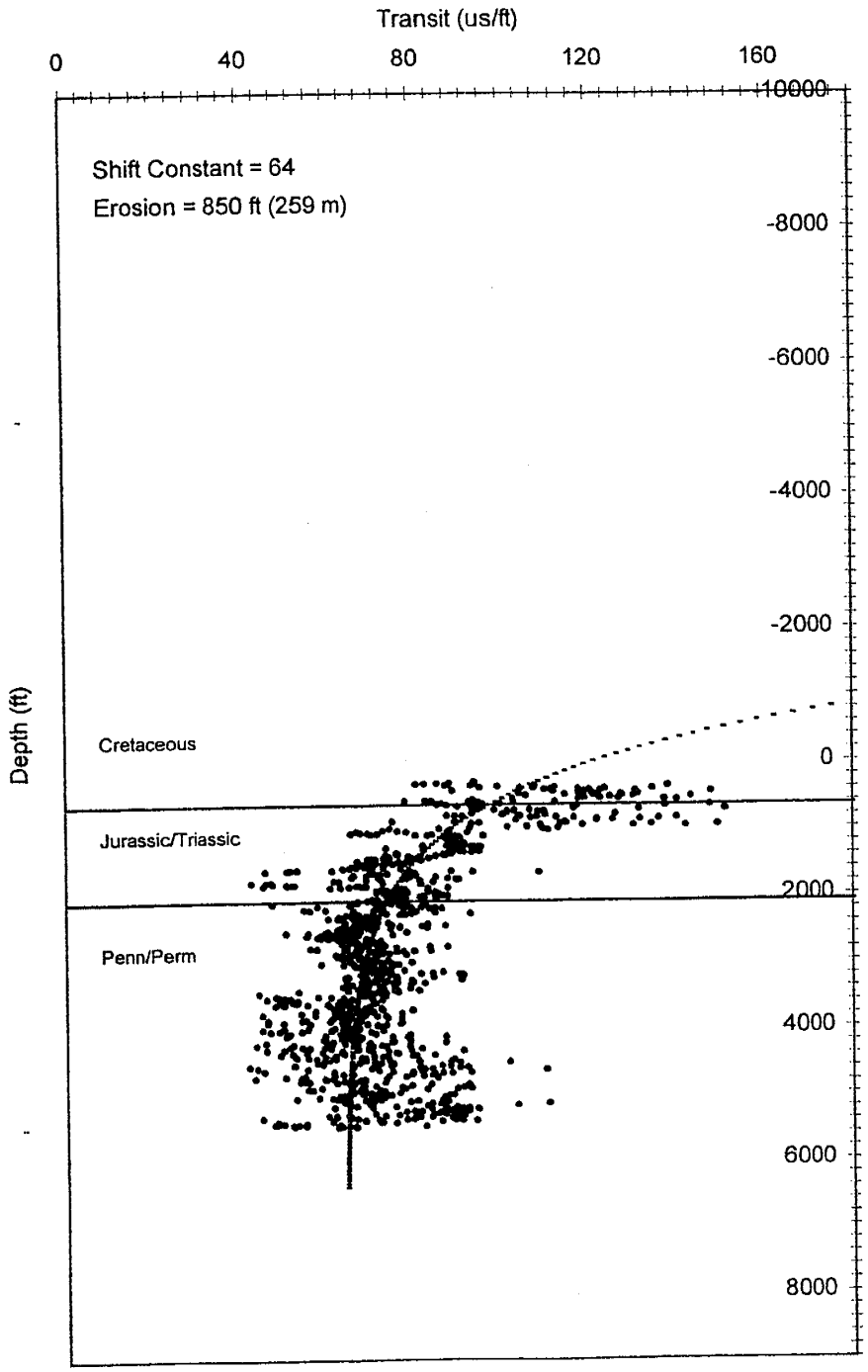

AP Tanner Unit #1

Twp 31S Rge 42W Sec 14

Baca, CO

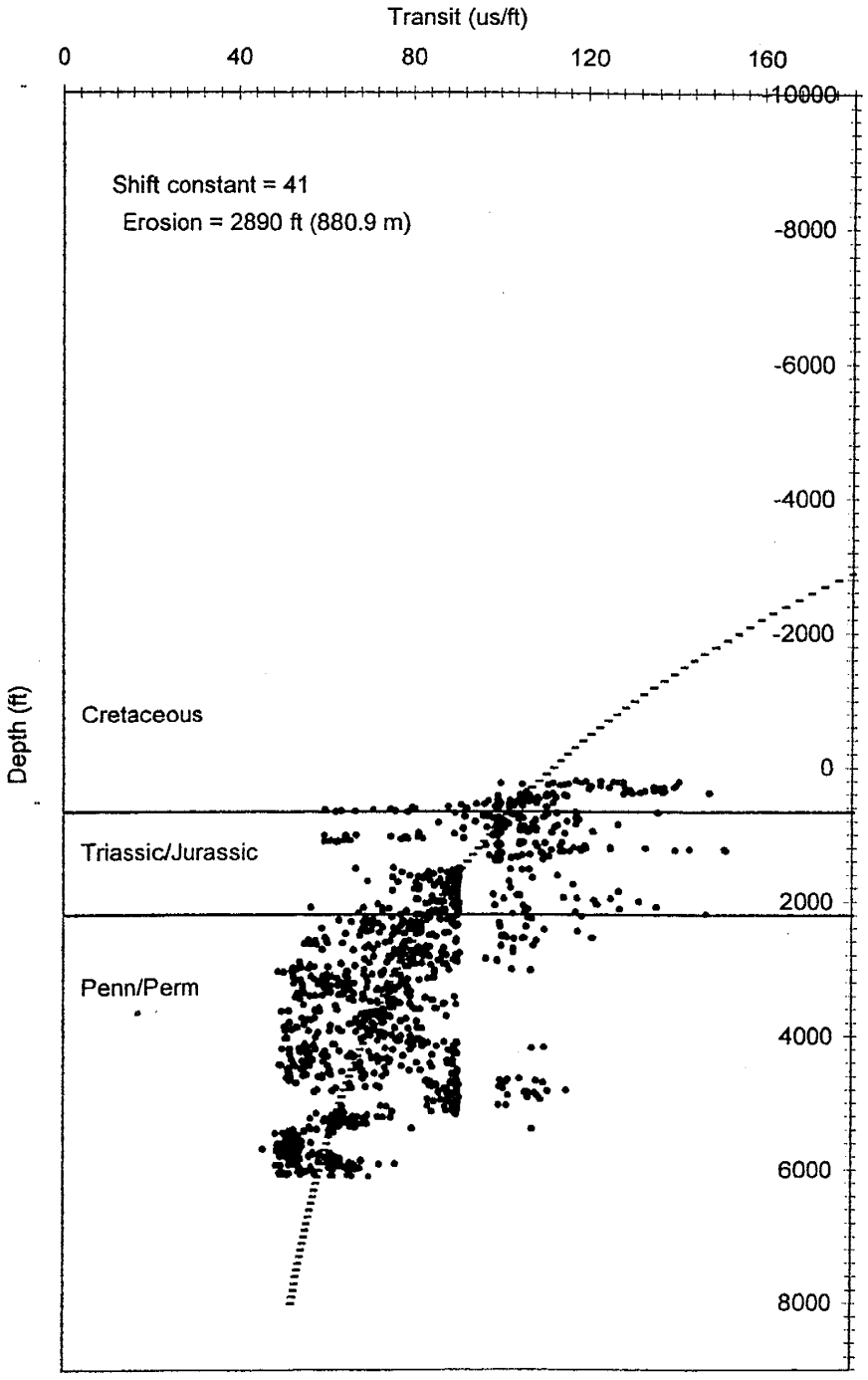

Dean #1-22

Twp 22S Rng 52W Sec 22

Bent, CO

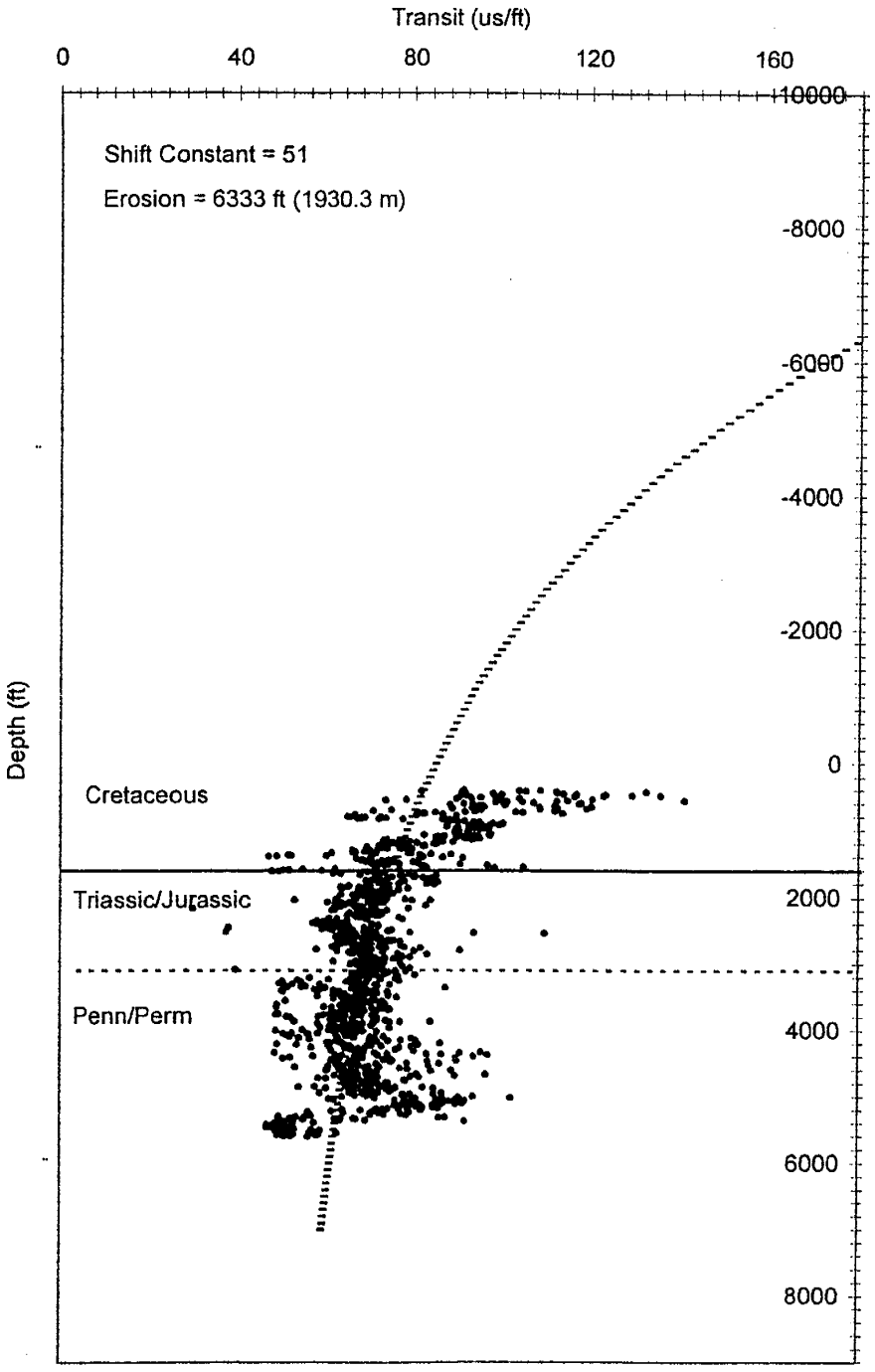

Jolla Land & Cattle Co. "F" #1

Twp 31N Rng 34E Sec

Union, NM

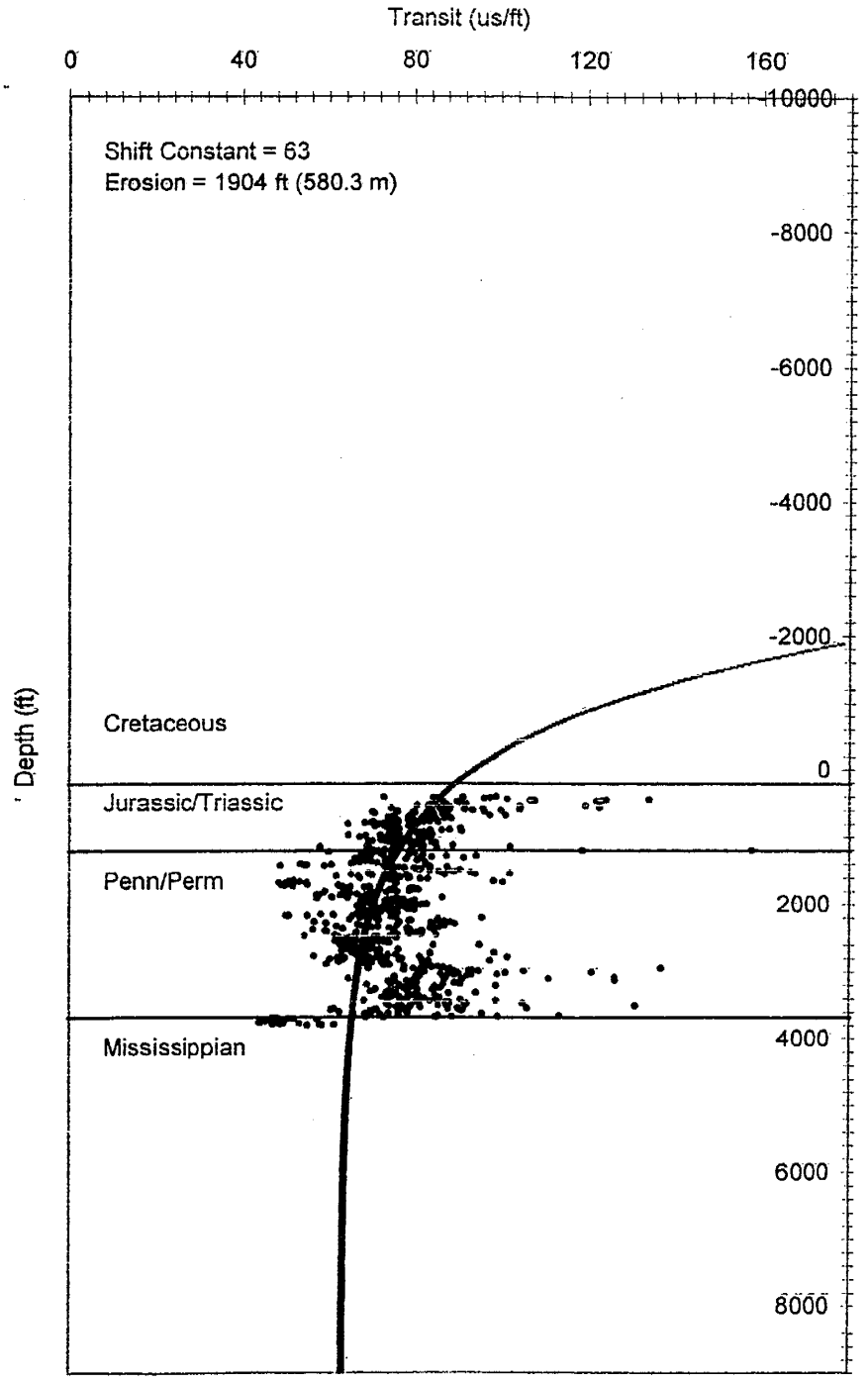

Caroline Gonzales #1

Twp 23N Rng 32E Sec

Union, NM

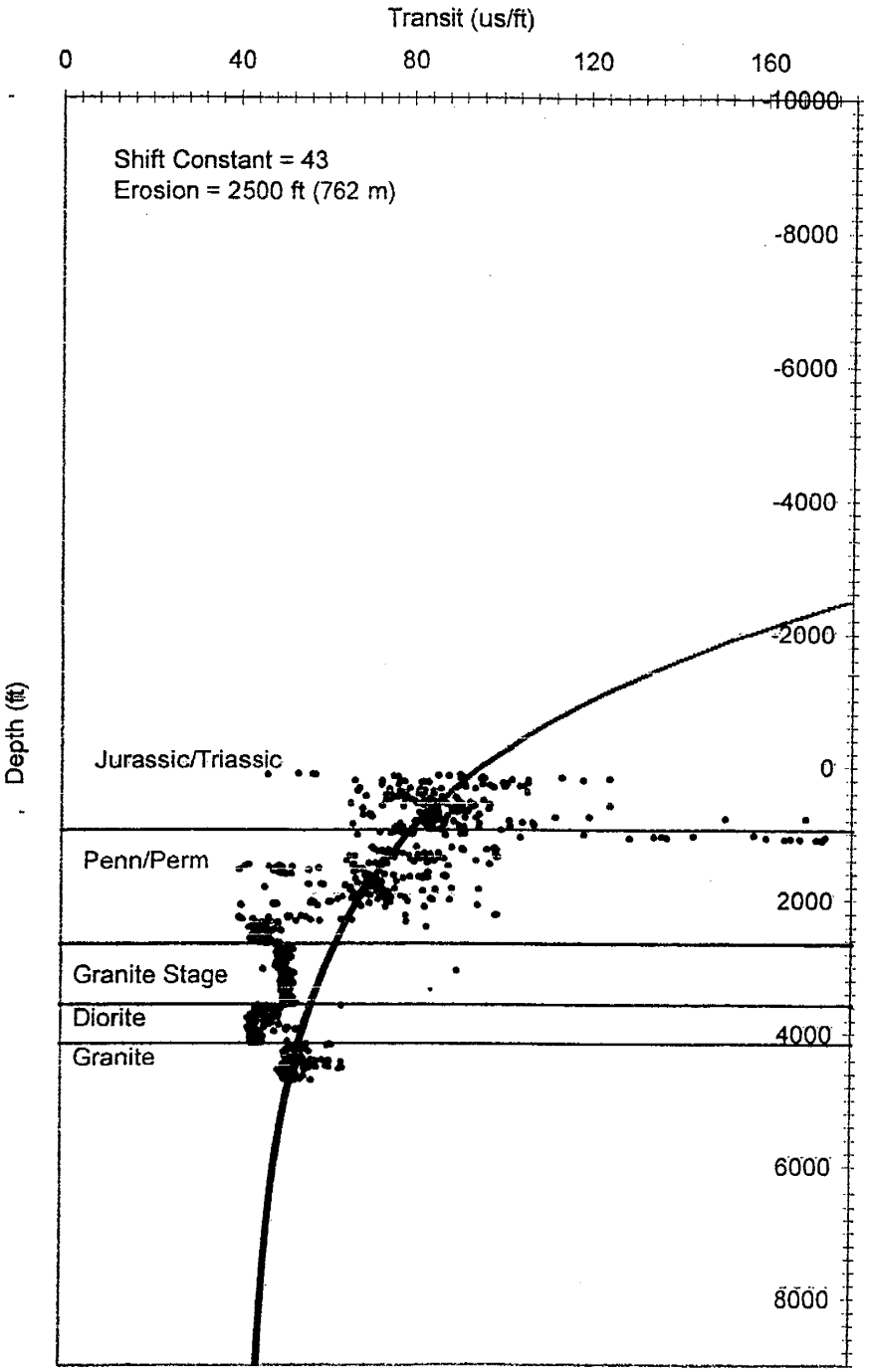

BDCDGU #241 2332

Twp 23N Rng 32E

Union, NM

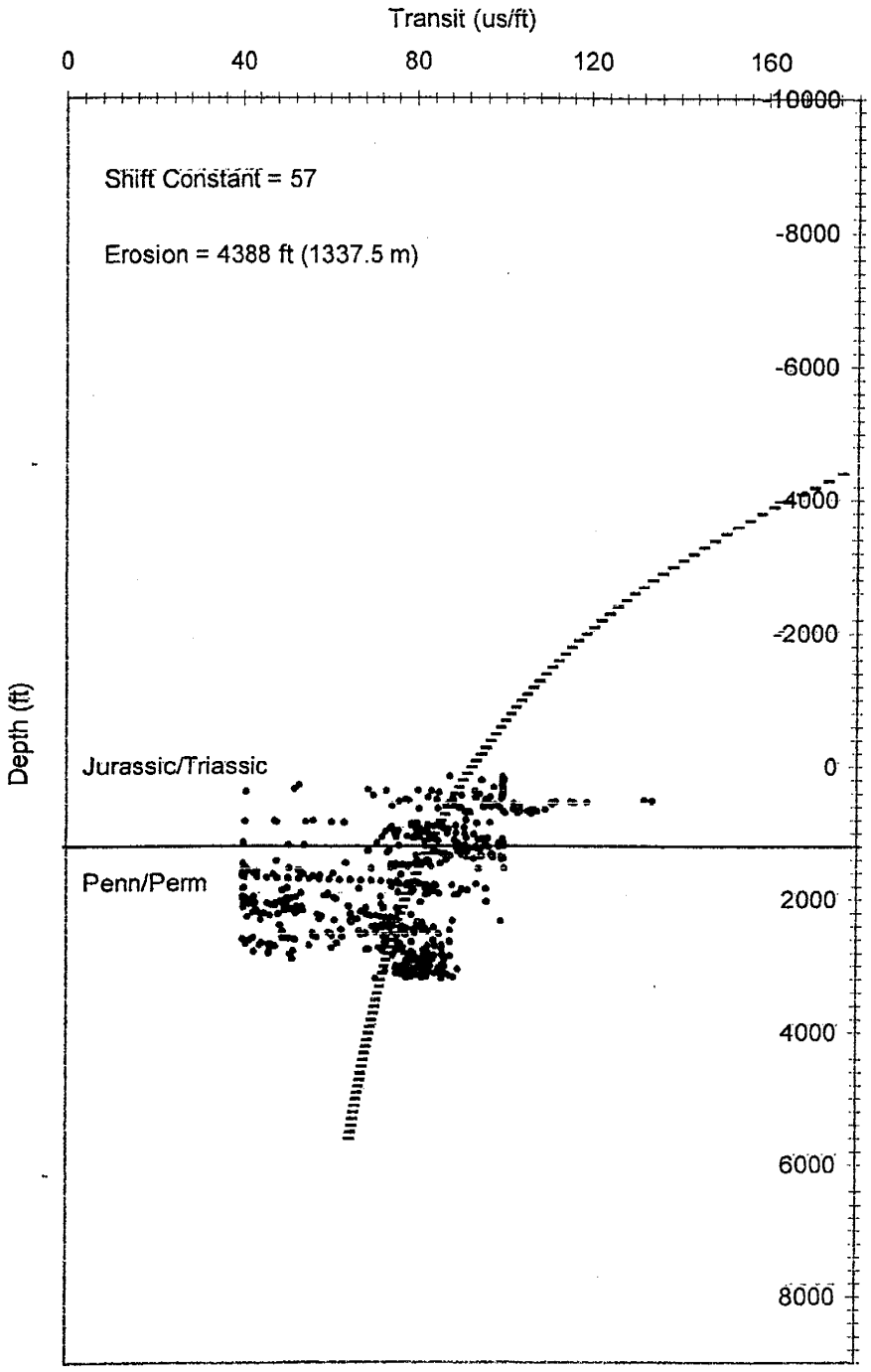

Union "B" State #1

Twp 31N Rng 33E

Union, NM